

**EVALUATION OF SHEAR FAILURE MECHANISM OF
RC MEMBER BASED ON ANALYSIS OF
BEAM ACTION AND ARCH ACTION**

FU Li

**EVALUATION OF SHEAR FAILURE MECHANISM OF
RC MEMBER BASED ON ANALYSIS OF
BEAM ACTION AND ARCH ACTION**

By

FU Li

A Dissertation Submitted to Nagoya University
In Partial Fulfillment of the Requirements for
The Degree of Doctor of Engineering

Department of Civil Engineering
Graduate School of Engineering, Nagoya University
Nagoya, Japan

ABSTRACT

In ordinary seismic design for a reinforced concrete (RC) structure, one of the basic requirements is that brittle shear failure shall be inhibited. In reality, however, a certain number of RC structures nevertheless could not survive under effect of great earthquake or cyclic loading because of severe shear behavior, although they conform shear design rules. Shear failure after yielding of longitudinal reinforcement (short for shear failure after yielding) and shear failure at cutoff point in longitudinal reinforcement (short for shear failure at cutoff point) are the most common shear failure patterns that has been widely reported. Meanwhile, cyclic loading plays a primary role in the two patterns of shear failure and it can lead to a different deformation behavior, i.e. section cracking at plastic hinge, from that under monotonic loading. Herein, the section crack refers to a crack penetrating RC member in transverse direction, which is usually caused by cyclic loading, shrinkage and thermal effect. Therefore, this study aims to clarify the mechanisms of above shear failures and investigate the effect of section crack on shear performance, for a more optimized shear design.

In order to better understand the failure mechanism, the shear failure after yielding of a RC column subjected to cyclic loading was simulated by three dimensional Rigid-Body-Spring-Method (3-D RBSM), and the shear strength degradation, which was responsible for ultimate failure, was quantitatively assessed. Afterwards, by decoupling shear strength into beam action and arch action, the mechanism of shear strength degradation, i.e. mechanism of shear failure after yielding, was explained based on the degradation behaviors of beam action and arch action. The result shows that the progressive degradation of arch action with increased displacement ductility results in the shear

strength degradation until lower than the shear demand corresponding to flexural strength and final failure. Additionally, a parametric study for the effect of main structural variables, i.e. shear reinforcement ratio, shear span to effective depth ratio, tension reinforcement ratio and axial compression load, on mechanism of shear failure after yielding was carried out. As the effect of variables on degradation rate of arch action, the result shows that more arrangement of shear reinforcement can effectively reduce the start displacement ductility for dramatic degradation of arch action.

Section crack at plastic hinge zone is regarded as a primary factor for the degradation of arch action, therefore, by using 3-D RBSM, the initial section crack was introduced into RC column and the effect of section crack on shear strength was surveyed by a following monotonic loading analysis. As a consequence, it was revealed that the formation of section crack located at the position $1.0d$ or $2.0d$ (d : effective depth) far away from footing-column intersection can obviously reduce the arch action and shear strength. Also, the reduction effect of initial section crack on shear strength was further demonstrated by loading test on RC beams with initial section crack, and the following numerical study on shear resistance mechanisms shows that the degradation of shear strength in section-cracked beam is attributed to the degradation of arch action, because the initial section crack obstructs the transfer of axial compressive stress in concrete.

The different shear performances of RC beams with and without rebar cutoff under monotonic loading were simulated by 3-D RBSM, and the different developments of beam action and arch action were obtained. As a result, it was understood that the beam with rebar cutoff presents a lower shear strength because the rebar cutoff significantly reduces the capacity of arch action. Moreover, it was learned that the decline of beam action, after shear cracking, leads to the shear failure of beam with rebar cutoff, while the drop of arch action is the main cause of shear failure of beam without rebar cutoff.

ACKNOWLEDGEMENTS

First and foremost, I would like to express my sincerest gratitude to my supervisor, Professor Hikaru Nakamura. He guided, inspired, assisted and supported me to pursue a doctoral degree. In the whole progress of my research, he has provided me encouragement, insightful discussions, valid advice, a lot of wonderful ideas and financial assistance. Without his patience and great efforts, this dissertation would have never been completed. I am very thankful to Associate Professor Yoshihito Yamamoto for his enthusiasm and his great help in my numerical analysis. I gratefully thank to Assistant Professor Taito Miura for this kind supports for my experimental work. Sincere thanks also give to the other members of my examination committee: Professor Akiyama Mitsuyoshi and Professor Kazuo Tateishi for their valuable academic comments on my mid-term examinations and feedback on this dissertation.

I would like to thank all members of Concrete Laboratory for the great and unforgettable time we spent together. I am particularly thankful to Dr. Di Qiao, senior student, for his help in my daily life and his advice on my study work. I also pay thankfulness and appreciation to Mr. Shun-yuan Chi and Mr. Yang Zhang for their continuous assistance to my experimental work.

I gratefully acknowledge that Nagoya University kindly exempts my tuition fee during my entire doctoral course.

I am deeply thankful to my parents, Mr. Ya-ping FU and Mrs. Xiu-jie Li, for their love, support, encouragement and sacrifices. At last, I want to thank my wife, Ke Liu, who is the best thing in my life and always stands by my side.

Table of Contents

ABSTRACT	I
ACKNOWLEDGEMENTS	III
Table of Contents.....	IV
List of Tables	VIII
List of Figures.....	IX
1. General Introduction.....	1
1.1 Background	1
1.2 Literature review	4
1.2.1 Effect of main structural variables on shear strength	4
1.2.2 Shear failure after yielding under cyclic loading.....	5
1.2.3 Introduction of shear resistance mechanisms	7
1.2.4 Effect of section crack on shear strength of RC structure	10
1.2.5 Effect of rebar cutoff on shear strength of RC structure	10
1.3 Study objective and research significance	11
1.4 Organization of dissertation contents.....	12
2. Basic Methodology of Analysis.....	16
2.1 Introduction.....	16
2.2 Numerical method.....	16
2.2.1 3-D RBSM.....	16
2.2.2 Concrete material model.....	17

2.2.3 Reinforcement and bond models	20
2.3 Decoupling approach of shear resistance mechanism.....	21
2.3.1 Decoupling approach of beam action and arch action.....	21
2.3.2 Decoupling approach of truss action and concrete contribution	24
2.4 Example of decoupling result for shear resistance mechanism	25
2.5 Summary	29
3. Mechanism of Shear Failure after Yielding due to Cyclic Loading	30
3.1 Introduction.....	30
3.2 Objective experiment	31
3.3 Analytical model	32
3.4 Analytical result	33
3.4.1 One-side repeated loading	33
3.4.2 Cyclic loading.....	35
3.5 Evaluation of shear strength degradation.....	36
3.5.1 Evaluation approach of shear strength at each ductility level	36
3.5.2 Shear strength degradation due to different loading conditions	39
3.6 Evaluation of shear resistance mechanism degradation.....	40
3.6.1 Shear resistance mechanism degradation under one-side repeated loading ...	41
3.6.2 Shear resistance mechanism degradation under cyclic loading.....	43
3.7 Summary and conclusions	46
4. Effect of Structural Variables on Shear Resistance Mechanisms	47
4.1 Introduction.....	47
4.2 Overview of parametric analysis.....	47
4.3 Analytical result	49
4.3.1 Analytical result for different shear reinforcement ratios.....	50
4.3.2 Analytical result for different shear span to effective depth ratios	51
4.3.3 Analytical result for different tension reinforcement ratios.....	52

4.3.4 Analytical result for different axial compression loads	54
4.4 Shear strength degradation curve	55
4.5 Effect of structural variables on shear resistance mechanisms	62
4.6 Summary and conclusions	67
5. A Factor on Degradation of Arch Action	69
5.1 Introduction	69
5.2 Evaluation method of shear strength of RC member with section pre-crack	70
5.3 Effect of section pre-crack on shear strength and arch action	72
5.3.1 Pre-crack located at footing-column intersection (Case 1)	72
5.3.2 Section pre-crack 1.0d far away from footing-column intersection (Case 2)	75
5.3.3 Section pre-crack 2.0d far away from footing-column intersection (Case 3)	77
5.4 Summary and conclusions	79
6. Experimental Investigation of Effect of Section Pre-crack on Shear Strength and Mechanism of Shear Strength Degradation due to Section Pre-crack.....	80
6.1 Introduction	80
6.2 Experimental setup.....	81
6.2.1 Design of specimens	81
6.2.2 Approach for introducing section pre-crack	83
6.3 Experimental result	84
6.3.1 Load-displacement relationship and failure mode.....	84
6.3.2 Opening and closure behaviors of section pre-crack.....	87
6.4 Numerical analysis for test beams	89
6.4.1 Analytical model.....	89
6.4.2 Procedure for introducing section pre-crack	89
6.4.3 Analytical result	91
6.5 Mechanism of shear strength degradation caused by section pre-crack	96
6.5.1 Decoupling result of shear resistance mechanism.....	96

6.5.2 Primary role of section pre-crack in degradation of shear resistance mechanism	98
6.6 Summary and conclusions	102
7. Effect of Rebar Cutoff on Shear Resistance Mechanisms	104
7.1 Introduction	104
7.2 Objective experiment	105
7.3 Analytical model	108
7.4 Analytical result	108
7.5 Effect of rebar cutoff on shear resistance mechanisms	111
7.6 Summary and conclusions	119
8. Summary and Conclusions	120
8.1 Conclusions	120
8.2 Recommendations for future study	122
References	124

List of Tables

Table 2. 1 Concrete model parameters for normal spring (Yamamoto et al. 2008).	19
Table 2. 2 Concrete model parameters for shear spring (Yamamoto et al. 2008) ...	19
Table 4. 1 List of analytical cases.....	48
Table 6. 1 Material property of RC beams	82
Table 6. 2 Result of shear load	85
Table 7. 1 Details of objective RC beams	106

List of Figures

Figure 1. 1 Shear strength degradation curves	5
Figure 1. 2 Reason for shear failure after yielding	6
Figure 1. 3 Strut-and-tie model (fib code 2010).....	7
Figure 1. 4 Beam action and arch action (AIJ 1988).....	8
Figure 1. 5 Organization of the dissertation	14
Figure 2. 1 3-D RBSM	17
Figure 2. 2 Concrete constitutive models for monotonic loading analysis (Yamamoto et al. 2008)	18
Figure 2. 3 Concrete constitutive models for cyclic loading analysis (Yamamoto et al. 2008).....	19
Figure 2. 4 Reinforcement model (Yamamoto et al. 2014)	20
Figure 2. 5 Constitutive model of reinforcement and bond stress-slip model (Yamamoto et al. 2014)	20
Figure 2. 6 Stress state in cross section of a RC member.....	22
Figure 2. 7 Interpretation of shear resistance components	23
Figure 2. 8 Change of compressive stress in cross section along member axis	23
Figure 2. 9 Setup of objective experiment.....	25
Figure 2. 10 Load-displacement relationship and shear resistance mechanisms	26
Figure 2. 11 An example of concrete compressive distributions at cross sections..	27
Figure 2. 12 Longitudinal distributions of shear resistance mechanisms.....	27
Figure 2. 13 Deformations and axial compressive stress distributions	28

Figure 3. 1 Setup of objective experiment.....	32
Figure 3. 2 Analytical model	33
Figure 3. 3 Load-displacement relationship (one-side repeated loading)	34
Figure 3. 4 Deformations and axial compressive stress distribution (one-side repeated loading).....	34
Figure 3. 5 Load-displacement relationship (cyclic loading).....	35
Figure 3. 6 Deformations and axial compressive stress distribution (cyclic loading)	36
Figure 3. 7 Approach for evaluation of shear strength at each ductility level.....	37
Figure 3. 8 Evaluation of shear strength at each ductility level	39
Figure 3. 9 Degradations of shear resistance mechanisms (one-side repeated loading)	41
Figure 3. 10 Shear resistance mechanisms VS displacement ductility (one-side repeated loading)	42
Figure 3. 11 Degradations of shear resistance mechanisms (cyclic loading).....	44
Figure 3. 12 Shear resistance mechanisms VS displacement ductility (cyclic loading)	45
Figure 4. 1 Analytical models “C1, C2”	49
Figure 4. 2 Load-displacement relationship (ρ_w).....	49
Figure 4. 3 Comparison of deformations (ρ_w)	50
Figure 4. 4 Load-displacement relationship (a/d)	51
Figure 4. 5 Comparison of deformations (parameter a/d).....	52
Figure 4. 6 Load-displacement relationship (ρ_t).....	53
Figure 4. 7 Comparison of deformations (ρ_t)	53
Figure 4. 8 Load-displacement relationship (P)	54
Figure 4. 9 Comparison of deformations (P).....	55
Figure 4. 10 Evaluation of shear strength at each ductility level (ρ_w)	56

Figure 4. 11 Evaluation of shear strength at each ductility level (a/d).....	56
Figure 4. 12 Evaluation of shear strength at each ductility level (ρ_t).....	57
Figure 4. 13 Evaluation of shear strength at each ductility level (P).....	58
Figure 4. 14 Shear strength degradation curves	59
Figure 4. 15 Procedure for estimation of shear strength degradation curves by test data	60
Figure 4. 16 Comparison of shear resistance mechanisms (ρ_w)	62
Figure 4. 17 Comparison of shear resistance mechanisms (a/d)	64
Figure 4. 18 Comparison of shear resistance mechanisms (ρ_t).....	65
Figure 4. 19 Comparison of shear resistance mechanisms (P).....	66
Figure 5. 1 Different deformation behaviors between monotonic loading and cyclic loading (Mizuno et al. 2010)	70
Figure 5. 2 Method for evaluation of shear strength of RC member with section pre- crack.....	71
Figure 5. 3 Introduction of section pre-cracks (Case 1)	72
Figure 5. 4 Load-displacement relationships (Case 1)	73
Figure 5. 5 Result of shear resistance mechanisms (Case 1).....	73
Figure 5. 6 Deformations and axial compressive stress distributions (Case 1).....	74
Figure 5. 7 Load-displacement relationships (Case 2)	75
Figure 5. 8 Result of shear resistance mechanisms (Case 2).....	76
Figure 5. 9 Deformations and axial compressive stress distributions (Case 2).....	76
Figure 5. 10 Load-displacement relationships (Case 3)	77
Figure 5. 11 Result of shear resistance mechanisms (Case 3).....	78
Figure 5. 12 Deformations and axial stress distributions (Case 3).....	79
Figure 6. 1 Details of RC beams.....	82
Figure 6. 2 Details of RC beams.....	83
Figure 6. 3 Load-displacement relationships.....	85

Figure 6. 4 Comparison of test result with the result by Pimanmas et al. (2001) ...	86
Figure 6. 5 Crack patterns after shear failure	87
Figure 6. 6 Behavior of section pre-crack	88
Figure 6. 7 Analytical model and procedure for introduction of section pre-crack.	90
Figure 6. 8 Crack propagation of beam No. A	93
Figure 6. 9 Crack propagation of beam No. B	94
Figure 6. 10 Crack propagation of beam No. C	95
Figure 6. 11 Decoupling of shear resistance into average beam action and arch action	97
Figure 6. 12 Longitudinal distributions of decoupling arch action and axial stress states in central cross section at maximum load.....	99
Figure 6. 13 Result of the factors for calculation of arch action	99
Figure 6. 14 Comparison of axial compressive stress states in cross section of concrete between beam No. A and C	100
Figure 7. 1 Classification of failure types.....	105
Figure 7. 2 Drawing of RC beams.....	107
Figure 7. 3 Analytical models.....	108
Figure 7. 4 Load-displacement relationships.....	109
Figure 7. 5 Deformations and crack patterns.....	110
Figure 7. 6 Decoupling beam action and arch action	111
Figure 7. 7 Beam actions and arch actions at stage A	112
Figure 7. 8 Result of local force for the two beams at stage A.....	113
Figure 7. 9 Beam actions and arch actions at stage B	114
Figure 7. 10 Result of local force for the two beams at stage B.....	114
Figure 7. 11 Beam actions and arch actions at stage C	115
Figure 7. 12 Result of local force for the two beams at stage C.....	116
Figure 7. 13 Beam actions and arch actions at stage D	117

Figure 7. 14 Result of local force for the two beams at stage D118

1. General Introduction

1.1 Background

In the ordinary seismic design for a reinforced concrete (RC) structure, one of the basic requirements is that the brittle shear failure shall be inhibited, i.e. the shear strength shall exceed the shear demand corresponding to flexural strength (ACI318M-14 2015, CEB model code 1985, JSCE standard specification 2012, Euro code 2). In the past several decades, shear failure was always a key issue in the design for RC structures and has been studied by a great number of researches. Many achievements have been obtained for more accurate prediction of shear strength, but in the real world, it still can be found that many RC structures damaged due to shear. According to a great amount of reports for the seismic damage (Kobe Earthquake, 1995; Mid-Niigata Prefecture Earthquake, 2004), the RC structures such as bridge piers mainly present two classifications of shear failure patterns: shear failure after flexural yielding of longitudinal reinforcement (short for shear failure after yielding) and shear failure at rebar cutoff point in longitudinal reinforcement (short for shear failure due to rebar cutoff).

A RC structure, designed for flexural behavior, may suffer shear failure after yielding at plastic hinge zone under cyclic loading. By far, much care has been put on the effect of main structural variables, i.e. shear reinforcement ratio, shear span to effective depth ratio, tension reinforcement ratio and axial compression load, on the deformability of RC

member subjected to cyclic loading, by experimental and numerical methods (Park 1982, Saatcioglu 1991, Panagiotakos et al. 2001, Priestley 1981, Ishibashi et al. 2001), and the corresponding achievements have been adopted in the seismic deformation-based design. And as one achievement of significance, the direct cause for the shear failure after yielding has been widely explained as that the original shear strength would progressively degrade with the increased deformation/displacement ductility; as a consequence, the shear strength ultimately is decreased lower than the shear demand corresponding to flexural strength, leading to the reduction of load carrying capacity and the shear failure. On the basis of the tremendous test data, a design method for shear failure after yielding was established, that is, several models of shear strength degradation curve (relationship between the ratio of degraded shear strength to the original shear strength and the displacement ductility level) (ATC 6-2 1983, Ang et al. 1989, Wong et al. 1993, Priestley et al. 1994a-c, Ohe and Yoshikawa 2002), have been built. The concept of shear strength degradation curve has been employed in the current JSCE standard specification (2012). The basic mechanism of shear strength degradation due to cyclic loading, however, is still not yet fully understood, although it is significant and urgent to give a proposal to inhibit the shear failure after yielding and enhance the existing structures based on it.

A certain number of RC bridge piers with rebar cutoff in longitudinal reinforcement presented severe shear damage at rebar cutoff point, instead of at footing-column joint, under the effect of destructive earthquake or cyclic loading. For this problem, several researches (Ferguson et al. 1959, Baron 1966, Kao et al. 1975, Ozaka et al. 1986 and 1987) have studied the design method for the shear strength of RC member with rebar cutoff based on the monotonic loading experiments, where different rebar cutoff lengths, number of cutoff bar and shear reinforcement ratios were considered as parameters. Yamamoto et al. (1984) investigated the effect of rebar cutoff on the ultimate displacement ductility by loading test on the bridge piers. Kawashima et al. (1995) and Kosa et al. (2008) developed seismic evaluation methods for determining whether shear

failure would occur to the rebar cutoff point in longitudinal rebar for existing RC structures. In recent years, the seismic retrofit methods for the rebar cutoff point, such as the FRP sheet jacketing and the steel jacketing (Zhang et al. 2012), became hot topics. As a basic research, the author here hoped to find out the difference between the shear resistance mechanisms of RC structures with and without rebar cutoff, with an intention to give suggestions for the improvement of shear performance at rebar cutoff point.

Cyclic loading rather than monotonic loading is regarded as a primary cause for the shear failure after yielding and the shear failure at rebar cutoff point. According to the numerous test reports (Ohta 1979, Kinugasa et al. 1994, Mizuno et al. 2010, Choi et al. 2010), an essential behavior of RC structure under cyclic loading, which cannot be observed under monotonic loading, is noted: a certain flexural crack propagates from one side under positive loading and afterwards may be connected by another flexural crack propagating from the opposite side under negative loading, namely, a crack penetrating RC member in transverse direction (called section crack, Pimanmas et al. 2001) forms at the plastic hinge zone. Actually, the rebar cutoff point is one of the causes for easy formation of section crack. Thus, it is concerned that the section crack may be a critical factor for shear failure. To date, only few researchers studied on section crack. Pimanmas et al. (2001a, 2001b, 2001c) for first time experimentally penetrated multiple section pre-cracks into RC beams designed in shear by 4-point reversed flexural loading, and investigated the effect of initial section cracks on shear strength. As a task in this study, the author hoped to quantitatively investigate the effect of section crack at plastic hinge zone on shear strength and shear resistance mechanisms.

In recent years, benefiting from the high development of super computers, various numerical methods for simulating structural performance of RC structures were developed. Among them, the three dimensional Rigid-Body-Spring-Method (3-D RBSM), a discrete-type numerical method, has been demonstrated can excellently reproduce the bending and the shear behaviors of RC structure (Yamamoto et al. 2008). As the

advantage of 3-D RBSM over the continuum theory such as finite element analysis, this tool not only provides an insight of cracking behavior, i.e. evaluation of crack width and crack number, but also creates finer element, which makes it possible to evaluate local stress state. Moreover, as the basic shear resistance mechanisms, the concept of beam action and arch action has been proposed by considering the relationship between shear and moment ($V=dM/dx$) (Park et al. 1975). Kim et al. 2011 developed a model to evaluate the shear contribution by arch action in RC beams, but their model needs an idealization of the compressive force path for arch profile and is not available to the evaluation of arch action at each deformation for a loading test. Although the variables related to local stress state for the integrated computation of beam action and arch action are not available by experimental method, the author, however, found that they are able to be obtained from the local stress output, i.e. stress states of concrete elements and steel reinforcement elements, in cross sections of RC member, by 3-D RBSM (Iwamoto et al. 2017, Fu et al. 2016b). Therefore, it becomes possible to quantitatively evaluate the shear resistance mechanisms by using numerical method, 3-D RBSM in this study.

1.2 Literature review

1.2.1 Effect of main structural variables on shear strength

A large amount of researches have studied the effect of main structural variables, such as shear reinforcement ratio ρ_w , shear span to effective depth ratio a/d and tension reinforcement ratio ρ_t , on shear strength. Kani (1964) for first time clearly defined two main groups of failure modes, i.e. flexural failure and shear failure, and attempted to establish a rational theory for the effects of shear on the behavior of RC members. His continuing study (Kani 1966) shows that shear strength for the RC members of $a/d=1.0$ are up to 700% higher than the corresponding values for the RC members of $a/d=5.0$,

and a change of ρ_w from 0.8% to 2.8% produced a further increase in shear strength in the order of 100%. Mattock (1969), Papadakis (1996), and Collins and Kuchma (1999) carried out extensive loading test on RC beams and their result shows that the different tension reinforcement ratio has little effect on the shear strength of short beams, particularly when $a/d < 2.5$, while the large amount of tension reinforcement would enhance the shear strength of slender beams, particularly when $a/d > 4.0$. Actually, based on the above database, the design code for shear strength has been statistically established (Okamura et al. 1980, Niwa et al. 1986).

1.2.2 Shear failure after yielding under cyclic loading

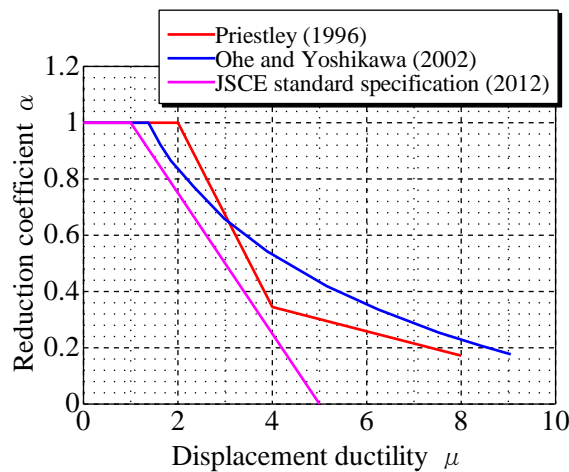


Figure 1. 1 Shear strength degradation curves

The original seismic design, such as seismic coefficient method and allowable stress method, has been found not rational for assessment of deformability of RC structures, since many structures suffered from brittle shear failure during great earthquakes. Therefore, Ohta (1979) investigated the different responses of RC bridge piers between cyclic loading and one-side repeated loading by experimental method, and pointed it out that the ultimate displacement ductility was obviously reduced by cyclic loading. The shear failure after yielding was also highlighted. For more rational prediction of deformability, ATC (1983), Nakamura et al. (1992), Ang et al. (1989), Wong et al. (1993),

Priestley et al. (1996), Ohe and Yoshikawa (2002) and JSCE standard specification (2012) have established various models for prediction of the ultimate displacement ductility by the relationships between the degradation rate of shear strength and the displacement ductility (see **Figure 1.1**). The basic consideration of these models is that the shear strength would progressively degrade with the increase of displacement ductility, and ultimately is decreased lower than the shear demand corresponding to flexural strength, which is also considered as the direct reason of shear failure after yielding (see **Figure 1.2**).

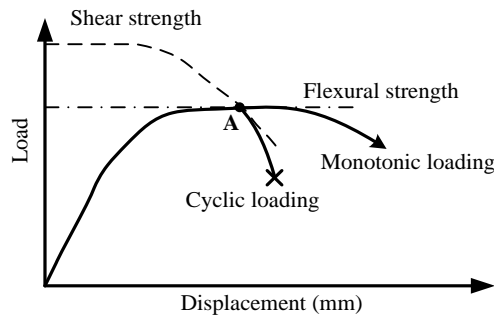


Figure 1. 2 Reason for shear failure after yielding

Thereafter, some researchers attempted to explain the mechanical characteristics of RC structures under cyclic loading. Mishima et al. (1992) simulated the shear failures after yielding of RC bridge piers by employing discrete crack model, and found that the plane of flexural crack caused by previous tension would progressively lose the ability to sustain compression force, under cyclic loading, because after entering plastic stage the longitudinal reinforcement in the plane would bear great compression force. This behavior, obviously, does not appear under one-side repeated loading. Watanabe et al. (1993) also reported the loss of shear transfer at the compression zone of concrete by cyclic loading for RC columns.

1.2.3 Introduction of shear resistance mechanisms

1.2.3.1 Strut-and-tie model

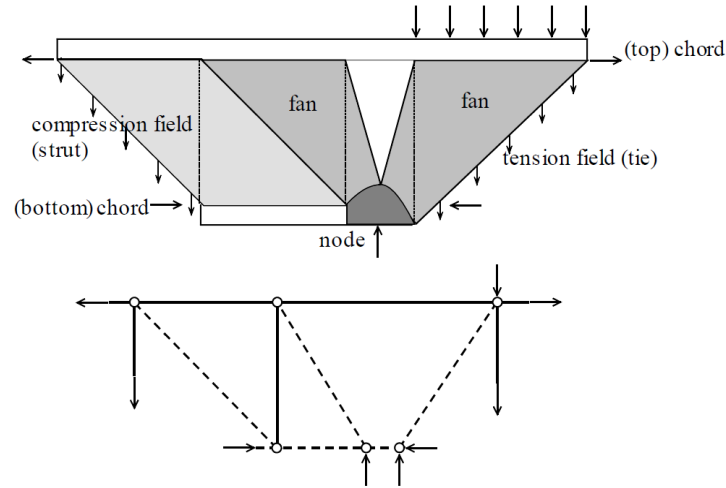


Figure 1. 3 Strut-and-tie model (fib code 2010)

Schleich et al. (1987) for first time extended the truss model for beams with uniformly inclined diagonal, all parts of structure in the form of strut-and-tie model, and defined the basic concept of B-region, where internal state of stress is easily derived from the sectional forces, and D-region, where D stands for discontinuity, disturbance or detail. The strut-and-tie model is generally to examine the ultimate limit state of structural concrete of discontinuity regions, i.e. D-regions, and has been adopted in design codes (fib code 2010). When a concentrated load is applied near the support (see **Figure 1.3**), a fan-shaped stress distribution occurs over the support and the depth of a concrete strut. The strength of steel ties shall be determined by multiplying the cross section area of reinforcement and the yield strength. In calculating the load carrying capacity of concrete struts, the effective strength of concrete is desirable to be obtained using the design compressive strength of concrete but appropriately considering the reduction effect caused by presence of crack.

The strut-and-tie model is very useful to assess the shear strength of deep beam damaged due to compression failure of concrete strut.

1.2.3.2 Beam action and arch action

Park et al. (1975) for first time proposed the principal shear resistance mechanism by combining the relationship between the external moment and the internal moment of resistance with the well-known relationship between shear and the rate of change of bending moment along a beam. And the shear resistance mechanism is decoupled into two terms: beam action and arch action. For a long time, the concept of beam action and arch action is only for a better understanding of basic shear theory when a RC member plastically deforms under shear loading, and it is hard to clarify the contributions of beam action and arch action in the development of shear resistance because the necessary local stress state for calculation is not available in ordinary experiment.

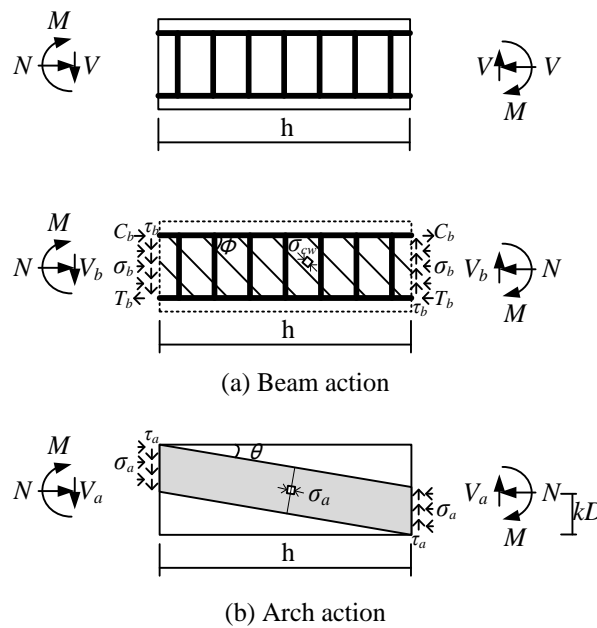


Figure 1. 4 Beam action and arch action (AIJ 1988)

The concept of beam action and arch action has been applied in the shear design proposed by Architectural Institute of Japan (1988) and has a great advantage for explicitly distinguishing the shear contributions provided by concrete and steel reinforcement (see **Figure 1.4**).

Kim et al. (2011) for first time attempted to decouple shear resistance into arch action, truss action and membrane action. Their result makes it clear that the arch action is the concrete contribution provided by the fan-shaped compressive stress distributing at the uncracked compression zone of RC member after diagonal shear cracking; the beam action is the combination effect of truss action, carried by shear reinforcement, and concrete contribution. Hereby, the concrete contribution, as one part of beam action, consists of the aggregate interlocking effect and the doweling effect. Their work in a degree improved the previous truss model which does not directly account for the concrete shear resistance components, but the decoupling procedure, which is on the basis of deformation condition and idealizes the force path of compression chord, is still not applicable to analyze the shear resistance mechanisms at each deformation of a RC structure under complicated loading conditions.

1.2.3.3 Truss action and concrete contribution

Truss action is a most typical consideration for the shear contribution carried by shear reinforcement, assuming a parallel chord truss with the strut angle of 45° (ACI 318M-14, JSCE standard specification 2012). Some other approach suggested to use a parallel chord truss with a variable angle of inclination of diagonal struts (Eurocode 2 2004). But since above truss models, which are standard, have no explicit concrete contribution, i.e. aggregate interlocking and dowel effect, which may cause a lower inclination of the concrete struts and more engagement of shear reinforcement, the modified truss model has been proposed for considering the variable-angle truss.

In truss theory, concrete contribution is regarded as the shear strength of RC member without arrangement of shear reinforcement consisting of aggregate interlocking effect and doweling effect, and has been estimated by a large number of loading experiments by considering the effect of a variety of concrete strengths, effective depths and shear span to effective depth ratios (Okamura et al. 1980, Niwa et al. 1986, Ang et al. 1989, Wong et

al. 1993, Priestley et al. 1994). Moreover, it has been repeatedly proved that the concrete contribution in truss theory agrees well with the experiment diagonal shear cracking load.

1.2.4 Effect of section crack on shear strength of RC structure

Up to present, nearly no research clearly define the section crack which is considered generally generated at plastic hinge zone of RC member under cyclic loading, that is, a certain flexural crack propagates from one side under positive loading and afterwards may be connected by another flexural crack propagating from the opposite side under negative loading. A lot of experimental researches, however, have confirmed the appearance of section crack (Ohta 1979, Kinugasa et al. 1994, Mizuno et al. 2010, Choi et al. 2010), although they have not defined it. Pimanmas and Maekawa (2001a) for first time experimentally penetrated multiple section pre-cracks into RC short beams designed failing by shear by 4-point reversed flexural loading. Thereafter, by 3-point loading, they found that the section pre-cracks enhanced the shear strength compared with that of the non-cracked beam, because the pre-cracks obstructed the continuous propagation of diagonal shear cracks, which was further demonstrated in their finite element analyses (Pimanmas and Maekawa 2001b, 2001c). As the characteristics, the section pre-cracks by 4-point reversed loading dispersedly located at the entire shear span, however, the section cracks due to cyclic loading generally initiate and propagate only at the zone where high moment affects. Thus, it is desirable to find out an experimental method to introduce a section crack at plastic hinge zone of shear span and investigate its damage to shear performance.

1.2.5 Effect of rebar cutoff on shear strength of RC structure

Rebar cutoff in main reinforcement has been regarded as a critical factor for reducing shear strength of RC member. Ferguson et al. (1959) for first time studied the relationship between the reduced shear strength, due to rebar cutoff, and the ordinary shear strength

by considering the parameters: length of cutoff bar and amount of cutoff bar. But his proposal assessment equation has a large scattering because of a lack of important parameters. Baron et al. (1966) pointed it out that the shear stress state at rebar cutoff point significantly increases because neutral axis changes. Kao et al. (1975) proposed an equation to estimate shear strength at rebar cutoff point by assuming that longitudinal reinforcement and shear reinforcement have been yielded. Thereby, the shear strength before yielding of reinforcement cannot be known. Ozaka et al. (1986 and 1987) conducted monotonic loading experiment for the RC beams with rebar cutoff by considering different structural variables to establish an assessment equation for shear strength, and summarized four classifications of shear failure types due to rebar cutoff. Yamamoto et al. (1984) clarified that the deformability of RC member with rebar cutoff was lower than that of the ordinary RC member. Then, Kawashima et al. (1995) developed a seismic evaluation method to determine whether shear failure would occur at rebar cutoff point for existing structures by means of the failure mode factor and the safety factor. Zhang et al. (2012) studied the retrofitting effect of FRP jacketing on the shear performance of rebar cutoff in RC bridge piers under cyclic loading, and their result shows that the sufficient height of FRP jacketing is significant for a sufficient retrofitting.

1.3 Study objective and research significance

Shear failure is always a hot topic in the design for RC structures and should be inhibited, since it is a brittle failure mode. According to numerous seismic damage reports, many RC structures, meeting shear design requirement, eventually were devastatingly shear damaged. And it has been summarized that the observed shear failures commonly appeared to be two modes: shear failure after yielding and shear failure at rebar cutoff point, both ordinarily triggered by cyclic loading or seismic effect. As the most important

deformation behavior caused by cyclic loading, section crack at plastic hinge zone, hard being observed under monotonic loading, is regarded as an essential factor for shear failure.

Since shear strength degradation under cyclic loading is the direct cause for shear failure after yielding, therefore, one target in this study is to quantitatively assess the shear strength degradation with increased displacement ductility, and to understand the mechanism of shear strength degradation by decoupling development of shear resistance into beam action and arch action, employing 3-D RBSM. Moreover, the second objective is to clarify the primary role of section crack in shear performance by experimental method and 3-D RBSM analysis. In addition, the third objective is to simulate the reduction effect of rebar cutoff on development of shear performance and consequently explain the reduction effect based on beam action and arch action.

This study contributes to a more comprehensive understanding of the mechanism of shear failure after yielding, i.e. mechanism of shear strength degradation, by the degradation processes of beam action and arch action, and the progressive degradation of arch action due to cyclic loading is clarified, which is very helpful to establish new method for improvement of shear performance. This study also provides a practical experiment method for introducing section crack in RC structure, which can be widely used for investigating the effect of pre-crack, and clarifies the effect of section crack on shear resistance mechanism. Additionally, the governing shear resistance mechanism for worse shear performance of RC beam with rebar cutoff is explained in this study and a basic knowledge for shear behavior in rebar cutoff zone is provided.

1.4 Organization of dissertation contents

The flow chart of this study is given in **Figure 1.5**. The dissertation overall consists of

three parts. The first part is on purpose to clarify the mechanism of shear failure after yielding of RC columns subjected to cyclic loading (chapters 3, 4 and 5). The second part investigates the effect of rebar cutoff in longitudinal reinforcement on shear resistance mechanism, i.e. the reason for low shear strength in RC beam with rebar cutoff was explained (chapter 6). And the third part clarifies the effect of section crack on shear performance of RC beam by experiment and numerical analysis. The contents of this dissertation are briefly described as follows.

Chapter 1 is the introduction of this study, including the research background, a review of previous key literatures, the research objectives and the organization of contents.

Chapter 2 discusses the basic methods applied in this study. Firstly, the numerical tool, 3-D RBSM, is introduced including concrete model and reinforcement model. Secondly, the method how to decouple shear resistance obtained from 3-D RBSM into beam action, arch action, truss action and concrete contribution is discussed.

In chapter 3, the mechanism of shear failure after yielding of a representative RC column is explained. The shear failure behavior of the RC column under cyclic loading is first simulated by 3-D RBSM analysis. Then, the shear strength degradation with increased displacement ductility was quantitatively evaluated by applying a numerical approach. Lastly, the mechanism of shear strength degradation is explained by the degradation characteristics of beam action and arch action.

In chapter 4, on the basis of the RC column discussed in chapter 3, as a parametric study, the effect of main structural variables, i.e. shear reinforcement ratio, shear span to effective depth ratio, tension reinforcement ratio and axial compression load, on mechanism of shear failure after yielding is investigated. The shear strength degradation curves for each parameter are drawn and compared with those summarized according to experimental database. Moreover, the effect of structural variables on degradation of shear resistance mechanism is presented.

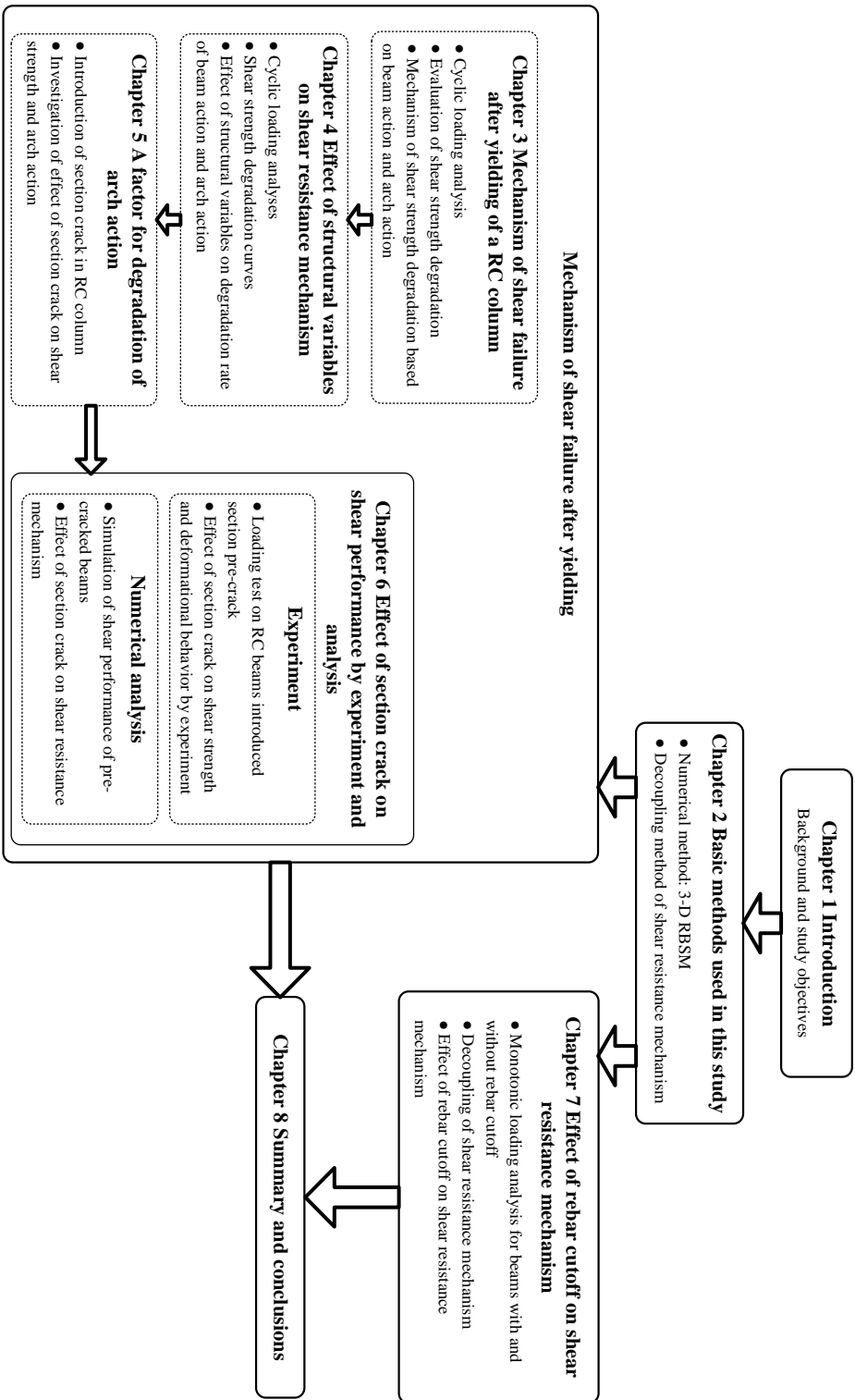


Figure 1. 5 Organization of the dissertation

In chapter 5, as a typical deformation behavior caused by cyclic loading and a possible factor for degradation of arch action, the section crack is numerically introduced into the three critical cross sections in the RC column studied in chapter 3, and its effect on shear strength and arch action is confirmed.

In chapter 6, a method is attempted to introduce section pre-crack into RC beam, and afterwards the effect of section crack on shear strength is investigated by loading test. As second part, the shear behavior of pre-cracked beam is simulated by 3-D RBSM and the effect of section crack on shear resistance mechanism is revealed.

In chapter 7, the different shear performances of RC beams with and without rebar cutoff under monotonic loading are simulated. In addition, the effect of rebar cutoff on shear resistance mechanism is clarified aiming to understand the reason of lower strength for beam with rebar cutoff.

In chapter 8, the conclusions included in this study are summarized and the recommendations for future study is pointed out.

2. Basic Methodology of Analysis

2.1 Introduction

In this chapter, firstly the three dimensional Rigid-Body-Spring-Method (3-D RBSM for short), which is the basic numerical method and tool to simulate mechanical behaviors of RC structures in this research, is explained. Secondly, as the most important method to analyze shear failure mechanism, the decoupling approach of shear resistance mechanism into beam action and arch action is discussed.

2.2 Numerical method

In this section, first of all, the basic concepts of 3-D RBSM, which is for model of concrete, is introduced. After that, the constitutive models of concrete for normal spring (tensile and compression behaviors) and shear spring (shear behavior) are reviewed. At last, the method for model of steel reinforcement is explained, together with its material properties.

2.2.1 3-D RBSM

3-D RBSM has been developed in order to quantitatively evaluate the mechanical responses including softening and localization fractures (Yamamoto et al. 2008), and has been shown that the model can well simulate the cracking and failure behaviors of RC

members (Gedik et al. 2011 and Yamamoto et al. 2014). In 3-D RBSM, concrete is modeled as an assemblage of rigid polyhedrons interconnected by springs at their boundary surfaces (see **Figure 2.1**). The crack development is affected by mesh design as cracks initiate and propagate through interface boundaries of polyhedrons. The random geometry of rigid polyhedrons is generated by Voronoi tessellation, which can reduce mesh bias on the initiation and propagation of potential cracks.

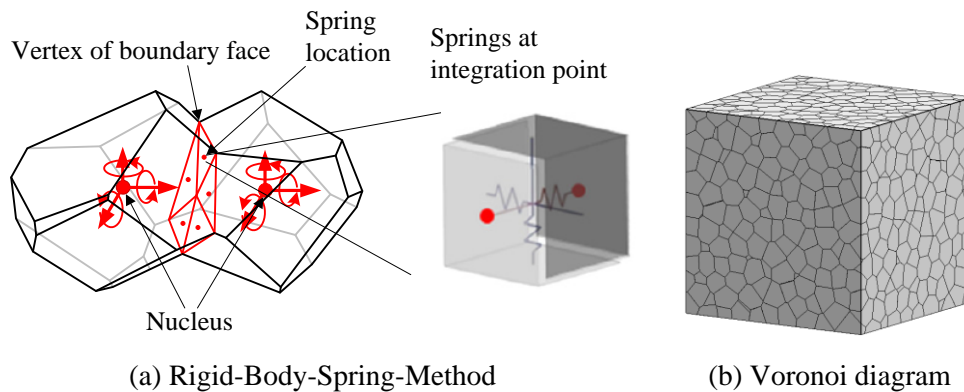


Figure 2. 1 3-D RBSM

The response of the spring model, which has one normal and two tangential springs, provides an insight into the interaction among the polyhedrons, which is different from the models based on continuum mechanics.

2.2.2 Concrete material model

The constitutive models for tension, compression of normal springs and for shear springs used in 3-D RBSM for monotonic loading analysis are constructed by uniaxial relationships between stress and strain, as shown in **Figure 2.2**. The details of the models and the relevant model parameters (see **Table 2.1** and **Table 2.2**) have been described and verified in the research conducted by Yamamoto et al. (2008), that is, the mechanical behaviors of normal strength concrete such as uniaxial tension and compression, tri-axial compression and confinement effect by stirrups could be accurately simulated. Hereby, it

should be mentioned that the tensile strength f_t^* and fracture energy g_f were determined based on the estimation equations dependent on compressive strength of concrete f_c^* , employed in the current design codes (JSCE standard specification 2012), if the corresponding test results were unknown in the original literature.

On the basis of the models for monotonic loading analysis, the models for cyclic loading analysis, which regards the previously introduced stress-strain relationships for monotonic loading as the envelop curve, were developed (Yamamoto et al. 2014).

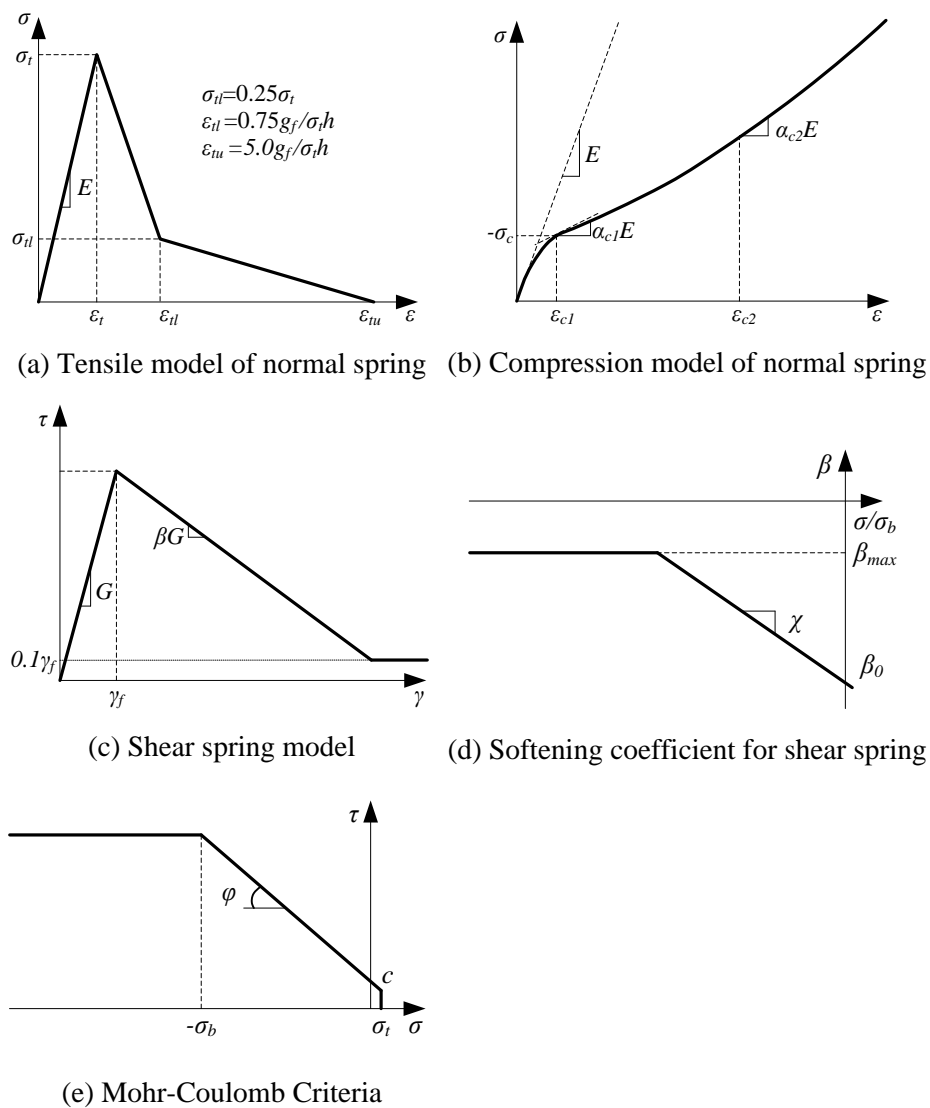


Figure 2. 2 Concrete constitutive models for monotonic loading analysis

(Yamamoto et al. 2008)

Table 2. 1 Concrete model parameters for normal spring (Yamamoto et al. 2008)

Normal spring						
Young modulus	Tensile response		Compressive response			
E (N/mm ²)	σ_t (N/mm ²)	g_f (N/mm ²)	σ_c (N/mm ²)	ε_{c2}	α_{c1}	α_{c2}
$1.4E^*$	$0.80f_t^*$	$0.5G_f^*$	$1.5f_c'^*$	-0.015	0.15	0.25

"*" indicates experimental measurements. E^* : Young Modulus
 f_t^* : Tensile strength, G_f^* : Fracture energy, $f_c'^*$: Compressive strength

Table 2. 2 Concrete model parameters for shear spring (Yamamoto et al. 2008)

Shear spring							
Young modulus $\eta = G/E$	fracture criterion			Softening behavior			
	c (N/mm ²)	φ (degree)	σ_b (N/mm ²)	β_0	β_{max}	χ	κ
0.35	$0.14f_c'^*$	37	$f_c'^*$	-0.05	-0.025	-0.01	-0.3

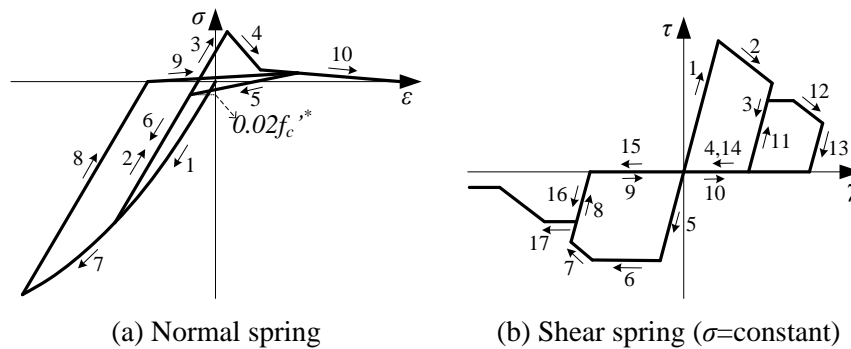


Figure 2. 3 Concrete constitutive models for cyclic loading analysis (Yamamoto et al. 2008)

Figure 2.3a shows the typical hysteresis loop of the normal spring for cyclic loading. The unloading paths in the tension zone pass towards the point of stress $\sigma = -0.02f_c'^*$ ($f_c'^*$ is the nominal concrete compressive strength) on the compression loading path. The reloading paths in the tension zone pass towards the start point of the unloading process.

Figure 2.3b shows the typical hysteresis loop of the shear spring. The initial elastic modulus G is used as the spring stiffness of the unloading and reloading processes. For unloading process, after the stress decreases to zero, it would keep zero until the strain

reaches the residual strain of the opposite sign.

2.2.3 Reinforcement and bond models

Steel reinforcement is modeled as a series of regular beam elements (**Figure 2.4**) that can simulate the bending effects. In this model, the reinforcement can be freely arranged within the member, regardless of the mesh design of concrete (Bolander and Hong 2002). At each beam node, two translational and one rotational degrees of freedom are defined by means of the springs. The reinforcement is attached to the concrete particles by zero-size link elements, which provides a load-transfer mechanism between a concrete particle and a beam node.

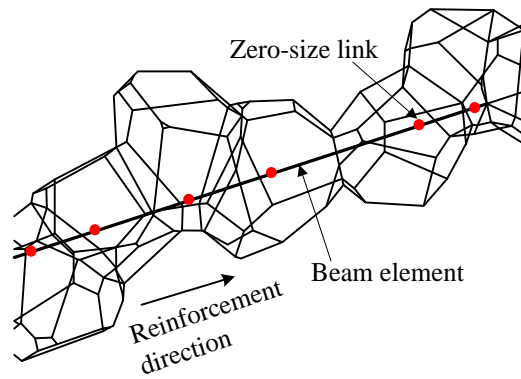


Figure 2. 4 Reinforcement model (Yamamoto et al. 2014)

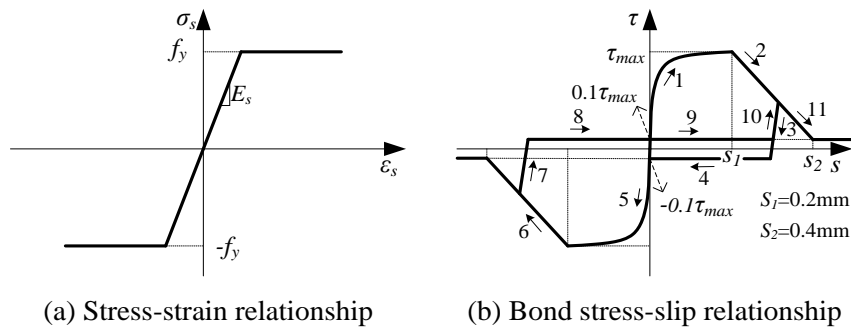


Figure 2. 5 Constitutive model of reinforcement and bond stress-slip model

(Yamamoto et al. 2014)

A bi-linear model is assumed for the stress-stain relationship of reinforcement (**Figure 2.5a**) (Yamamoto et al. 2014). Crack development is strongly affected by the bond interaction between concrete and reinforcement of linked element. **Figure 2.5b** shows the bond stress-slip relationship. Up to the shear strength τ_{max} , the relation proposed by Suga et al. (2001) is applied and the relation proposed by CEB-FIB (1990) is used for the post peak behavior. As the typical hysteresis loop, the initial secant stiffness corresponding to the $\pm 0.1\tau_{max}$ stress points is assumed as the stiffness of reloading and unloading. After the stress reaches the level of $\pm 0.1\tau_{max}$ on the unloading paths, the stress keeps this level until the slip reaches the residual slip of the opposite sign.

2.3 Decoupling approach of shear resistance mechanism

In chapter 1.2.3, the concepts of a number of shear resistance mechanisms such as beam action and arch action have been introduced, and in this section, the approach decoupling shear resistance into contributions provided by beam action and arch action based on local stress output from 3-D RBSM is explained.

2.3.1 Decoupling approach of beam action and arch action

It is acknowledged that the mechanical equilibrium of a cross section in RC beam is ordinarily expressed by Equation 2.1 (see **Figure 2.6**).

$$M = (T + C_s) \cdot \frac{j_s}{2} + C_c \cdot j_{C_c} + T_c \cdot j_{T_c} \quad 2.1$$

where, M is the bending moment acting on a cross section of RC beam, T and C_s are the tensile and compressive resistances sustained by longitudinal reinforcement; C_c is the compressive resultant in concrete; T_c is the tensile resultant in concrete; j_s is the arm length between the centroids of tensile and compressive longitudinal reinforcements; j_{C_c} is the arm length between the centroid of compressive resultant in concrete and the beam axis; j_{T_c} is the arm length between the centroid of tensile resultant in concrete and the beam

axis.

Based on the previous work (Park et al. 1975, Fu et al. 2016b, Iwamoto et al. 2017), by differentiating Equation 2.1 in a small segment dx between two adjacent cross sections of RC member (see **Figure 2.7a**), an equation for calculation of shear resistance can be derived, i.e. Equation 2.2, and it can be divided into the two components of beam action V_b and arch action V_a expressed by Equation 2.3 and Equation 2.4.

$$V = \frac{dM}{dx} = V_b + V_a \quad 2.2$$

$$V_b = \left(\frac{dT}{dx} + \frac{dC_s}{dx} \right) \cdot \frac{j_s}{2} + \frac{dC_c}{dx} \cdot j_{Cc} + \frac{dT_c}{dx} \cdot j_{Tc} \quad 2.3$$

$$V_a = C_c \cdot \frac{dj_{Cc}}{dx} + T_c \cdot \frac{dj_{Tc}}{dx} \quad 2.4$$

where, according to the definitions given by Park et al. 1975, V is the combined shear resistance; the shear resistance; V_b is defined as beam action, which is attributed to the change rates of tensile resistance dT and compressive resistance dC_s along longitudinal reinforcement, and the change rates of compressive and tensile resultants in concrete dC_c , dT_c between two adjacent cross sections (see **Figure 2.7b**); the shear resistance V_a is defined as arch action, which is resulted from the change rate of centroids of compressive and tensile resultants in concrete dj_{Cc} , dj_{Tc} along beam axis (see **Figure 2.7c**).

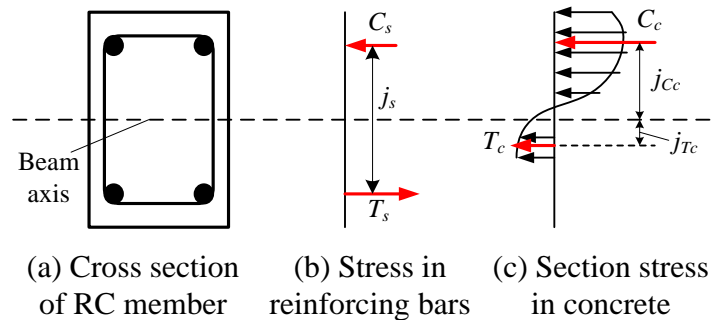


Figure 2. 6 Stress state in cross section of a RC member

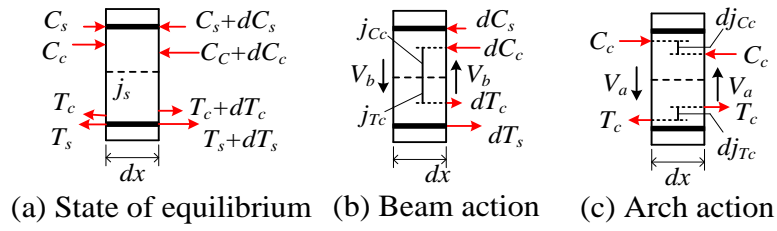


Figure 2. 7 Interpretation of shear resistance components

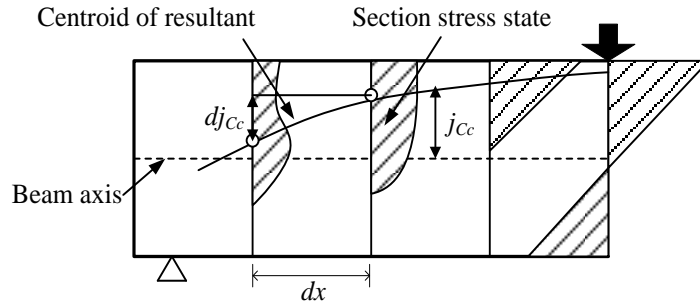


Figure 2. 8 Change of compressive stress in cross section along member axis

For example, the section stress states in concrete along beam axis are conceptually shown in **Figure 2.8**. It was clear that if the stress states and the centroids of compression resultants in two adjacent cross sections spacing dx are determined, the arch action provided by the second item ($C_c \cdot dj_{cc}/dx$) in Equation 2.4 in the segment dx can be computed. By the same way, the variables required for determination of beam action in any segment (dx) are able to be obtained from the local stress states in concrete and reinforcement elements from 3-D RBSM, although they are not available by experimental measurement. The reliability of 3-D RBSM for computation of local behavior in RC member has been demonstrated by experimental method. In the work by Iwamoto et al. (2017), four RC beams (with two different a/d ratios of 1.57 and 3.14) were 3-point loading tested. Moreover, the local strains distributed in cross sections of member and the local strain in stirrups were measured by strain gages. Consequently, it was verified that the development of the local strains in cross sections and stirrups from start of loading to failure point was accurately computed by 3-D RBSM analysis.

In the following chapters, the average beam action and arch action, at each displacement of loading analysis, of all units (dx) located in target shear span would be computed and applied to evaluation.

2.3.2 Decoupling approach of truss action and concrete contribution

Furthermore, based on the traditional truss theory, as one part of beam action, the shear resistance provided by truss action V_s due to shear reinforcement can be evaluated by Equation 2.5.

$$V_s = A_w \cdot \sigma_w \cdot \sin \alpha \cdot (\cot \theta + \cos \alpha) \cdot jd / s \quad 2.5$$

where, A_w is the cross section area of shear reinforcement placed in spacing s ; σ_w is the stress stage in shear reinforcement; jd is the moment arm length ($j=1/1.15$, d is the effective depth); s is the spacing of shear reinforcement; θ is the orientation of shear crack to member's axis; α is the orientation of shear reinforcement arrangement to member's axis.

The orientations of shear reinforcements of RC specimens mentioned in this study are confirmed as 90° . And according to the JSCE standard specification (2012), the orientation of shear crack is assumed as 45° , with an intention to conveniently compare the numerical result with the design value, so that the Equation 2.5 can be simplified as the Equation 2.6.

$$V_s = A_w \cdot \sigma_w \cdot jd / s \quad 2.6$$

Therefore, based on the Equation 2.6, the truss action for each set of shear reinforcement arranged in shear span can be calculated by using maximum stress in beam elements. Similar to the evaluation for beam action and arch action, the average truss action of all shear reinforcements are applied for evaluation. In addition, at each displacement, by subtracting the average truss action from the average beam action, the average concrete contribution V_c for beam action can be determined.

2.4 Example of decoupling result for shear resistance mechanism

With an intention to comprehensively understand the decoupling approach of shear resistance mechanisms, in this section, an example of decoupling result is described.

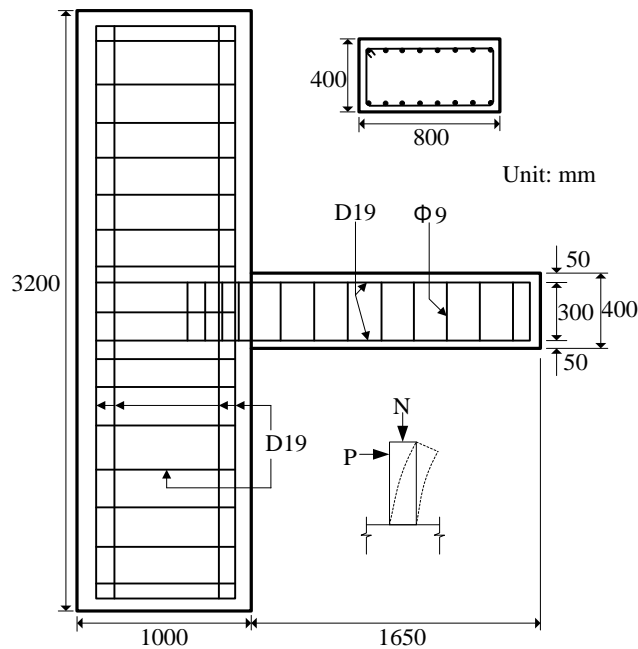


Figure 2. 9 Setup of objective experiment

The objective specimen for decoupling is a RC column (Ohta 1979), designed for bridge pier (see **Figure 2.9**), the details of which will be introduced in chapter 3.2. This column was flexure-designed and the yield strength of longitudinal reinforcement was 365.5 MPa. Hereby, in order to transfer the failure mode to shear, a monotonic loading analysis, by using increased yield strength of longitudinal reinforcement (900 MPa), was conducted. The analytical load-displacement relationship is shown in **Figure 2.10**.

A representative local stress output, i.e. the concrete stress distributions in cross sections at the maximum load, is given in **Figure 2.11**, for understanding how to integrate arch action. Obviously, the centroid of compression resultant in concrete (j_c) gradually changed along column axis because of the changed shape of stress distribution, and the relevant variables for the calculation of arch action for each elementary unit (dx) such as

the compression resultant in concrete (C_c) and its centroid (j_{Cc}) were able to be determined by integrating elementary stresses in cross section. In a similar way, the beam action was able to be determined for each elementary unit (dx) by integrating local stress in beam elements for steel reinforcement. With regard how to determine the width of unit dx , it has been confirmed that the estimation accuracy of shear force by the combination effect of average beam action and arch action is sufficiently high in the case that dx is no more than 100 mm (if dx exceeds 100 mm, the accuracy rapidly decreases), and smaller dx contributes to higher accuracy. Hereby, taking the average size of concrete element, 30 mm, into account, the width of dx was determined to be 50 mm.

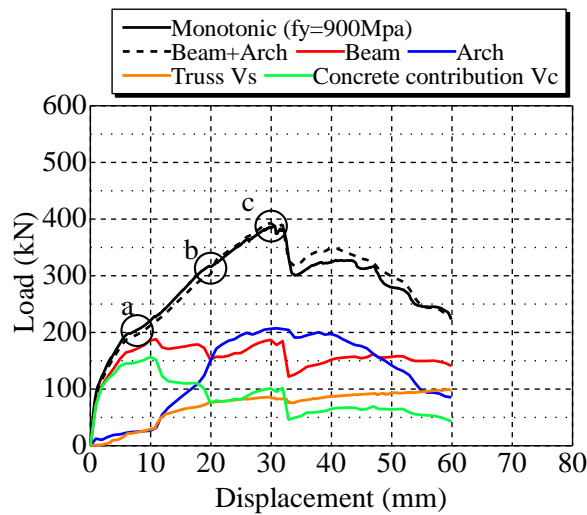


Figure 2. 10 Load-displacement relationship and shear resistance mechanisms

Consequently, the capacity curves of average shear resistance mechanisms for load-displacement relationship by 3-D RBSM were obtained, as shown in **Figure 2.10**, and the longitudinal distributions of shear resistance mechanisms in shear span along column axis at the three critical points a-c are shown in **Figures 2.12a-c**. Additionally, the dotted lines represent the shear force computed by the average of the summation of the beam actions and arch actions for each unit dx . It was first noted that the capacity curve of the combined effect of beam action and arch action calculated by local stress output agreed well with

the analytical load-displacement relationship as macro behavior (see **Figure 2.10**), which proved the applicability of the decoupling approach.

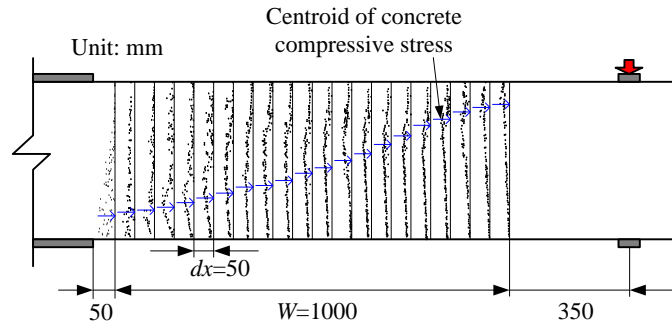


Figure 2. 11 An example of concrete compressive distributions at cross sections

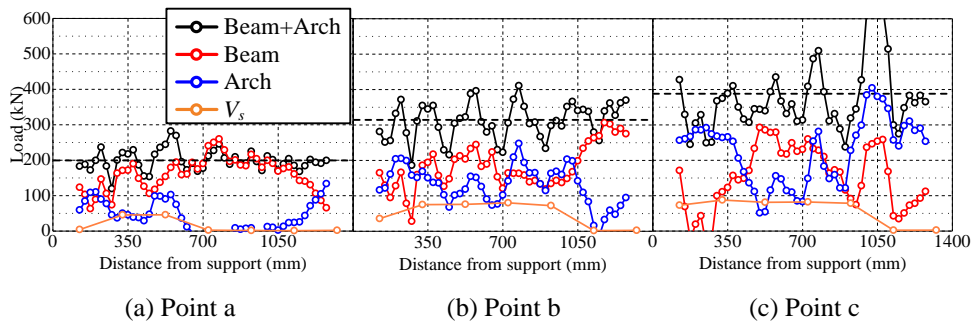


Figure 2. 12 Longitudinal distributions of shear resistance mechanisms

With regard to the development process, before the critical shear cracking, the beam action initially developed and increased consistently, whereas the arch action only had neglectable effect in the meantime (see **Figure 2.10**). This trend could be verified by the distributions of shear resistance mechanisms at point a shown in **Figure 2.12a** that shear resistance was entirely provided by beam action, although the truss action had little effect. At point a, the bending deformation was dominant, that is, the flexural cracks generated at the footing-column joint and the axial compressive stress was highly localized at the compression zone of column (see **Figure 2.13a**).

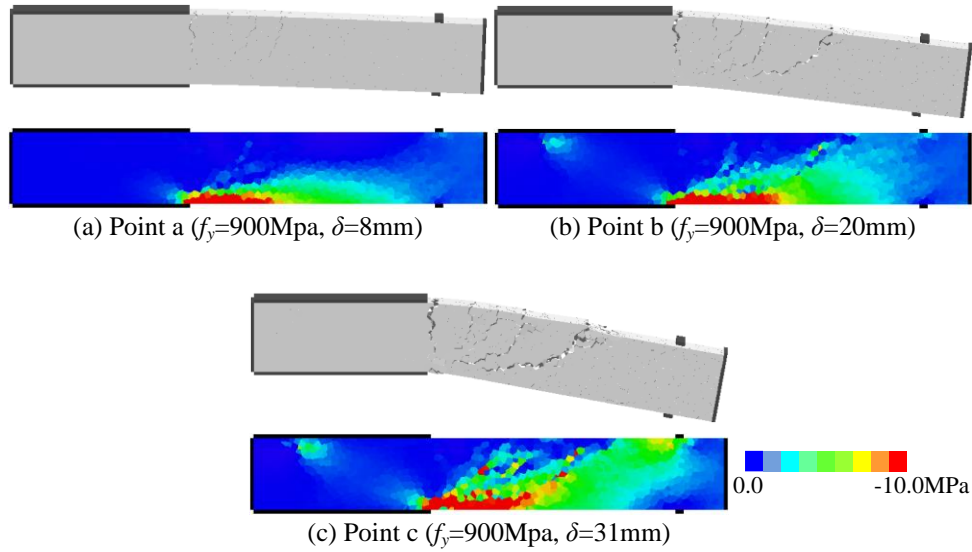


Figure 2. 13 Deformations and axial compressive stress distributions

Then after the critical shear cracking, the arch action formed and further improved the shear resistance while the beam action stopped growth (see **Figure 2.10**). This can be known from the distributions at point b illustrated in **Figure 2.12b**, where the arch action overall increased a lot to a same grade as the beam action. Because of the dramatic development of shear deformation, the truss action was increased and played an important role (see **Figure 2.10**). At point b, the preceding localization of axial compressive stress extended to the loading plate along the critical shear crack and presented a fan-shape (see **Figure 2.13b**).

Ultimately, the occurrence of shear strength (see point c in **Figure 10**) was found to be governed by the development of arch action, which was reflected by the highest grade of arch stress flow at the maximum load accompanied with a great shear deformation (see **Figure 2.13c**). Since the shear reinforcement was yielded nearby the point b, the truss action did not obviously rise at the point c (see **Figure 2.12b** and **Figure 2.12c**).

In addition, by subtracting the truss action from the beam action at each displacement, the average concrete contribution V_c was also obtained (**Figure 2.10**). It was known that the consistent growth of beam action before critical shear cracking was provided by the

increased concrete contribution, whereas the truss action (V_s) had minor effect. After critical shear cracking, the concrete contribution was gradually decreased while the truss action rose from a low grade which prevented the decline of beam action.

Based on the above decoupling results for a representative monotonic loading analysis, it was verified that the analytical load-displacement hysteresis can be decoupled into the capacity curves of shear resistance mechanisms, namely the beam action, arch action, truss action and concrete contribution corresponding to the shear strength can be determined. By investigating the change of each action, the shear resistance mechanism can be clearly discussed. This methodology provides us a way to accurately assess the critical factor for shear failure.

2.5 Summary

In this chapter, firstly, the basic numerical tool for analyze the structural behavior of reinforced concrete, i.e. 3-D RBSM, is introduced. Secondly, the basic theory of shear resistance mechanism for RC member, i.e. beam action and arch action, and the numerical approach for decoupling shear load into the shear components of beam action and arch action, by using the numerical local stress output, is explained. Moreover, as an example, the decoupling of the shear load for a RC column into each shear component is performed, in order to comprehensively understand the development progresses of beam action and arch action. The analysis of the developments of beam action and arch action is a standard approach for evaluation of the shear performance of RC member in the following content in this study.

3. Mechanism of Shear Failure after Yielding due to Cyclic Loading

3.1 Introduction

In preceding chapter 1.2.2, the realistic problem of shear failure after yielding under cyclic loading or great earthquake effect has been explained. It is a relatively brittle failure mode, which can reduce the deformability of RC member designed failing by flexure.

The reason of shear failure after yielding of a RC member has been conceptually explained as that the shear strength progressively degrades with the increase of displacement level and ultimately becomes lower than the shear demand corresponding to flexural strength, which leads to the decrease of load carrying capacity. The mechanism of the progressive degradation of shear strength due to cyclic loading, however, is not yet fully understood. Therefore, it is of great significance and very urgent to explain the shear failure mechanism in order to improve the seismic performance of RC members.

On the purpose of investigating the mechanism of shear strength degradation of RC member subjected to cyclic loading, in this study, the author first reviewed the previous work carried out by Nakamura et al. (2014), in which, the shear failure after yielding of a RC column was simulated by 3-D RBSM and the corresponding shear strength degradation was quantitatively evaluated. Afterwards, based on the decoupling approach of shear resistance mechanism introduced in chapter 2.3, the degraded shear strengths

after each load cycle were decoupled into the contributions of beam action and arch action, based on the local stress results from 3-D RBSM. Finally, the mechanism of shear strength degradation of the RC column was discussed by means of the degradation characteristics of beam action and arch action.

3.2 Objective experiment

The cyclic and one-side repeated loading analyses (3-D RBSM) of the RC column designed as bridge pier tested by Ohta (1979) were conducted and it has been confirmed that the analyses can accurately simulate the deformation behaviors until failure. The details of the objective RC column are shown in **Figure 3.1**. The footing and the column are 1000 mm and 1650 mm in height, respectively. And the column has a cross section of 800 mm×400 mm with an effective depth of 350 mm. The loading plate is 1400 mm high from the column base, i.e., the shear span-to-depth ratio equals to 4.0. Sixteen longitudinal reinforcing bars of D19 type were arranged with a concrete cover thickness of 50 mm (the tension reinforcement ratio is 0.82%). The stirrups of D9 type were arranged with a space of 200 mm in shear span (the shear reinforcement ratio is 0.08%). The yield strengths of longitudinal reinforcing bars and stirrups are 365.5 MPa and 372.2 MPa, respectively, and the compressive strength of concrete is 28.6 MPa. The shear load (P) was applied by displacement control and the peak displacement in each load cycle of cyclic and one-side repeated loadings were increased stepwise with an increment of yield displacement ($\pm\delta_y, \pm2\delta_y, \pm3\delta_y, \dots$) which is around 10mm. And ten cycles of loading were repeatedly imposed for each displacement level. In addition, during the shear loading, a 1.0 MPa axial compression load (N) was applied to the top of column. The load was selected to simulate the axial compression load on bridge pier, which are relatively low compared to the axial compression loads on building columns.

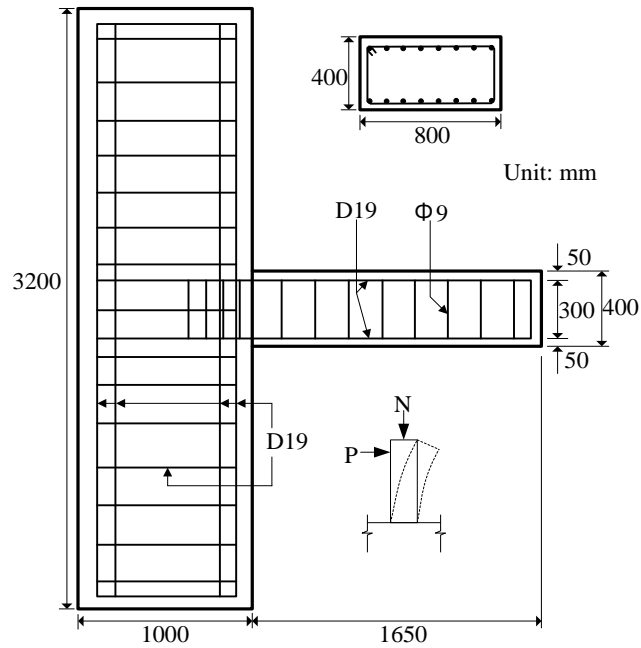


Figure 3. 1 Setup of objective experiment

As a result of the tests, under cyclic loading, the load carrying capacity of the column decreased at the displacement level of $-4\delta_y$ when the shear failure after yielding occurred; under one-side repeated loading, however, the load carrying capacity could be maintained until the displacement level of $+8\delta_y$.

3.3 Analytical model

In order to reduce computing time, the one-quarter 3-D RBSM model (cross section: 200 mm×400 mm) of the RC column was constructed as shown in **Figure 3.2**, and the average element size of concrete rigid particles used is 30 mm as recommended by Yamamoto et al. (2008). The reinforcing bars were modeled by beam and zero-link elements discretely and the six loading plates were modeled by prism rigid-body elements. The material properties of concrete and reinforcing bars were adopted according to the standards given by Yamamoto et al. (2008). The footing area was fixed by three plates and the axial compression load was applied to the plate on the top of the column. By

controlling displacement, cyclic and one-side repeated loadings were imposed on the shear loading plates. Furthermore, it has been confirmed that the load carrying capacity of the objective column dropped due to the increase of displacement ductility rather than the increase of the number of load cycles, thus, in this study, only one load cycle was simulated for each displacement level.

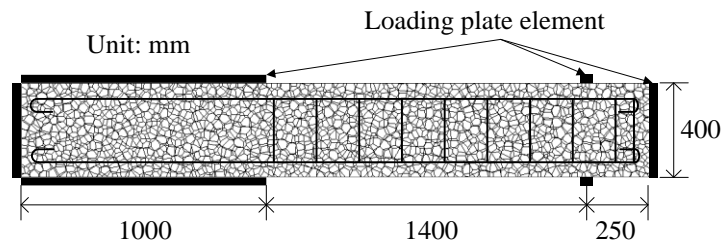


Figure 3. 2 Analytical model

3.4 Analytical result

3.4.1 One-side repeated loading

Figure 3.3 compares the load-displacement relationships by one-side repeated loading test and 3-D RBSM analysis. Since the one-quarter model was used, the analytical load in this study was magnified four times the original output. Consequently, both the analytical and experimental load-displacement curves showed the same trend that the RC column could maintain the original load carrying capacity with the increase of displacement level.

The analytical deformations (magnified by eight times in this study) corresponding to each displacement level and the axial compressive stress distributions in the column central section (at the deformation of $+4\delta_y$) of one-side repeated loading analysis are illustrated in **Figure 3.4**. It could be observed that flexural cracks first initiated near the footing-column joint at small displacement of $+1\delta_y$ (see **Figure 3.4a**). Then, the flexural cracks propagated toward the compression side and the crack widths became larger, with

the increased displacement level (see **Figure 3.4b**; **Figure 3.4c**; **Figure 3.4d**). At the deformation of $+4\delta_y$, the compressive stress localization due to bending was confirmed, as seen in **Figure 3.4e**, which indicated that bending deformation was dominant to the behavior of RC column under one-side repeated loading.

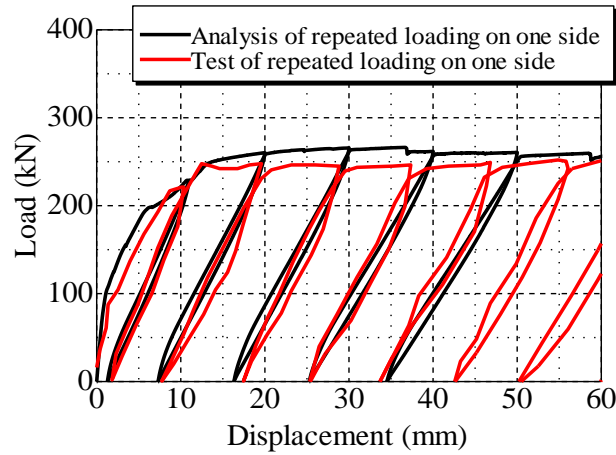


Figure 3. 3 Load-displacement relationship (one-side repeated loading)

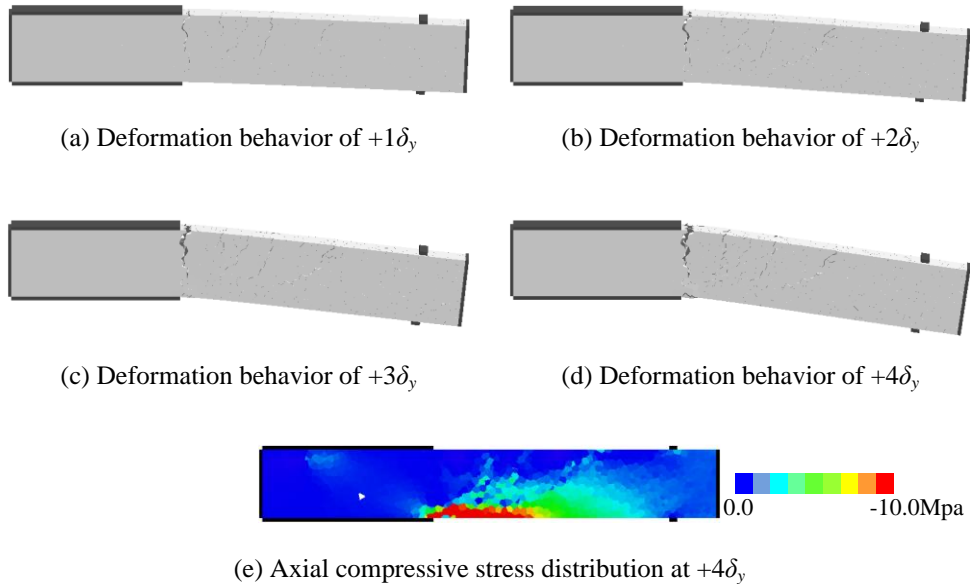


Figure 3. 4 Deformations and axial compressive stress distribution (one-side repeated loading)

3.4.2 Cyclic loading

Figure 3.5 compares the load-displacement relationships obtained by cyclic loading test and 3-D RBSM analysis. It was observed that the spindled shape of load-displacement curves at initial load stage changed to inverse S-shape with the increase of displacement level and the load carrying capacities decreased at a high rate at the deformation of $-4\delta_y$.

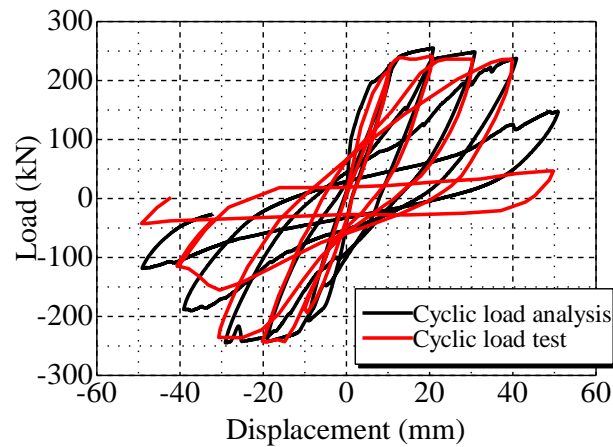


Figure 3. 5 Load-displacement relationship (cyclic loading)

Figure 3.6 gives the analytical deformations and the axial compressive stress distributions of cyclic loading analysis. Up to the deformation of $+2\delta_y$, same flexural crack propagation (see **Figure 3.4a**; **Figure 3.4b**) as that under one-side repeated loading was observed (see **Figure 3.6a**; **Figure 3.6b**). At the displacement of $-2\delta_y$, however, differently, an obvious inclined shear crack initiated at the footing-column joint (see **Figure 3.6b**). Furthermore, another inclined crack initiated across the previous one and a diagonal shear crack generated at the displacement of $+3\delta_y$, which was regarded as the typical shear deformation of a yielded RC member under cyclic loading (see **Figure 3.6c**). Finally, the shear deformation developed extremely rapidly at the displacement of $-4\delta_y$, which resulted in the shear failure of the RC column (see **Figure 3.6d**). As shown in **Figure 3.6e**, it was found that in contrast from that under one-side repeated loading, the axial compressive stress distributed along the diagonal shear cracks at the displacement

of $+4\delta_y$, which indicated that shear behavior became dominant at the ultimate stage.

Therefore, it was clear that 3-D RBSM can accurately simulate not only the bending deformation under one-side repeated loading but also the transfer of deformation from bending to shear and the shear failure due to cyclic loading of a RC member.

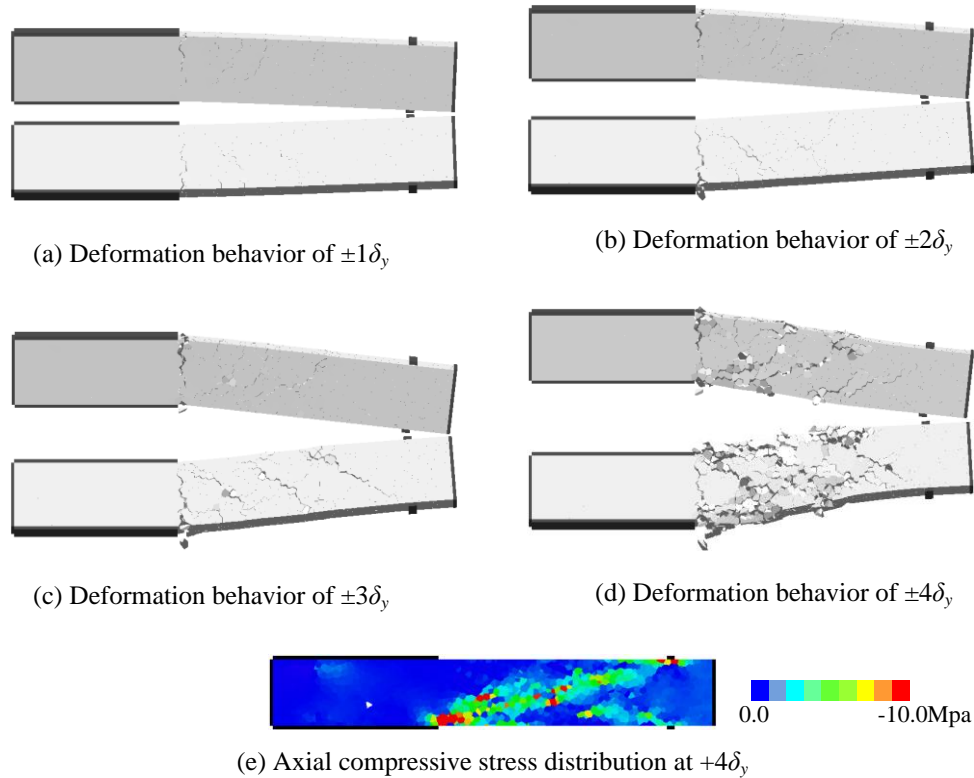


Figure 3. 6 Deformations and axial compressive stress distribution (cyclic loading)

3.5 Evaluation of shear strength degradation

3.5.1 Evaluation approach of shear strength at each ductility level

The reason for shear failure after yielding of a RC member under cyclic loading has been explained conceptually as the shear strength progressively degrades and ultimately becomes lower than the flexural strength with the increase of displacement level. Therefore, it is significant for seismic deformation-based design to quantitatively evaluate

the degraded shear strengths after each load cycle. Considering the problem that the degraded shear strengths cannot be investigated by experimental load hysteresis unless the load carrying capacity decreased lower than the flexural strength, the author has proposed a numerical approach by using 3-D RBSM to quantitatively assess the shear strength at each ductility level.

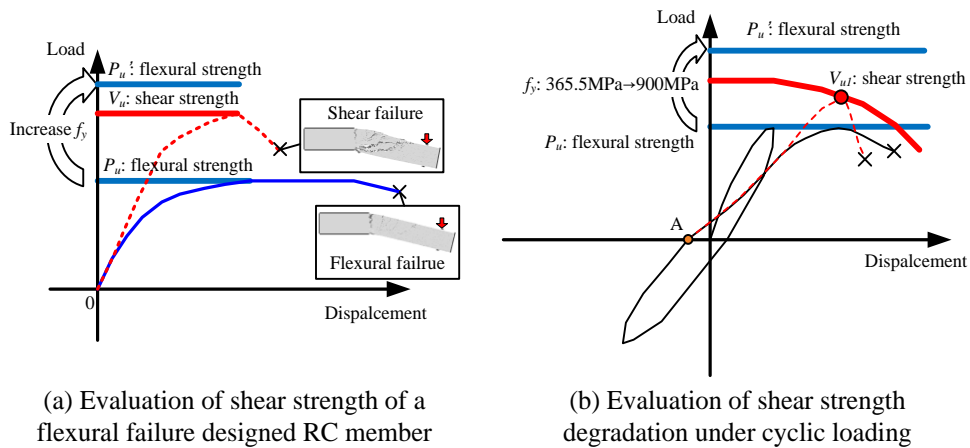


Figure 3. 7 Approach for evaluation of shear strength at each ductility level

Figure 3.7a illustrates the approach for evaluation of shear strength of a RC member designed failing by flexure. It is known that under monotonic loading test, the load carrying capacity of the RC member will not exceed the flexural strength (P_u) after yielding of longitudinal reinforcement and show a dramatic bending behavior, thus the shear strength (V_u) which is usually much higher than the flexural strength is unknown and cannot be measured directly by loading test. On the other side, a basic knowledge is noted that the flexural strength can be significantly improved by increasing yield strength of longitudinal reinforcement without affecting the grade of shear strength according to the design code (Equation 3.1-3.3) in JSCE standard specification (2012).

$$P_u = f_y \cdot A_s \cdot (d - 0.4x) / a \quad 3.1$$

$$V = V_{con} + V_s \quad 3.2$$

$$V_{con} = 0.20 \cdot f_c^{1/3} \cdot \rho_t^{1/3} \cdot d^{1/4} \cdot (0.75 + 1.4/(a/d)) \cdot b_w \cdot d \quad 3.3$$

where, P_u is the flexural strength corresponding to flexural tension failure; f_y is the yield strength of longitudinal reinforcement; d is the effective depth; x is the depth of the equivalent rectangular stress block within concrete cross section; a is the length of shear span; V is the combined shear strength; V_{con} is the shear strength provided by concrete including arch action and the concrete contribution for beam action; f_c' is the nominal concrete compression strength; ρ_t is the tension reinforcement percentage; b_w is the width of RC member; V_s is the shear strength provided by shear reinforcement (see Equation 2.5).

Hence, in 3-D RBSM analysis, the previous problem in loading test that the load carrying capacity cannot reflect the grade of shear strength is solved and the shear strength is assessed by monotonic loading hysteresis, after improving the flexural strength (P_u') greater than the shear strength (V_u) by increasing the yield strength of longitudinal reinforcement (f_y). In the meantime, a behavioral transfer from bending to shear is also observed (see **Figure 3.7a**).

On the basis of the methodology shown in **Figure 3.7a**, a numerical approach for evaluation of the shear strength at each ductility level under cyclic loading was developed and the evaluation of the degraded shear strength after first load cycle is explained in **Figure 3.7b**. The black hysteresis represents the load-displacement relationship calculated by regular cyclic loading analysis, and because of the mentioned trouble that the load carrying capacity cannot exceed the flexural strength P_u , the degraded shear strength V_{ul} after first load cycle (ordinarily higher than P_u) is unknown. By the same approach increasing yield strength of longitudinal reinforcement as introduced in **Figure 3.7a**, however, if the flexural strength (P_u') is instantly enhanced to be higher than the shear strength V_u at the end of the first load cycle (Point A), and thereafter a monotonic loading (dash red hysteresis) is imposed until the ultimate shear failure, the degraded shear strength V_{ul} after first load cycle is able to be captured by referring the maximum load. Based on the same procedure the degraded shear strength after each load cycle is

determined. Moreover, the relationship between the degraded shear strengths and the displacement ductility levels (shear strength degradation curve) can be achieved by this methodology (Nakamura et al. 2014).

Based on the mentioned numerical approach, the 3-D RBSM analyses for evaluation of the degraded shear strengths after each load cycle of one-side repeated and cyclic loadings for the objective RC column were carried out. The yield strength of longitudinal reinforcing bars was remarkably enhanced from the original 365.5 MPa to 900 MPa at the ends of load cycles, in order to achieve an extremely great flexural strength.

3.5.2 Shear strength degradation due to different loading conditions

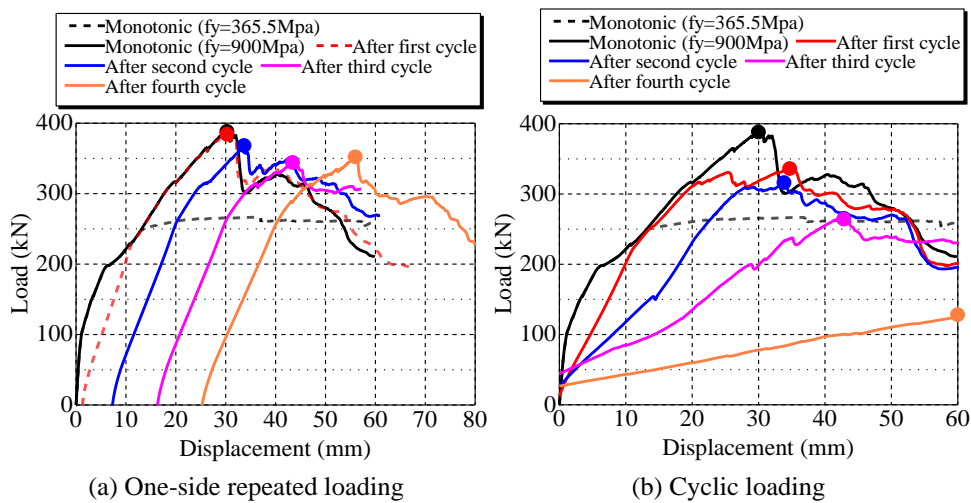


Figure 3. 8 Evaluation of shear strength at each ductility level

The corresponding analytical load-displacement hysteresis located at the first quadrant for evaluation of the degraded shear strengths of one-side repeated loading and cyclic loading are shown in **Figure 3.8**, respectively. Moreover, the load-displacement relationships of the monotonic loading analyses by using increased yield strength ($f_y=900\text{MPa}$) for reference of the original shear strengths and the monotonic loading analysis by using regular yield strength ($f_y=365.5\text{MPa}$) for reference of the flexural strength are also illustrated. In addition, the maximum loads after each load cycle, as the degraded shear

strengths, are marked (the load at the displacement of 60 mm is regarded as the maximum load for the case after fourth load cycle under cyclic loading).

Consequently, for the shear strength degradation due to one-side repeated loading (see **Figure 3.8a**), it was observed that the degraded shear strengths preserved a higher grade than the flexural strength all the time, hence the load carrying capacity was well maintained (see **Figure 3.3**). For the shear strength degradation due to cyclic loading (see **Figure 3.8b**), differently, it was notable that the shear strength was decreased at a higher rate than that of the one-side repeated loading, with the increase in load cycles, and ultimately, it became lower than the flexural strength after fourth load cycle, resulting in the decrease of load carrying capacity and shear failure (see **Figure 3.5**).

It was demonstrated that the different tendencies of shear strength degradation under one-side repeated loading and cyclic loading can be quantitatively assessed, according to the proposed approach for evaluation of shear strength degradation discussed in chapter 3.5.1.

3.6 Evaluation of shear resistance mechanism degradation

In chapter 3.5, the shear strength degradation of the RC column under cyclic loading was quantitatively evaluated by 3-D RBSM. The mechanism of shear strength degradation, however, has not been explained. In previous chapter 2.4, as an example to explain the decoupling approach of shear resistance mechanisms, the analytical load-displacement hysteresis for monotonic loading analysis ($f_y=900$ MPa) shown in **Figure 3.8** has been decoupled and the decoupling results has been discussed in detail. In this section, by the same approach, all the load-displacement hysteresis for evaluation of shear strength degradation (the hysteresis in **Figure 3.8**) were decoupled into the contributions of beam action (V_b) and arch action (V_a), and the beam action was further decoupled into the contributions of truss action (V_s) and concrete contribution (V_c). The mechanism of

shear strength degradation would be explained by the degradation characteristics of each shear resistance mechanism.

3.6.1 Shear resistance mechanism degradation under one-side repeated loading

The load-displacement hysteresis for evaluation of degraded shear strengths due to different loading conditions (results in **Figure 3.8**) were decoupled into hysteresis of shear resistance mechanisms in order to understand the critical actions that govern the shear strength degradation.

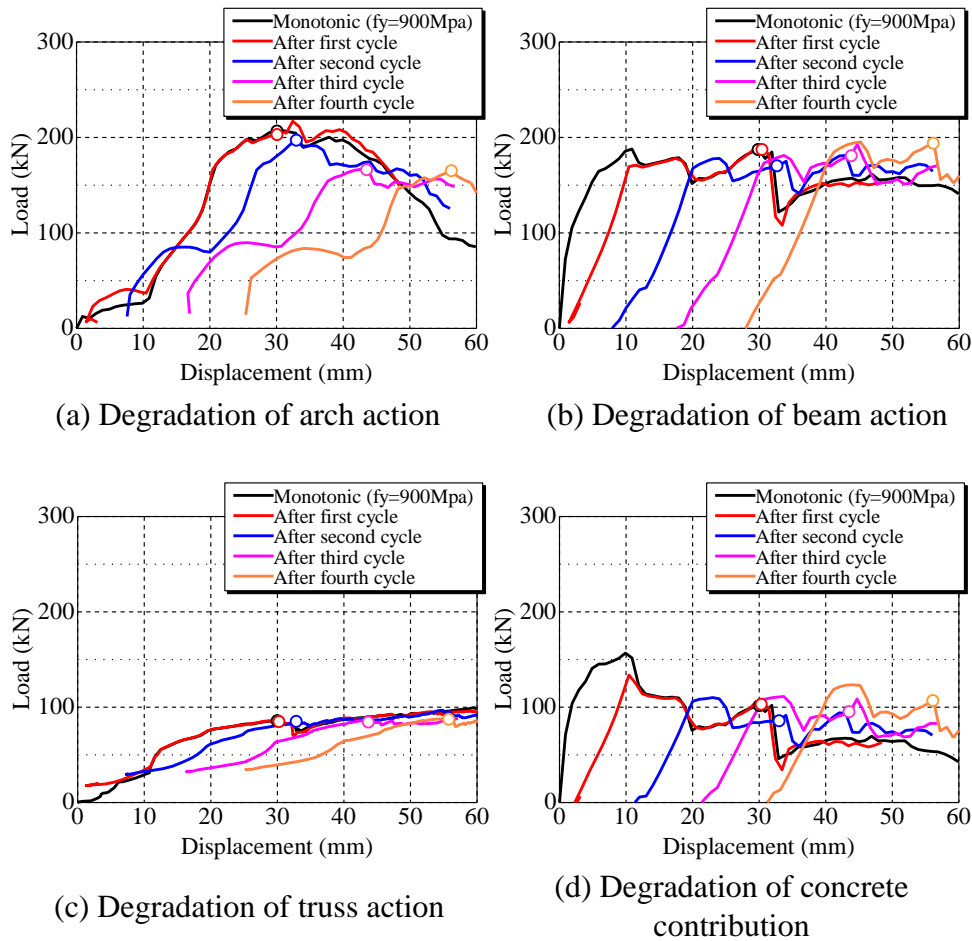


Figure 3. 9 Degradations of shear resistance mechanisms (one-side repeated loading)

In terms of one-side repeated loading, the decoupling results of shear resistance

mechanisms after each load cycle are shown in **Figure 3.9**. The beam actions, arch actions, truss actions and concrete contributions for degraded shear strengths (maximum loads in **Figure 3.8a**) were flagged and would be focused on.

Consequently, it was found that with the increase in load cycles, the arch action slowly decreased and 80% of the original capacity was maintained even after fourth load cycle (see **Figure 3.9a**). In the meantime, the beam action was not affected and kept a constant (see **Figure 3.9b**). Since both the beam action and arch action did not suffer remarkable loss, the shear strength could be kept much higher than flexural strength and the load carrying capacity could be sustained (see **Figure 3.3**).

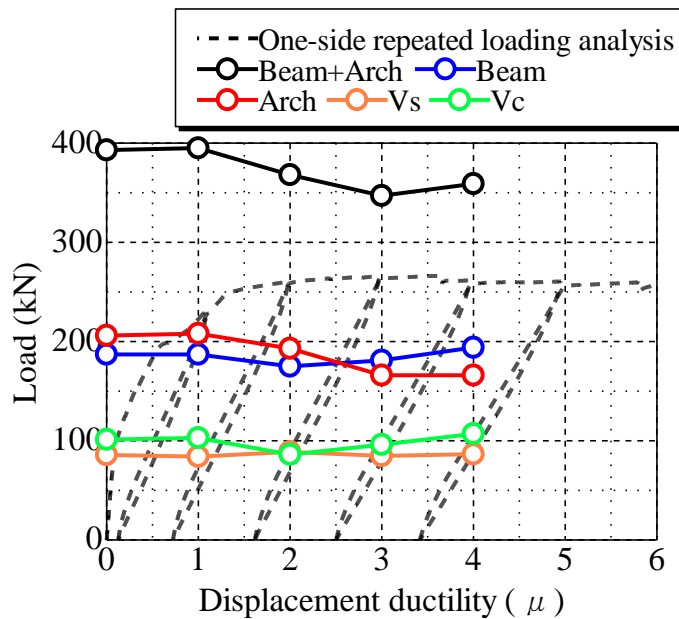


Figure 3. 10 Shear resistance mechanisms VS displacement ductility (one-side repeated loading)

The beam action for shear strength provided by truss action remained stable and was not affected by load cycles, since the truss action was only related to the stress state of shear reinforcement and would not increase after the yielding of stirrups (see **Figure 3.9c**). The truss action for shear strength, after fourth cycle of loading, was determined as 93

kN, which was slightly lower than the calculation by Equation 2.6, i.e. 98 kN. Similarly, the capacity of the concrete contribution, as a result, was well maintained and was not reduced with the increase of load cycles (see **Figure 3.9d**).

The result of the beam actions, arch actions, truss actions and concrete contributions corresponding to the degraded shear strengths after each load cycle (marked points in **Figure 3.9**) are summarized in **Figure 3.10**, combined with the load-displacement ductility relationship obtained by one-side repeated loading analysis. Herein, for the correspondence of the shear components to displacement ductility, the zero displacement ductility corresponds to the initial actions not affected by load cycles, while the positive displacement ductility means the number of load cycles that the shear strength has experienced (same correspondence was adopted in the following content in chapter 3 and chapter 4), and the degraded shear strengths after each load cycle are presented by the combined effect of beam action and arch action. As consequence, the shear resistance mechanisms were not significantly affected by one-side repeated loading condition, except for a low decrease of arch action, which guaranteed the stable load carrying capacity and the good deformability of the RC column.

3.6.2 Shear resistance mechanism degradation under cyclic loading

In terms of cyclic loading, the decoupling results of the shear resistance mechanisms after each load cycle are shown in **Figure 3.11**. Similarly, the beam actions, arch actions, truss actions, and concrete contributions for degraded shear strengths (maximum loads in **Figure 3.8b**) were flagged.

Consequently, as illustrated in **Figure 3.11**, it was noted that the shear strength provided by arch action was rapidly decreased with the increased load cycles, which quite differed from that of the one-side repeated loading. When the shear failure occurred after fourth load cycle, the arch action nearly had completely lost its capacity, which indicated that the arch action could not rebuild with the increase in load cycles (see **Figure 3.11a**).

In contrary, as shown in **Figure 3.11b**, the beam action could maintain the majority of its original capacity in the first four load cycles. But after the severe degradation of arch action (after fourth load cycle), the beam action began decrease at a high rate, together with the occurrence of shear failure.

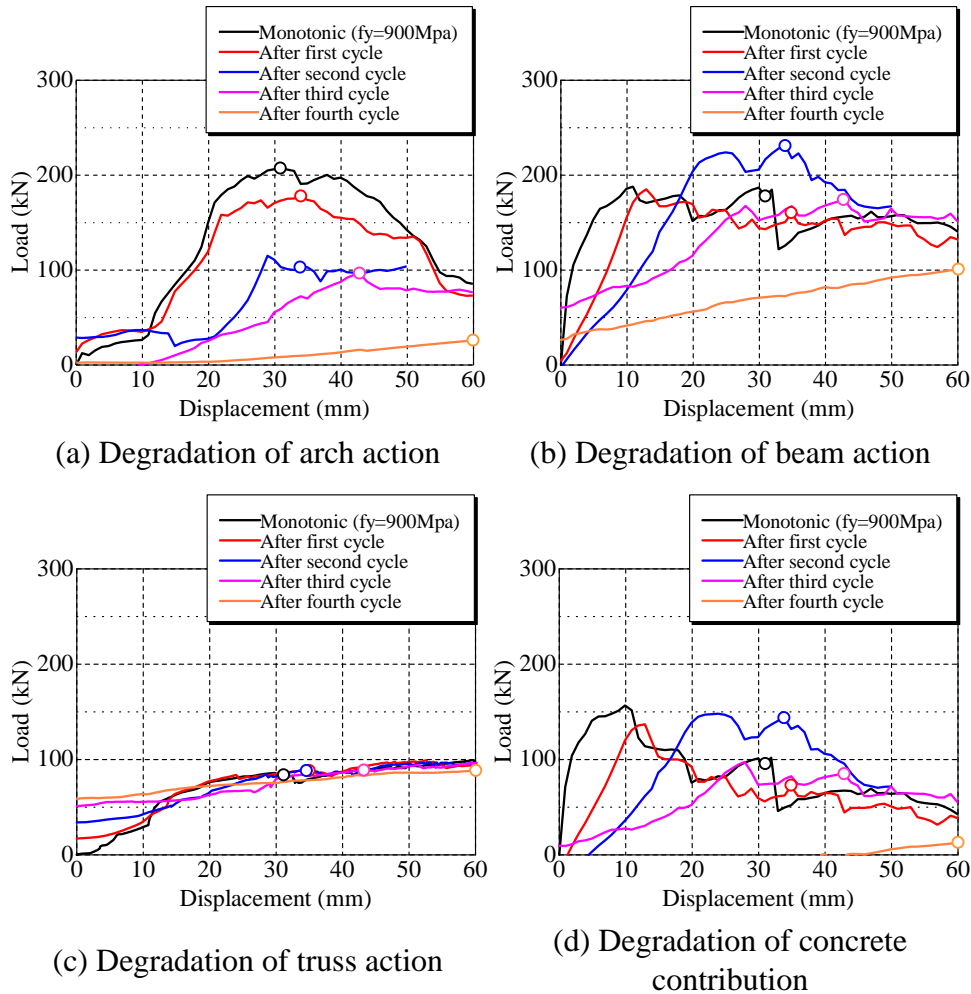


Figure 3. 11 Degradations of shear resistance mechanisms (cyclic loading)

With respect to the decoupling results of beam action, the shear strength provided by the truss action remained stable and was not affected by the increased load cycles (see **Figure 3.11c**) because of the same reason explained in previous chapter 3.6.1. On the other side, the concrete contribution although could maintain the majority of its original

capacity in the first four load cycles, after the severe degradation of arch action (after fourth load cycle), however, it lost the ability to rebuild and was subsequently decreased at a high rate (see **Figure 3.11d**) caused by the extreme large shear deformation (see **Figure 3.6d**). Thus, it was acknowledged that the degradation of concrete contribution was the critical factor for the degradation of beam action after fourth load cycle.

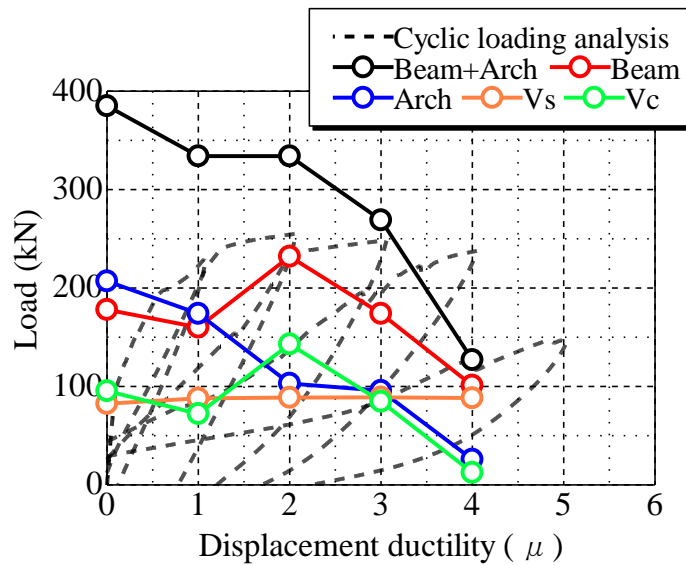


Figure 3. 12 Shear resistance mechanisms VS displacement ductility (cyclic loading)

Moreover, the data of the beam actions, arch actions, truss actions, and concrete contributions corresponding to the degraded shear strengths after each load cycle (marked points in **Figure 3.11**) are summarized in **Figure 3.12**, combined with the load-displacement ductility relationship obtained by cyclic loading analysis. Herein, the degraded shear strengths after each load cycle are presented by the combined effect of beam action and arch action. As the mechanism of shear strength degradation due to cyclic loading, it could be concluded that the original shear strength was first decreased to a grade close to the flexural strength after third load cycle ($\mu=3$) because of the progressive degradation of arch action, while the beam action at this stage well maintained its original capacity; then after the severe degradation of arch action after

fourth load cycle ($\mu=4$), the beam action began decrease induced by the degradation of concrete contribution; finally the shear strength became lower than the flexural strength and the shear failure occurred.

Therefore, the lesson that the first degradation of arch action is the critical factor for the shear strength degradation to the grade of flexural strength and the occurrence of shear failure can be acknowledged, and this is the major distinction in shear resistance mechanism degradations between on-side repeated loading and cyclic loading.

3.7 Summary and conclusions

In this chapter, aiming to study the mechanism of shear failure after yielding of RC member under cyclic loading, the author first simulated the different shear behaviors of a RC column under one-side repeated loading and cyclic loading by 3-D RBSM. Secondly the processes of shear strength degradation were quantitatively assessed and it was found that the shear strength under cyclic loading is progressively decreased at a much higher rate than that under one-side repeated loading, which leads to an earlier failure of RC column under cyclic loading.

Moreover, the key mechanism of shear failure after yielding is explained, that is, the original shear strength is first decreased to a grade close to the shear demand corresponding to the flexural strength because of the progressive degradation of arch action, while the beam action at this stage well maintains its original capacity; then after the high percentage loss of arch action, the beam action begins decrease induced by the degradation of concrete contribution; finally the shear strength is reduced lower than the shear demand corresponding to flexural strength and the shear failure occurs. On the contrary, the arch action, under one-side repeated loading, presents very limited degradation with the increase of displacement ductility, contributing to an excellent deformability of the RC column.

4. Effect of Structural Variables on Shear Resistance Mechanisms

4.1 Introduction

The author has studied the mechanism of shear failure after flexural yielding for a RC column subjected to cyclic loading, and have achieved a conclusion that the first degradation of arch action is the primary cause of shear strength degradation until lower than the shear demand corresponding to flexural strength. As mentioned in chapter 1.2.1, it has been widely studied that a number of structural variables such as shear reinforcement ratio (ρ_w), shear span to effective depth ratio (a/d), longitudinal reinforcement ratio (ρ_l) and axial compression load (P) significantly affect the shear performance of RC member including shear strength. Therefore, in this chapter, in order to make it clear that how those structural variables affect the mechanism of shear strength degradation, a parametric study was carried out on the basis of the structural details of the RC column studied in chapter 3.

4.2 Overview of parametric analysis

Based on the structural details of the RC column analyzed in chapter 3, the author carried out parametric analyses for shear reinforcement ratio, i.e. ρ_w , shear span to

effective depth ratio, i.e. a/d , tension reinforcement ratio, i.e. ρ_t , and axial compression load, i.e. P , and investigated how these variables affect shear resistance mechanism. All analytical cases are listed in **Table 4.1**, where case S1 represents the standard column analyzed in chapter 3; case series “A1-A3” are for studying the effect of shear reinforcement ratio, while the other variables are kept same as the standard case S1; case series “B1-B2” are for investigation on the effect of shear span to effective depth ratio; case series “C1-C2” are prepared for studying the effect of tension reinforcement ratio; case series “D1-D2” are for the survey on the effect of axial compression load. Hereby, reinforcement ratio was changed by directly increasing or decreasing cross section area of reinforcement, and shear span to effective depth ratio was changed by changing shear span length (see **Figure 4.1**).

Table 4. 1 List of analytical cases

Case No.	Shear span to effective depth ratio a/d	Tension reinforcement ratio ρ_t (%)	Shear reinforcement ratio ρ_w (%)	Axial load P (MPa)
S1	4.0	0.82	0.08	1.0
A1			0.16	
A2	4.0	0.82	0.32	1.0
A3			0.00	
B1	3.0	0.82	0.08	1.0
B2	2.0			
C1		0.41	0.08	1.0
C2	4.0	1.02		
D1	4.0	0.82	0.08	4.0
D2				6.0

When creating analytical models, same element size in average, 30 mm, was applied and same procedure was employed for cyclic loading analysis, i.e. displacement was stepwise increased with an increment of yielding deformation δ_y .

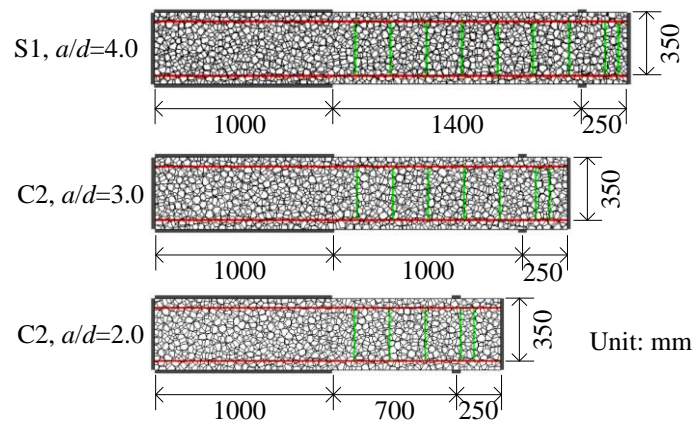


Figure 4. 1 Analytical models “C1, C2”

4.3 Analytical result

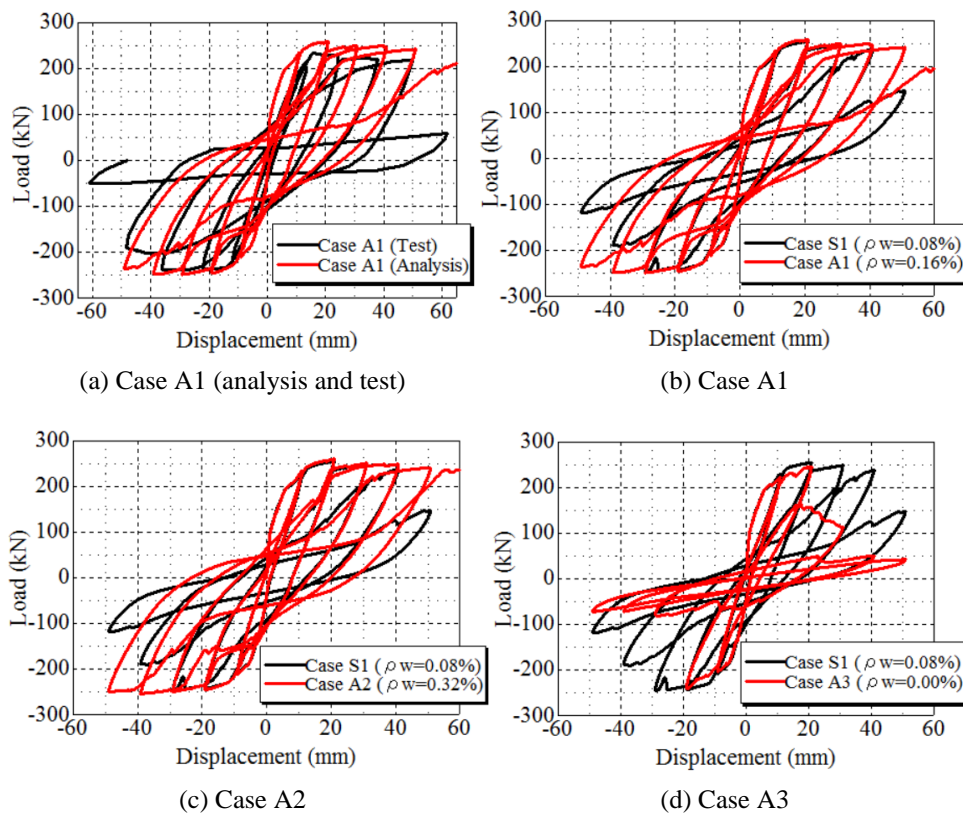


Figure 4. 2 Load-displacement relationship (ρ_w)

In this section, the analytical results, i.e. load-displacement relationship and deformation behavior, for the objective cases are first described.

4.3.1 Analytical result for different shear reinforcement ratios

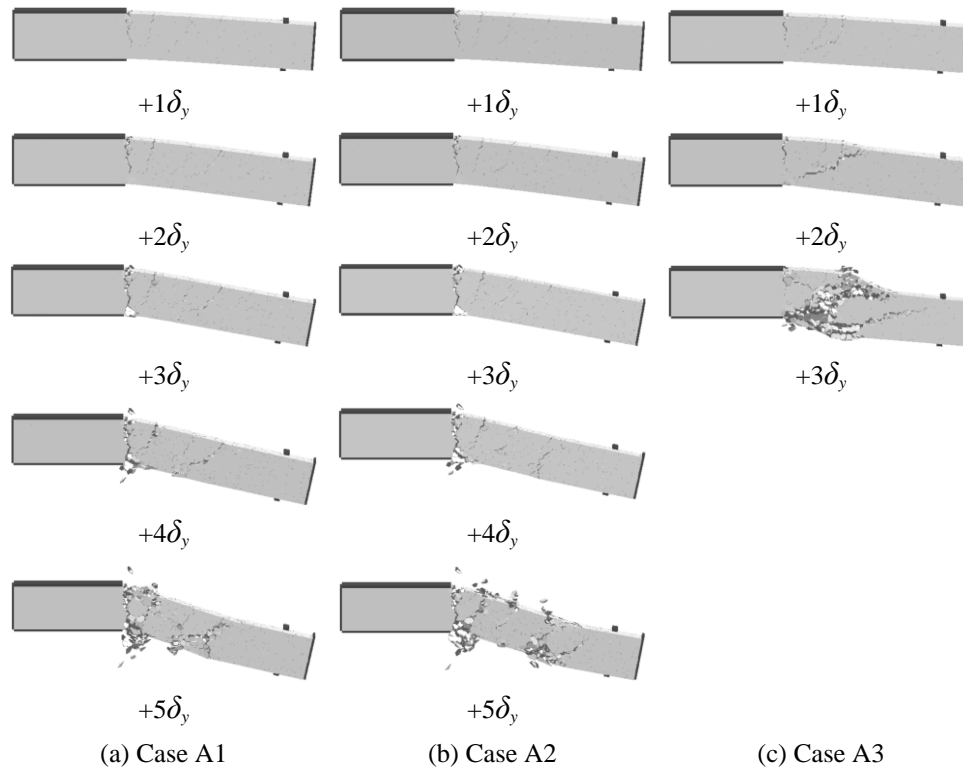


Figure 4. 3 Comparison of deformations (ρ_w)

The analytical result for case series “A1-A3” with shear reinforcement ratio as parameter are shown in **Figure 4.2** and **Figure 4.3**. We could see from the load-displacement relationships for case A1 shown in **Figure 4.2a** that the test load-carrying capacity and its evident decrease at the displacement of +6 δ_y (δ_y is yielding deformation, 10 mm) were well reproduced by 3-D RBSM. Furthermore, it was understood that because of more shear reinforcement arrangement, the deformational ability of case A1 and A2 were remarkably improved, i.e., standard case S1 failed at the displacement of -4 δ_y ; case A1 destroyed at the displacement of +6 δ_y (see **Figure 4.2b**); case A2 did not

fail even the displacement was over $+6\delta_y$ (see Figure 4.2c). On the contrary, since the lack of shear reinforcement, case A3 failed in shear at an earlier stage at $+3\delta_y$ (see **Figure 4.2d**).

For deformation behavior (deformations were magnified by eight times), it was observed that the shear behaviors were considerably reduced for cases A1 and A2 (see **Figure 4.3a-b**), in contrast to the result for standard S1 shown in **Figure 3.6**. Case A3, however, exhibited much severer shear cracking behavior at an earlier stage $+3\delta_y$ (see **Figure 4.3c**).

4.3.2 Analytical result for different shear span to effective depth ratios

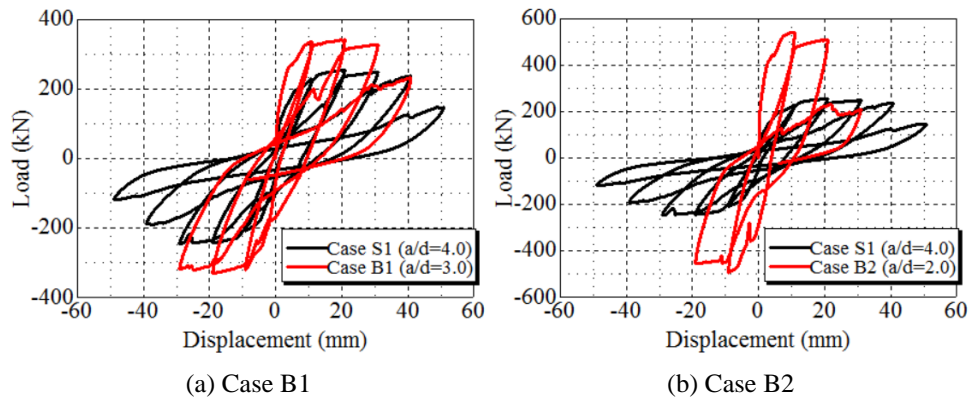


Figure 4. 4 Load-displacement relationship (a/d)

Afterwards, the analytical result for case series “B1-B2” with shear span to effective depth ratio as parameter are described by **Figure 4.4** and **Figure 4.5**. As a consequence, it was notable that shorter column provided greater load carrying capacity, i.e. around 250 kN for standard S1, 330 kN for case B1 and 500 kN for case B2, but presented worse deformational ability: standard S1 failed at the displacement of $-4\delta_y$; case B1 failed at the displacement of $+4.0\delta_y$; case B2 destroyed at the displacement of $+3\delta_y$.

The corresponding deformation behaviors are exhibited in **Figure 4.5** (result of case S1 referring to **Figure 3.6**). Obviously, shear cracks in short columns B1 and B2 initiated at initial loading stage ($+1\delta_y$), which was quite different from that in standard S1. Also,

these early formed shear cracks developed much more rapid which led to earlier shear failure.

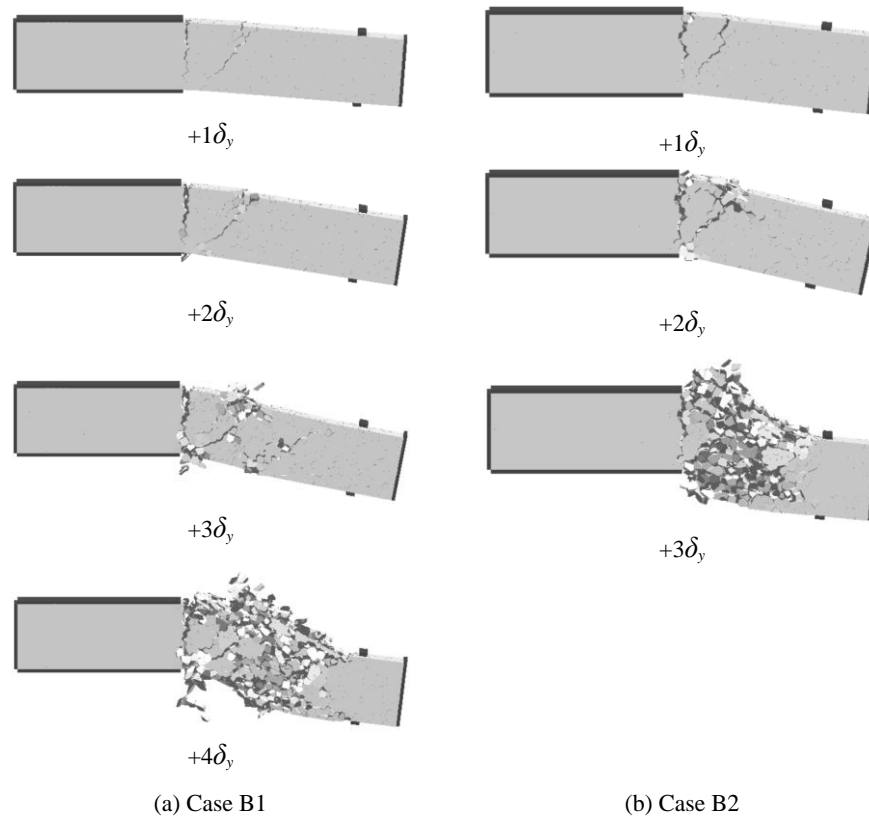


Figure 4. 5 Comparison of deformations (parameter a/d)

4.3.3 Analytical result for different tension reinforcement ratios

Figure 4.6 and **Figure 4.7** illustrate the result for case series “C1-C2” with tension reinforcement ratio as parameter. It was observed, from the load-displacement relationships (see **Figure 4.6**), that deformational ability of column with higher tension reinforcement ratio became worse with the increased displacement ductility: standard S1 failed at the displacement of $-4\delta_y$; case C1 presented good deformation ability more than $+5\delta_y$ (see **Figure 4.6a**); case C2 failed at the displacement of $+4\delta_y$ (see **Figure 4.6b**).

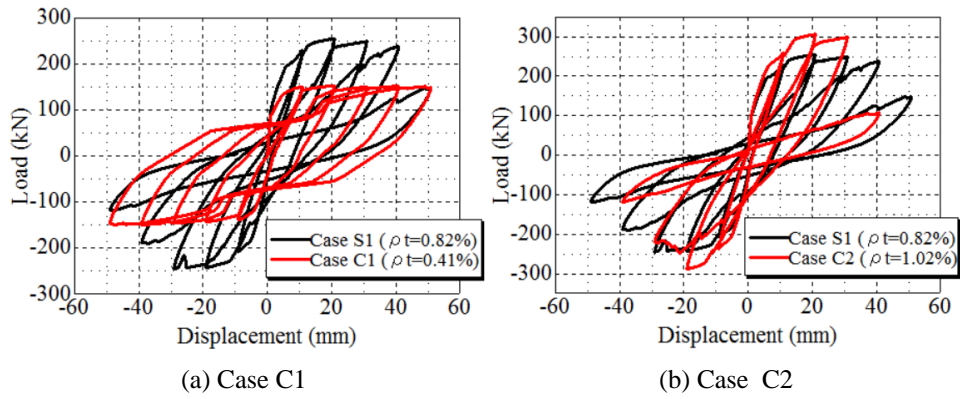


Figure 4. 6 Load-displacement relationship (ρ_t)

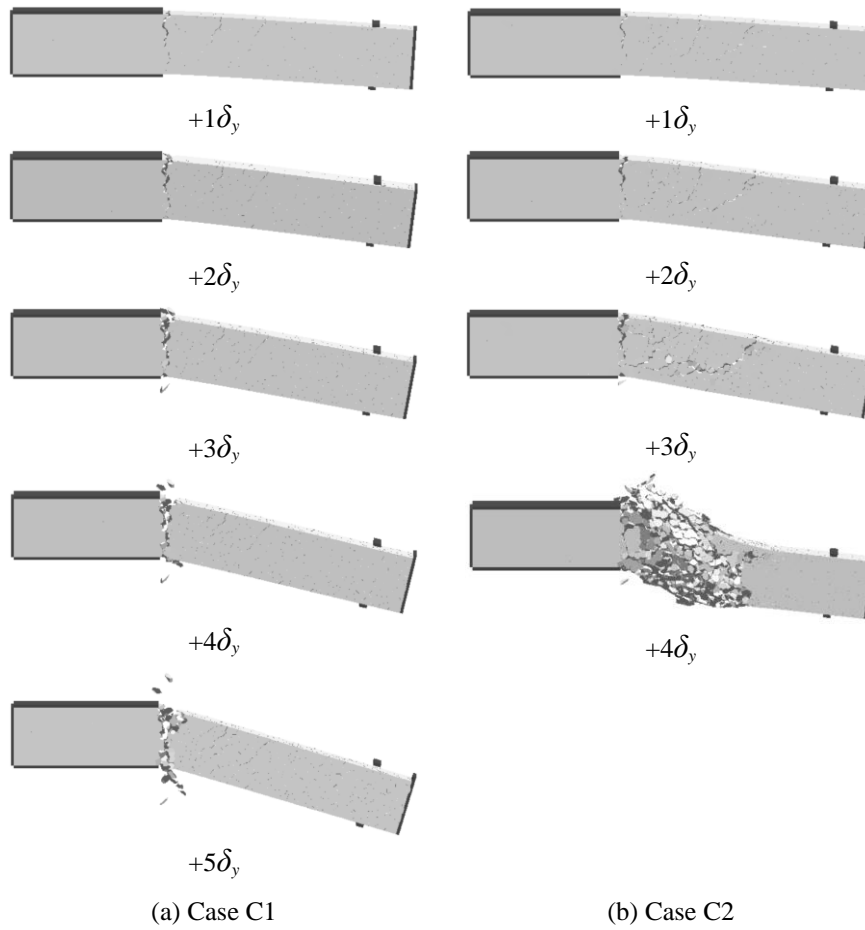


Figure 4. 7 Comparison of deformations (ρ_t)

Regarding to deformation behavior, flexural cracks dramatically developed and shear deformation was extremely minor for case C1, even the displacement reached $+5\delta_y$ (see **Figure 4.7a**), while shear deformation became obvious at the displacement of $+4\delta_y$ for case S1 (see **Figure 3.6**) and case C2 (see **Figure 4.7b**), which ultimately led to the shear failure at the displacement of $-4\delta_y$ for case S1 and $+4\delta_y$ for case C2.

4.3.4 Analytical result for different axial compression loads

Figure 4.8 and **Figure 4.9** illustrate the result for case series “D1-D2” with axial compression load as parameter. It was observed, from the load-displacement relationships (see **Figure 4.8**), that the deformational ability of the column withstanding higher axial compression load became worse: standard S1 failed at the displacement of $-4\delta_y$; case D1 presented worse deformation ability, failing at the displacement of $-3\delta_y$ (see **Figure 4.8a**); case D2 failed at the displacement of $+3\delta_y$ (see **Figure 4.8b**).

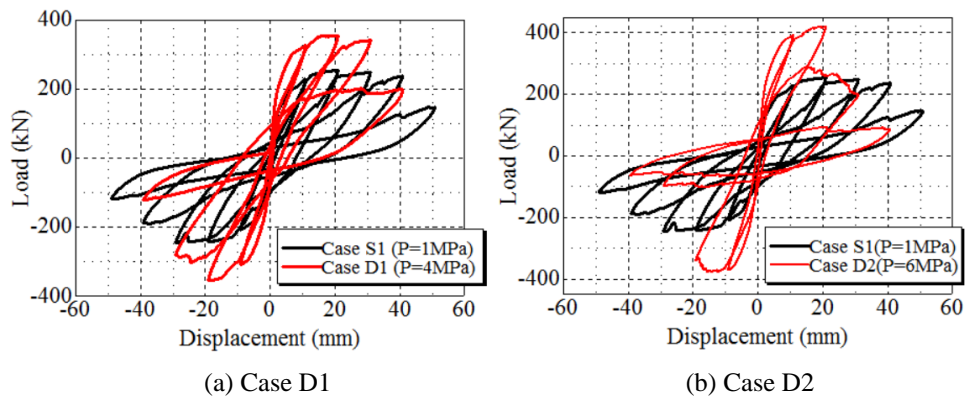


Figure 4. 8 Load-displacement relationship (P)

With regard to the deformation behaviors, it was obvious that the generation and propagation of shear crack became much earlier and more dramatic due to the increasing effect of axial compression load (see **Figure 4.9**), compared with that of the standard case S1.

According to above discussion about analytical results for objective cases, it was clear

that 3-D RBSM can well reproduce the different shear performances of RC members with varying structural variables.

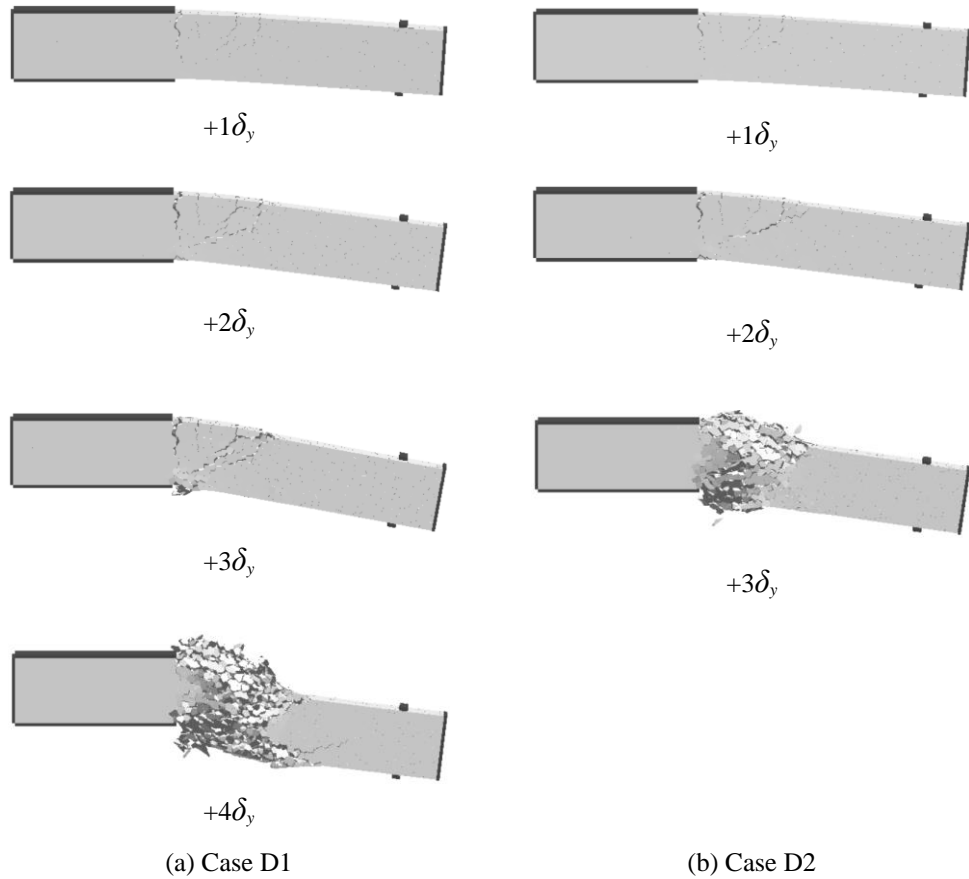


Figure 4. 9 Comparison of deformations (*P*)

4.4 Shear strength degradation curve

The approach for evaluation of shear strength degradation, applied in chapter 3.5.1, was employed again to estimate the processes of shear strength degradation for objective RC columns, and the analytical load-displacement hysteresis in first quadrant for evaluation of shear strength degradation are shown in **Figure 4.10-4.13** (the result of standard S1 referring to **Figure 3.8b**), where shear strength at each ductility is marked. Besides, monotonic loading analyses by using regular yield strength of tension

reinforcement ($f_y=365.5$ MPa) are also plotted for reference of the flexural strengths.

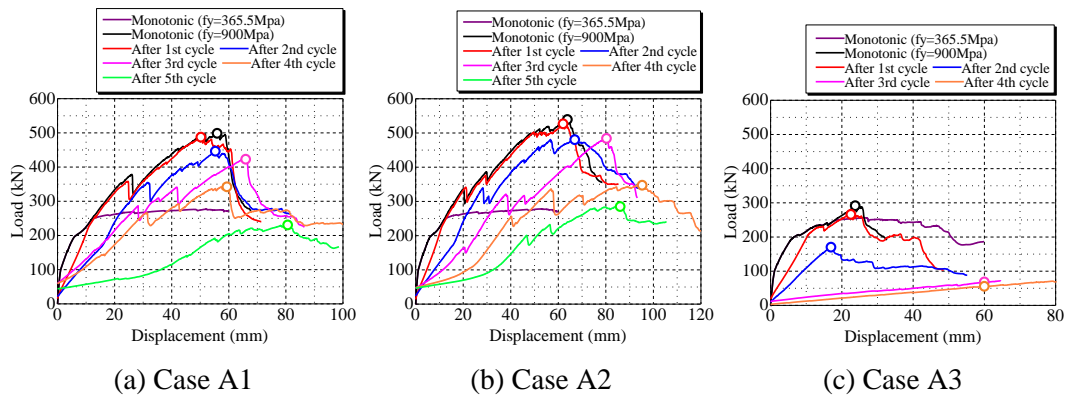


Figure 4. 10 Evaluation of shear strength at each ductility level (ρ_w)

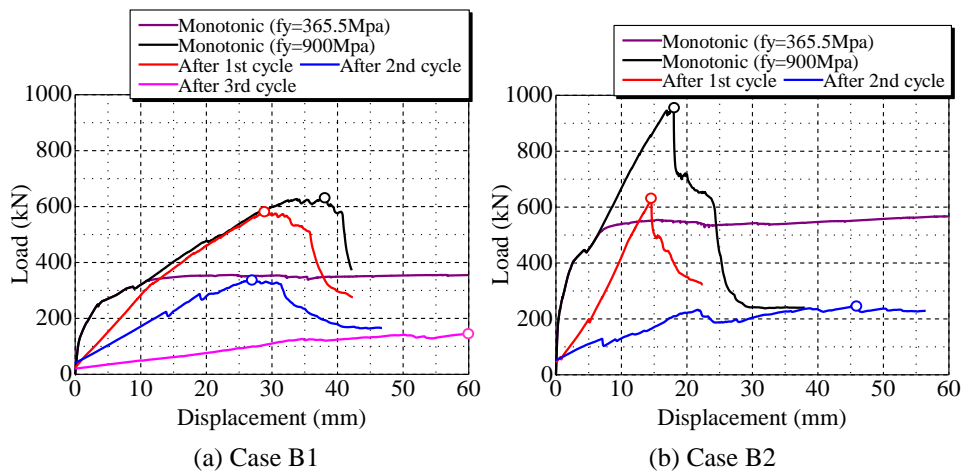


Figure 4. 11 Evaluation of shear strength at each ductility level (a/d)

For case series “A1-A3”, it was seen that the shear strength is decreased lower than the shear demand corresponding to the flexural strength after fifth cycle of loading for case A1 (see **Figure 4.10a**) while after second cycle of loading for case A3 (see **Figure 4.10c**); the shear strength of case A2, however, is always greater than the shear demand corresponding to the flexural strength even after fifth cycle of loading (see **Figure 4.10b**). The condition that shear strength lower than the shear demand corresponding to flexural strength will cause decrease of load carrying capacity and shear failure, which has been

introduced by the result shown in **Figure 4.2**.

Figure 4.11 shows the result for case series “B1-B2”. The result that the start ductility point for dramatic degradation of shear strength occurred earlier in the shorter columns, which was the direct cause of the earlier shear failures than standard S1.

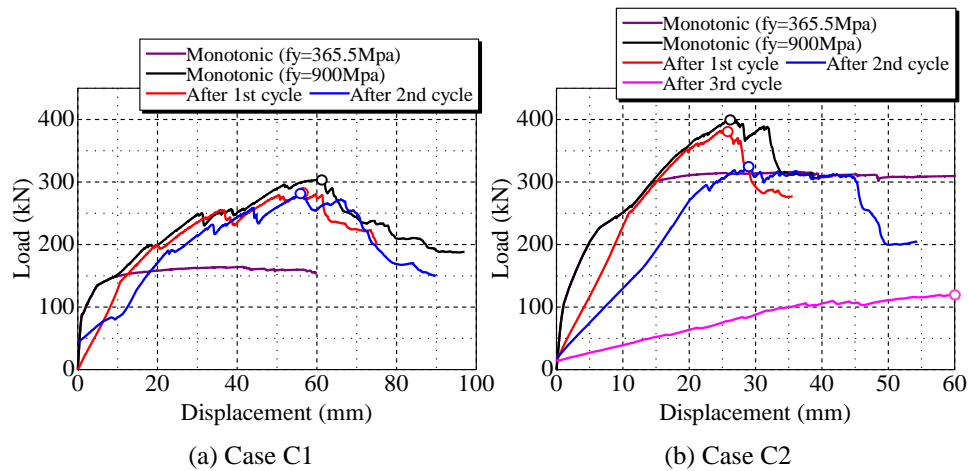


Figure 4. 12 Evaluation of shear strength at each ductility level (ρ_t)

The analytical load-displacement hysteresis shown in **Figure 4.12** are for case series “C1-C2”. Herein, after third cycle of loading, since even conducting monotonic loading analysis by using increased yield strength of tension reinforcement ($f_y=900$ MPa), case C1 still suffered flexural failure, namely the degraded shear strength could not be determined, only the degraded shear strengths in first three cycles of loading were taken into account (see **Figure 4.12a**). As a result, it was found that the shear strength was only slightly decreased due to the increased displacement ductility for case C1, while the shear strength was decreased lower than the shear demand corresponding to the flexural strength after fourth cycle of loading for case S1 and after third cycle of loading for case C2, which agrees well with the failure points obtained by cyclic loading analyses (see **Figure 4.6**).

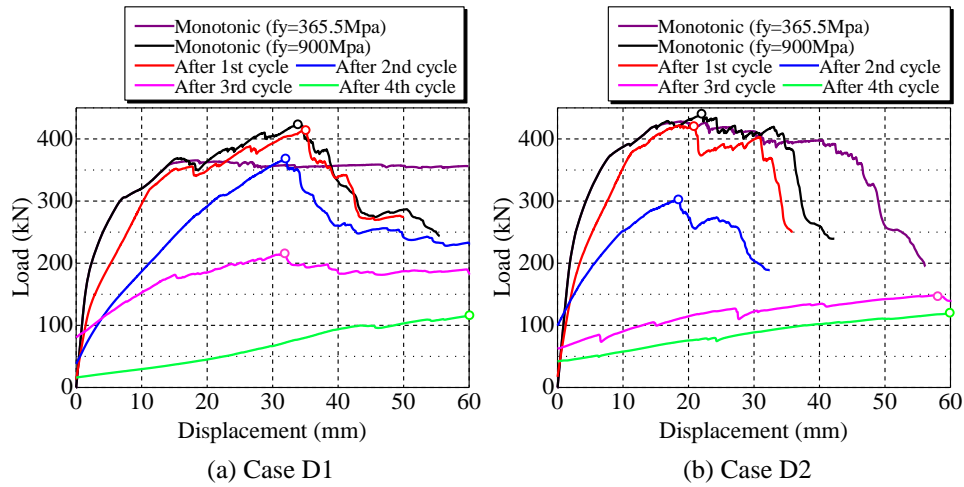


Figure 4. 13 Evaluation of shear strength at each ductility level (P)

Figure 4.13 shows the result for case series “D1-D2”. It was apparent that the increased axial compression load advanced the start ductility point for significant degradation of shear strength, that is, the shear strength degraded lower than the shear demand corresponding to the flexural strength after third load cycle for case D1 and after second load cycle for the case D2, respectively, which is also clarified by the failure points obtained by cyclic loading analyses (see **Figure 4.8**).

Finally, according to the above result for shear strength degradation, the shear strength degradation curve, which is introduced in chapter 1.2.2 and very important to seismic shear design, for each case was achieved. As the definition of shear strength degradation curve, it represents the relationship between the ratio α of degraded shear strength to initial shear strength and displacement ductility level μ , and the shear strength here means the entire concrete contribution V_{con} apart from contribution denoted by shear reinforcement V_s , referring to Equation 3.2.

Hereby, it was considered that the shear strength degradations previously estimated, i.e. the decreased shear strengths in **Figure 4.10-4.13**, are attributed to the degradation of V_{con} while V_s is a constant which is not affected by increased load cycles. Therefore, we can

estimate V_{con} at each displacement ductility level by the way removing the constant V_s from previously estimated shear strengths.

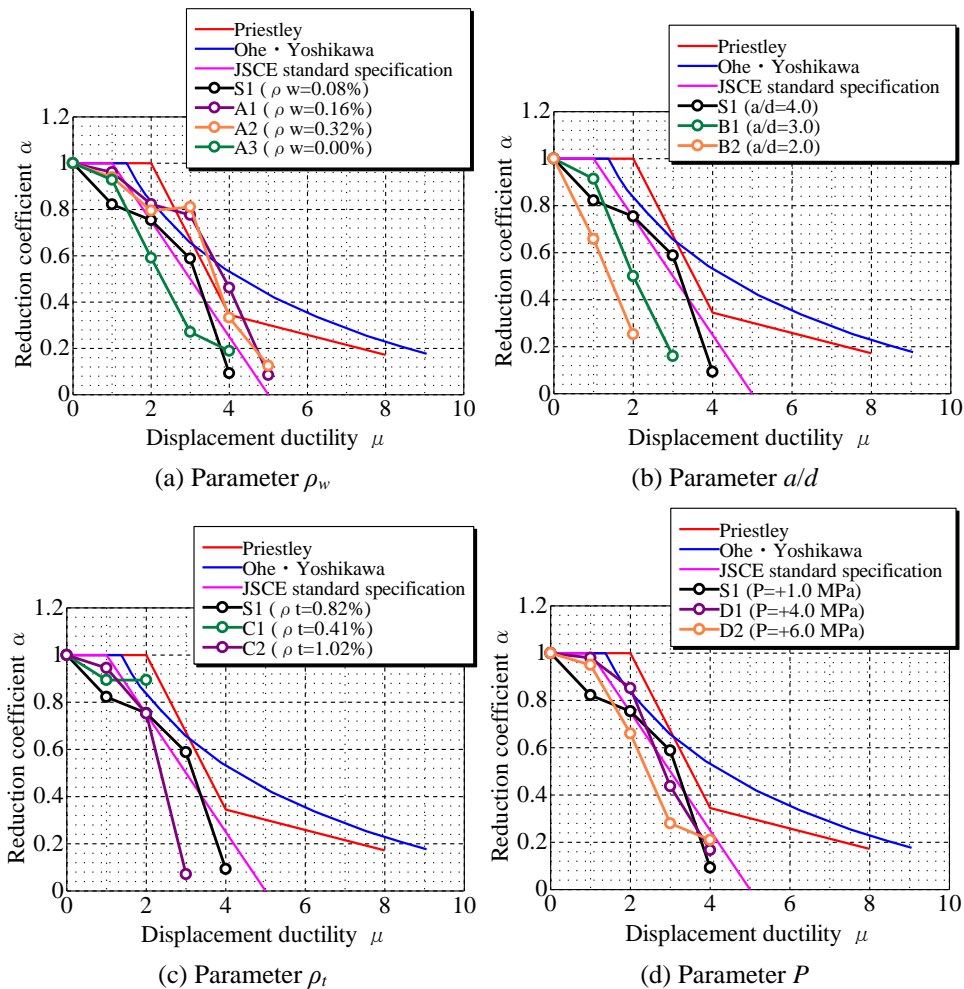


Figure 4.14 Shear strength degradation curves

As the approach to estimate constant V_s for each case, the following approach was employed: taking standard S1 as an example, the evaluation for shear strength of a same column as S1 but without shear reinforcement was first carried out, and this shear strength can be regarded as the initial V_{con} without degradation; then the constant V_s was able to be obtained by the difference between the initial shear strength of S1 ($V_{initial}$, shear strength by monotonic loading analysis shown in **Figure 3.8b**) and initial V_{con} , i.e. $V_s=V_{initial}-V_{con}$;

thereby, as mentioned before, the degraded V_{con} at each displacement ductility level was estimated by the difference between the degraded shear strength in **Figure 3.8b** and the V_s , and the resulting shear strength degradation curve, i.e. α (ratio of degraded V_{con} to initial V_{con}) VS μ , can be drawn.

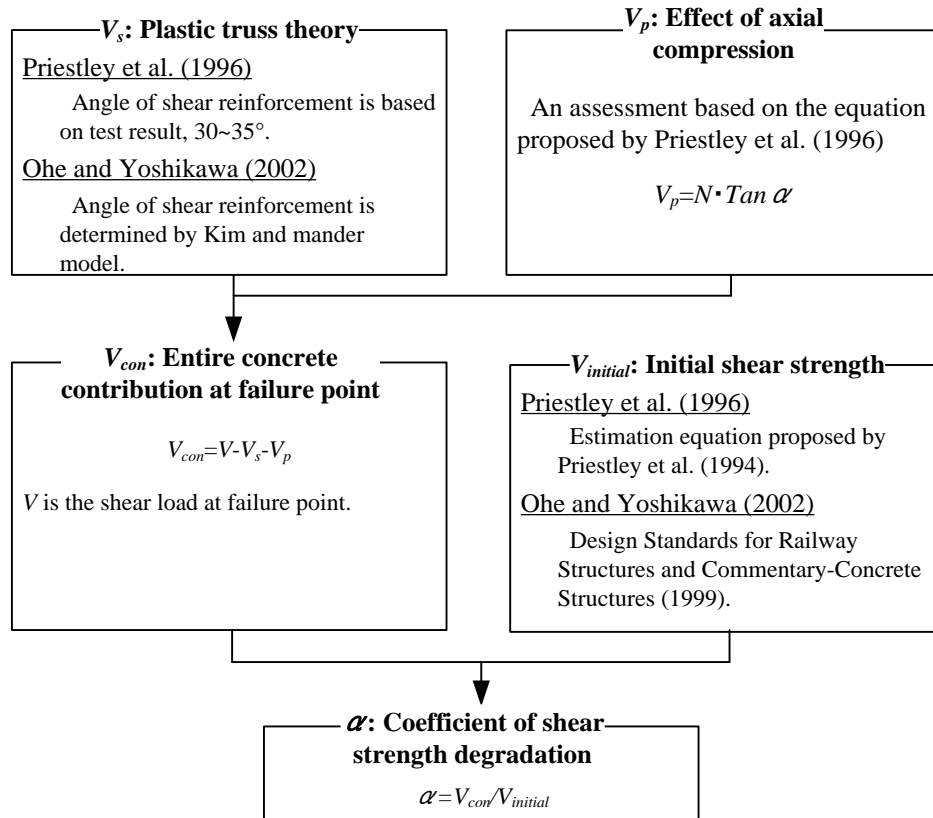


Figure 4. 15 Procedure for estimation of shear strength degradation curves by test data

Based on this approach, the shear strength degradation curve for each case was achieved and the result for each case series are summarized in **Figure 4.14**, combined with the design shear strength degradation curves proposed by Priestley et al. (1996), Ohe and Yoshikawa (2002) and JSCE standard specification (2012) basing on summary of test data. And their procedure for estimating shear strength degradation curves is briefly shown in the flow chart, **Figure 4.15**. In general, the decreased shear strength V_{con} was

estimated by subtracting the constant shear components by shear reinforcement V_s and the effect of axial compression V_p from the entire shear load monitored at failure point V , while the initial shear strength by concrete was estimated according to the applicable equations, that is, in Priestley's work, the equation in Priestley et al. (1994) was employed and in Ohe and Yoshikawa's work, the equation in Design Standards for Railway Structures and Commentary-Concrete Structures (1999) was adopted.

Consequently, first of all, for case series "A1-A1" as parameter study for shear reinforcement, it was found that the degradation trends of shear reinforced cases S1, A1 and A2 presented good agreement with the proposed curves; the start ductility point for rapid degradation of case A3 without shear reinforcement, however, was earlier than the other cases and overestimated by the proposed degradation curves. Thus, it was concluded that the arrangement of shear reinforcement could significantly delay the start ductility point for rapid degradation of shear strength, and larger percentage of shear reinforcement provided more evident effect. For case series "B1-B2" as parameter study for shear span to effective depth ratio, the result was obvious that the start ductility point for rapid degradation of short column B1 and B2 were much earlier than the standard S1 and the proposed degradation curves. The start ductility point for rapid degradation was increased with the decrease of shear span to effective depth ratio. And it should be emphasized that the previously proposed degradation curves by Priestley and Ohe and Yoshikawa greatly overestimate the start ductility point for rapid degradation of the short members, the columns B1 and B2. For case series "C1-C2" as parameter study for tension reinforcement ratio, like that of standard S1, the degradation trend of case C1 roughly agreed with the proposed degradation curves, whereas the case C3 presented earlier start ductility point for rapid degradation than the other cases and the proposed curves. And it was also concluded that the start ductility point for rapid degradation was advanced by the increasing of tension reinforcement ratio. And it was lessoned that the previously proposed degradation curves by Priestley and Ohe and Yoshikawa might overestimate the

start ductility point for rapid degradation for the member with great tension reinforcement, for example, the column C2. Finally, for case series “D1-D2” as parameter study for axial compression load, it was notable that the increased axial compression load led to earlier start ductility point for rapid degradation, and the statistical curves by Priestley and Ohe and Yoshikawa was likely to overestimate the start ductility point for rapid degradation for the RC members under relatively great axial compression load.

4.5 Effect of structural variables on shear resistance mechanisms

In this section, the load-displacement hysteresis for evaluation of shear strength degradation, discussed in chapter 4.4, were decoupled into a variety of shear resistance mechanisms, i.e. beam action, arch action, truss action and concrete contribution, which was a same procedure as that employed in chapter 3.6. And the author collected the shear resistance mechanisms corresponding to the degraded shear strengths and conducted comparative analyses for each case series.

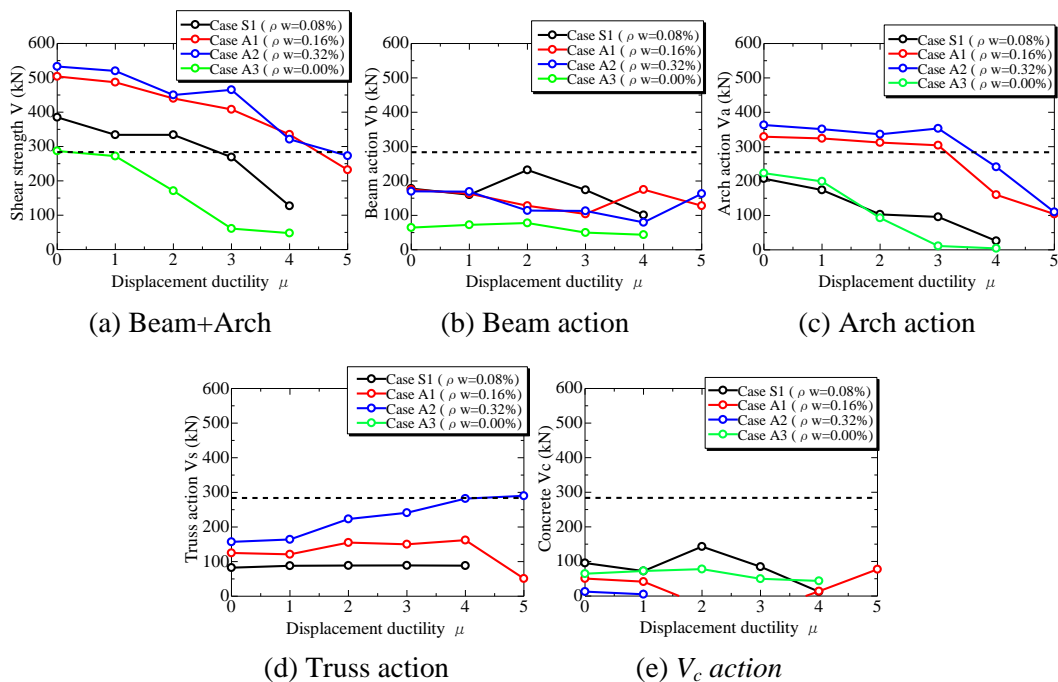


Figure 4. 16 Comparison of shear resistance mechanisms (ρ_w)

Firstly, the decoupled result for case series “A1-A3” are introduced. **Figure 4.16a** shows the shear strength degradations, in the form of combined effect of beam action and arch action, with the increased displacement ductility. By the way, the dotted line represents the grade of shear cracking load calculated based on the equation proposed by Niwa et al. (1986) and same for the dotted lines in **Figures 4.16b-e, Figure 4.17, Figure 4.18** and **Figure 4.19**. The original shear strength ($\mu=0$) was enhanced with the increased shear reinforcement ratio except for that of case A2 presenting a close grade to that of case A1, as case A2 in the numerical analyses for evaluation of shear strength suffered shear compression failure, because of the excessive amount of shear reinforcement. The shear compression failure of case A2 was understood because the stirrups were not yielded at failure points in the analyses for evaluation of shear strength. In the other cases S1, A1, A3, however, quite differently, the stirrups had been yielded before shear failure. Thereby, the result of case A2 was suggested to be removed from discussion. It was also noted that the increase of shear reinforcement ratio in a degree slowed the degradation rate of shear strength.

The results of beam action and arch action are illustrated in **Figure 4.16b-c**, and as the essential reason of shear strength degradation lower than the shear demand corresponding to flexural strength, the evident degradation of arch action with increased displacement ductility was noted. The lesson that higher shear reinforcement would more effectively slow the degradation rate of arch action should be kept in mind. Differently, the beam action generally was kept stable before shear failure and did not affect much on the shear strength degradation.

In addition, the decoupling truss actions and concrete contributions for beam actions are given in **Figure 4.16d-e**. The higher original truss action ($\mu=0$) due to higher shear reinforcement ratio was confirmed, and the truss actions were found not being affected by increased displacement ductility, as stirrups in columns were already yielded that has been explained in chapter 3.6.2. The concrete contributions of case S1 and A3 were kept

stable before shear failure. But those of the cases A1 and A2 were decreased lower than zero in the cases that $\mu > 1$, because the orientations of critical shear cracks in the numerical analyses for evaluation of shear strength were found greater than our assumption, i.e. 45° , resulting in overestimation of truss actions.

Secondly, the decoupling result for case series “B1-B2” are discussed. The degradation of each classification of shear resistance mechanism is compared by **Figure 4.17**. **Figure 4.17a** shows the shear strength degradations with the increased displacement ductility. Although the original shear strength of shorter column was higher, it was reduced at higher rate with the increased displacement ductility. After decoupling shear strength into beam action and arch action, it became clear that degradation of arch action determined the shear performance and shear strength degradation, that is, the more rapid degradation of shear strength in shorter column was attributed to the more rapid reduction of arch action (see **Figure 4.17c**). On the other side, the beam actions were kept stable before shear failure (see **Figure 4.17b**).

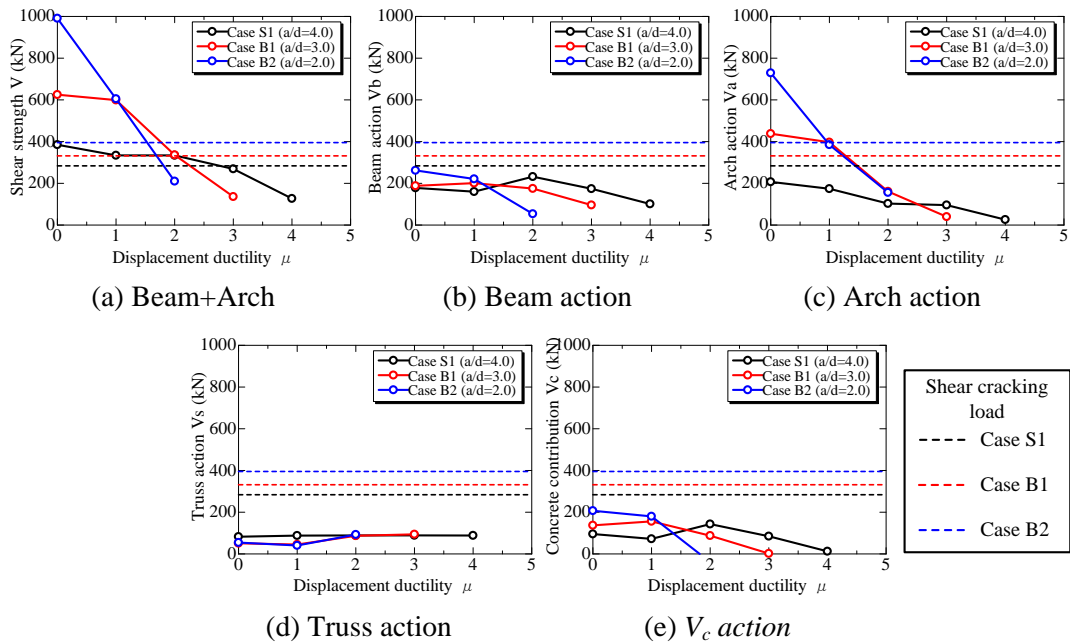


Figure 4. 17 Comparison of shear resistance mechanisms (a/d)

With respect to truss action and concrete contribution, the same percentage of shear reinforcement contributed to a close grade of truss action among the three cases, which was nearly not affected by the increased displacement ductility (see **Figure 4.17d**); and the concrete contribution showed same degradation process as beam action, that is, it was nearly kept stable before shear failure (see **Figure 4.17e**).

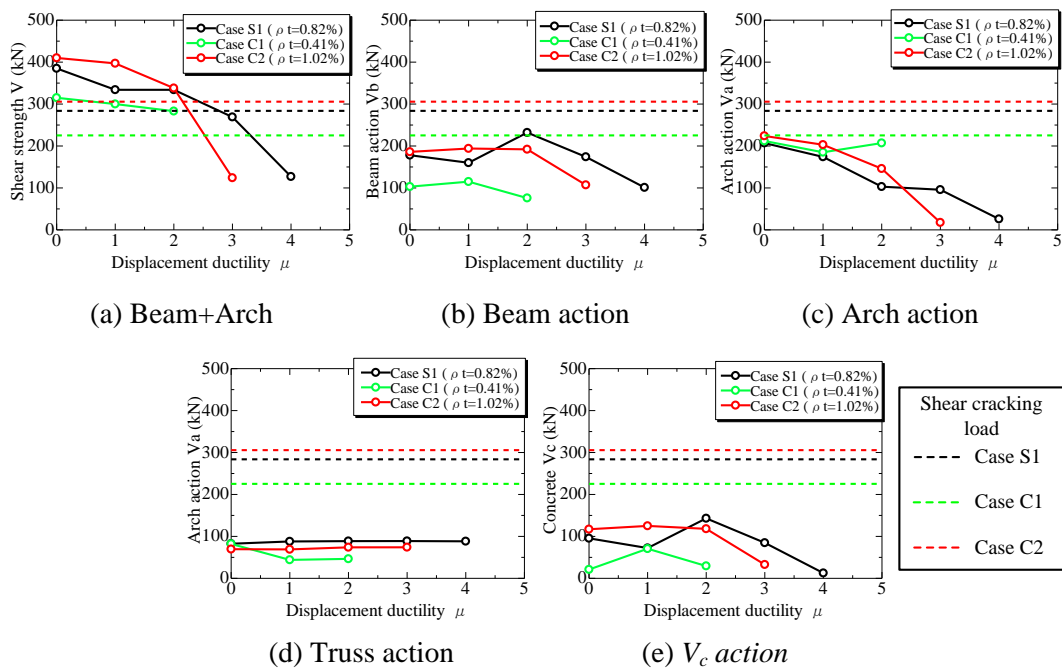


Figure 4. 18 Comparison of shear resistance mechanisms (ρ_t)

The decoupling shear resistance mechanisms for shear strengths of case series “C1-C2” is explained by **Figure 4.18**. **Figure 4.18a** is the comparison of shear strength degradations with the increased displacement ductility, where it was understood that higher percentage of tension reinforcement led to more rapid degradation of shear strength although it could contribute to relatively high original shear strength. And the rapid degradation of shear strength was found being caused by the more rapid degradation of arch action (see **Figure 4.18c**), while beam actions were kept stable before shear failure (see **Figure 4.18b**). Thus, like the result discussed in previous sections, arch action

governed the degradation of shear strength, regardless of the change of tension reinforcement ratio.

Regarding to the truss action and concrete contribution, once more, it was confirmed that the same percentage of shear reinforcement for the three cases contributed to a close grade of truss action, which was not decreased with the increased displacement ductility (see **Figure 4.18d**); and the concrete contributions sustained same degradation tendencies as the beam actions (see **Figure 4.18e**).

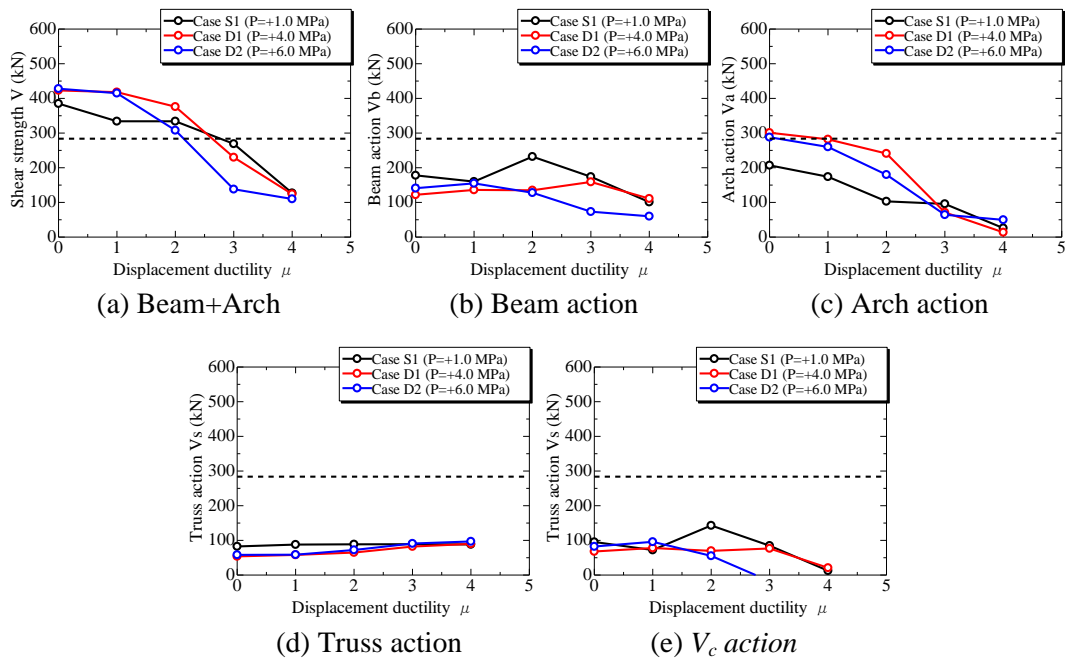


Figure 4. 19 Comparison of shear resistance mechanisms (P)

Lastly, the decoupling shear resistance mechanisms for shear strengths of case series “D1-D2” is explained by **Figure 4.19**, in which, the dotted lines represent the shear cracking load for standard case S1 by Niwa equation (Niwa et al. 1986). **Figure 4.19a** is the comparison of shear strength degradations with the increased displacement ductility, where it was apparent that higher grade of axial compression load led to more rapid degradation of shear strength. And similar to the previous result for other case series, the

rapid degradation of shear strength was resulted from the more rapid degradation of arch action (see **Figure 4.19c**), while the beam actions were kept stable before shear failure (see **Figure 4.19b**).

Moreover, it was further confirmed that the truss actions for the three cases were in close grade and not changed with the increased displacement (see **Figure 4.19d**); and the concrete contributions presented the same degradation tendencies as that of the beam actions (see **Figure 4.19e**).

4.6 Summary and conclusions

In this chapter, as a continuing study of chapter 3, the author first simulated the shear performances of RC columns with different structural variables, i.e. shear reinforcement ratio (ρ_w), shear span to effective depth ratio (a/d), longitudinal reinforcement ratio (ρ_t) and axial compression load (P) by 3-D RBSM, and then investigated the effect of structural variables on shear strength degradation process by the way of shear strength degradation curve. Finally, the effects of structural variables on degradation of shear resistance mechanisms of RC member were investigated.

As achievements, above all, it was confirmed that the shear strength degradation curves of RC columns with different structural variables assessed by 3-D RBSM presented similar degradation tendencies to those proposed based on test data, which in turn proved the reliability of analysis.

Secondly, it was lessoned that the progressive degradation of arch action with increased displacement ductility was the essential reason of the degradation of shear strength, which resulted in shear failure after yielding of RC member subjected to cyclic loading, regardless of the varying factors ρ_w , a/d , ρ_t , P considered in this chapter. And this finding confirmed the mechanism of shear strength degradation summarized in chapter 3.

Thirdly, it was revealed that more arrangement of shear reinforcement could effectively

delay the start ductility point for rapid degradation of arch action and shear strength.

Moreover, it also became clear that the smaller shear span to effective depth ratio could significantly advance the start ductility point for rapid degradation of arch action and shear strength.

In addition, an achievement that more arrangement of tension reinforcement would lead to earlier start ductility point for rapid degradation of arch action and shear strength.

Finally, the result implied that the higher grade of axial compression load could also lead to earlier start ductility point for rapid degradation of shear strength and arch action.

5. A Factor on Degradation of Arch Action

5.1 Introduction

Based on the achievements obtained from the preceding chapters 3 and 4, it was clear that the first progressive degradation of arch action with the increased load cycles was the critical factor for the shear failure after yielding of the RC member subjected to cyclic loading, and this degradation behavior could not be found under one-side repeated loading analysis. The reason of arch action degradation due to cyclic loading, however, is still unrevealed and needs deeper explanation.

A typical behavior of RC member under cyclic loading is noted that a flexural crack propagates from one side under positive loading and afterwards might be connected by another flexural crack propagates from opposite side under negative loading, namely, the section cracks usually form and propagate (see **Figure 5.1**). And the formation of section crack is regarded as the most essential different behavior from that under one-side repeated loading or monotonic loading where the flexural cracks merely propagate from tension side. Hence, it is supposed that the typical deformation of section crack is a primary reason for the arch action degradation.

This chapter aims to confirm the effect of section crack on the shear strength and the arch action of a RC member, by 3-D RBSM, and the method for introducing section crack by tension analysis of longitudinal reinforcement is also presented.

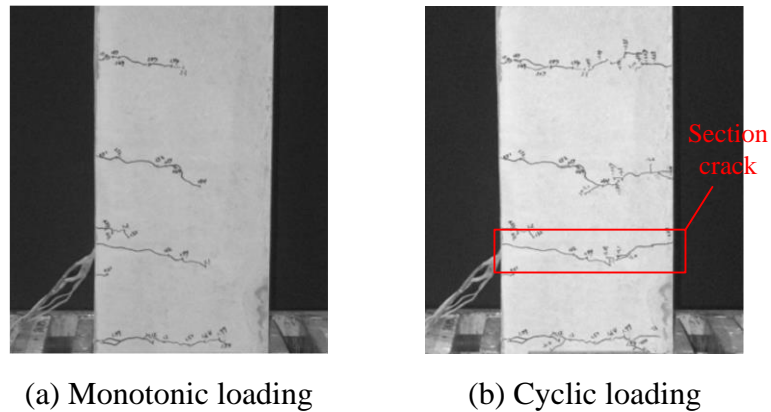


Figure 5. 1 Different deformation behaviors between monotonic loading and cyclic loading (Mizuno et al. 2010)

5.2 Evaluation method of shear strength of RC member with section pre-crack

The RC column that analyzed in chapters 2 and 3 is regarded as the objective model in this chapter, and the concrete and steel reinforcement properties can refer to chapter 3. Before the loading analysis for evaluation of shear strength, a section pre-crack was first introduced by an approach applying axial tension load on the link elements of longitudinal reinforcement (see **Figure 5.2**).

In the procedure of section pre-crack introduction, as the first step, four link elements in longitudinal reinforcement located at the same section, a certain distance from footing, are fixed, and meanwhile another four link elements located at the same section 200 mm farther away from footing are horizontally pulled by displacement control (see step 1 in **Figure 5.2**). Consequently, after entering plastic stage of the tensioned longitudinal reinforcement, a section pre-crack is generated approximately in the middle plane between the previous two sections where the eight link elements located at. The initiation of section pre-crack is attributed to the relatively low plastic tensile deformability of concrete, compared with that of the steel reinforcement. With respect to the width of

section pre-crack, it can be determined by the tensile displacement of link elements.

In the second step, once a section pre-crack with the target width is introduced, the previously tensioned and fixed link elements would be unloaded and become completely free in movement. The section pre-crack, however, would remain there due to the residual plastic deformation of longitudinal reinforcement (see step 2 in **Figure 5.2**).

Through the above two steps, a section pre-crack with a target width can be introduced. At last, in the third step, after increasing yield strength of longitudinal reinforcement to 900 MPa, the monotonic loading analysis is performed by displacement control to evaluate the shear strength, which is a same method as the evaluation of degraded shear strength described in chapter 3 (step 3 in **Figure 5.2**).

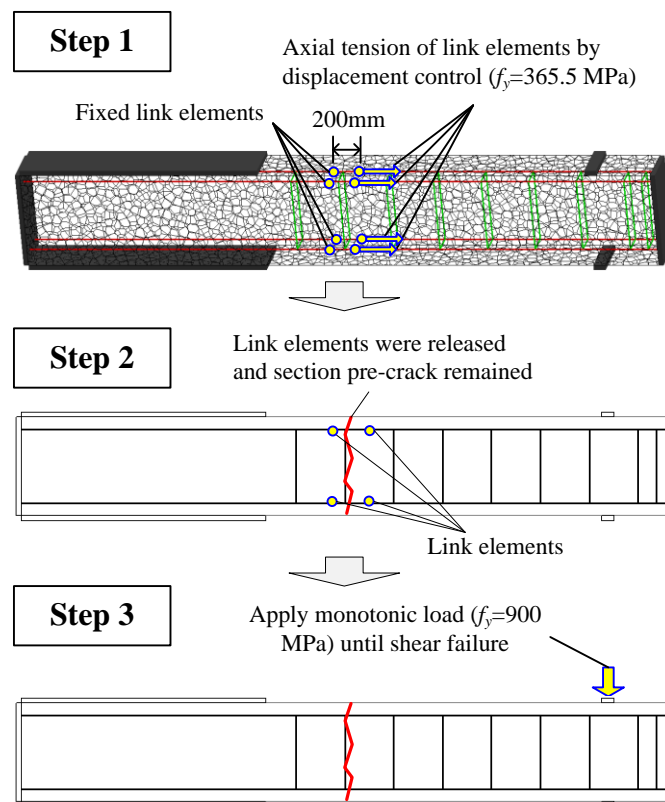


Figure 5. 2 Method for evaluation of shear strength of RC member with section pre-crack

5.3 Effect of section pre-crack on shear strength and arch action

In order to conduct a sufficient investigation, the pre-cracks were introduced in three critical sections where section pre-cracks usually form under cyclic loading: footing-column intersection, the section $1.0d$ (d is the effective depth of RC column) far away from the footing-column intersection and the section $2.0d$ far away from the footing-column intersection. Moreover, for each critical section, three grades of crack widths (0.5, 1.5, 2.5 mm) were taken into account.

5.3.1 Pre-crack located at footing-column intersection (Case 1)

The images of introduced pre-cracks with different widths located at footing-column intersection are illustrated in **Figure 5.3** (the deformations are magnified by ten times), and it was evident that the approach introduced in chapter 5.2 was effective to achieve a section pre-crack with target width.

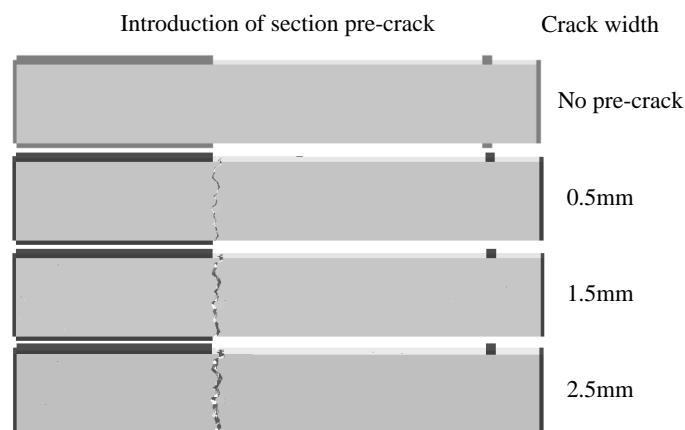


Figure 5. 3 Introduction of section pre-cracks (Case 1)

The load-displacement relationships for evaluation of shear strengths of the four pre-cracked columns in **Figure 5.3** are plotted in **Figure 5.4**. As a result, it was found that with the increase of crack width, although the initial stiffness of RC column was gradually decreased, which was resulted from the softening at the position of pre-crack, the shear

strength did not drop so much (less than 15% of the non-cracked case). Thus, it was clarified that the section pre-crack no wider than 2.5 mm at footing-column intersection had quite limited effect on shear strength.

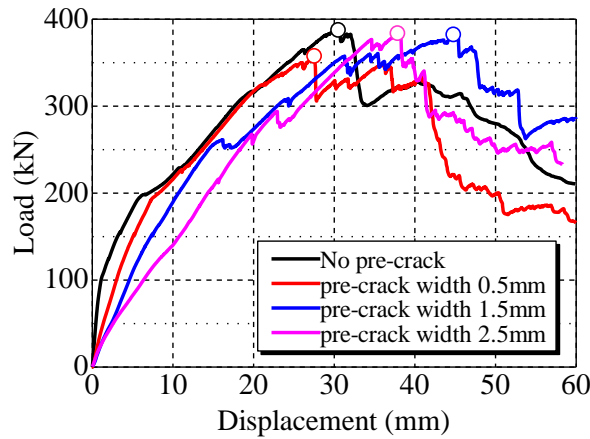


Figure 5. 4 Load-displacement relationships (Case 1)

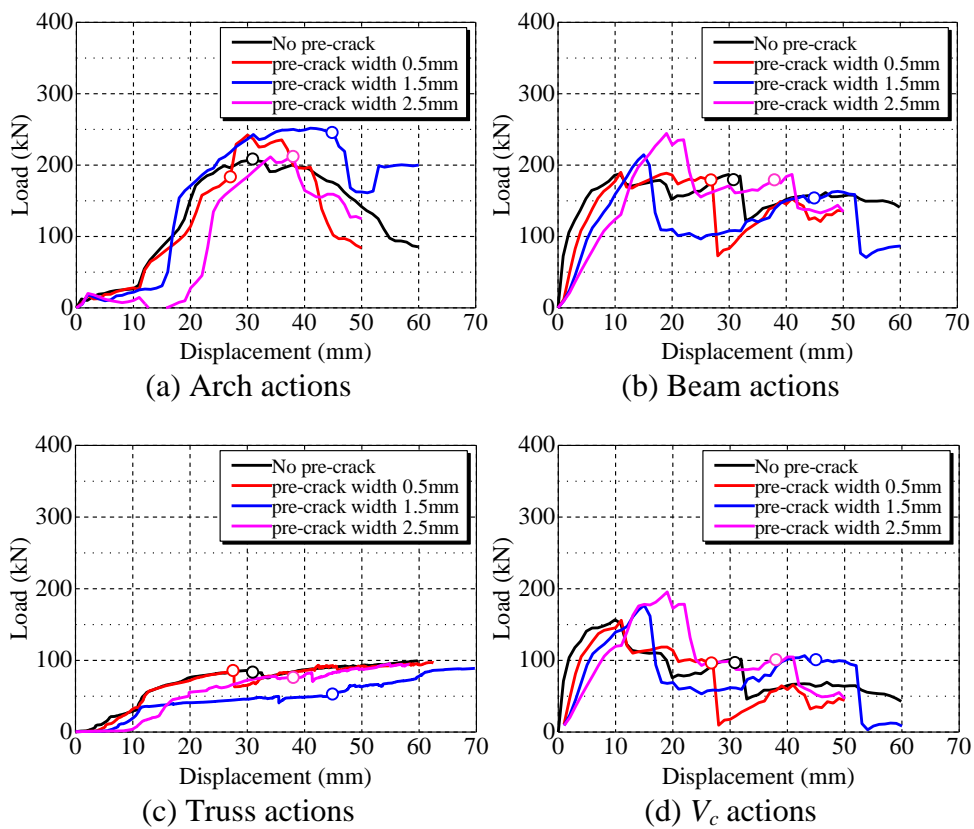


Figure 5. 5 Result of shear resistance mechanisms (Case 1)

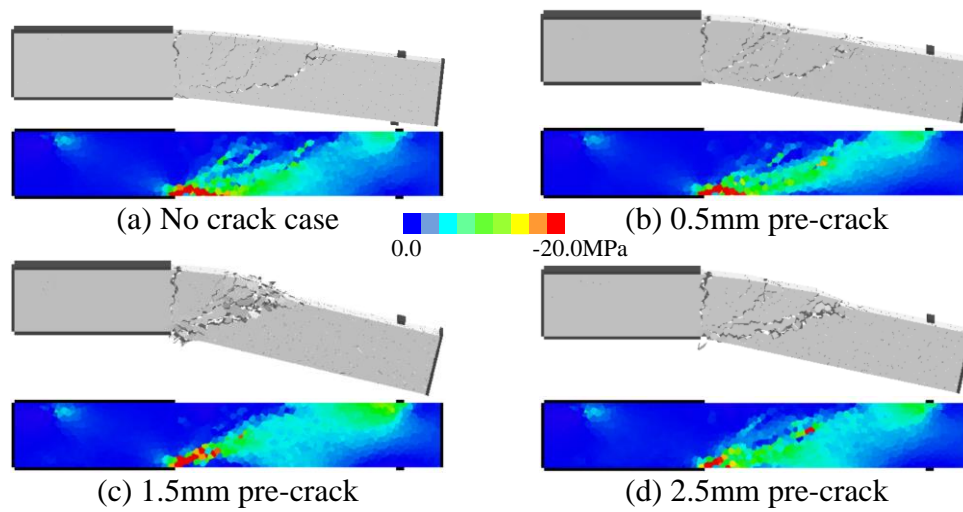


Figure 5. 6 Deformations and axial compressive stress distributions (Case 1)

Furthermore, the load-displacement relationships for evaluation of shear strength shown in **Figure 5.4** were decoupled into the beam actions, arch actions, truss actions and concrete contributions by the same approach discussed in previous chapter 2.3 and the decoupling results are shown in **Figure 5.5**. Above all, it was notable that the shear resistance mechanisms of the pre-cracked columns overall developed in the same way as those of the non-pre-cracked one, that is, the shear resistance was mainly provided by the beam action before shear cracking and was dominated by the arch action after the shear cracking. Herein, the marked points which correspond to the maximum loads marked in **Figure 5.4** are focused on, and it was found that the shear resistance mechanisms for shear strengths were not significantly affected by the section pre-cracks, that is, the shear resistance mechanisms of the pre-cracked columns were in the similar grade to those of the non-pre-cracked case. Therefore, it was clarified that the section pre-crack located at the footing-column intersection would not significantly reduce the capacity of arch action

In addition, the deformation behaviors (magnified by eight times) and the axial compressive stress distributions (negative in criterion standards for compressive effect) at maximum loads are compared in **Figure 5.6**. It was seen that the section pre-cracks almost did not change the shear crack pattern, and the fan-shaped axial compressive

stresses along the critical shear cracks of the pre-cracked columns could form in a close grade to that of the no pre-crack case.

5.3.2 Section pre-crack $1.0d$ far away from footing-column intersection (Case 2)

In this section and the following chapter 5.3.3, same investigation as the work performed in section 5.3.1 are carried out and the analytical results will be discussed one by one. In terms of the results for the section pre-crack $1.0d$ far away from the footing-column intersection, the load-displacement relationships for evaluation of shear strengths are shown in **Figure 5.7**. Different from the effect of section pre-crack on shear strength shown in **Figure 5.4**, the shear strength was obviously decreased with the increased pre-crack width, particularly if the pre-crack width exceeded 0.5 mm, the decreasing rate became relatively high, and the shear strength of the 2.5 mm pre-cracked column dropped to 68% of the non-pre-cracked one. Therefore, it was clear that the section pre-crack $1.0d$ far away from the footing-column intersection would cause great loss of shear strength.

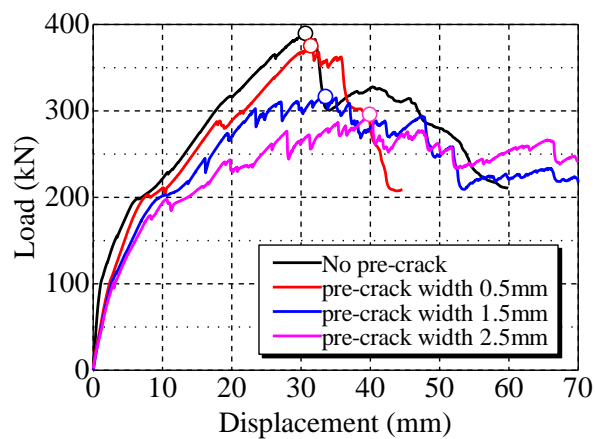


Figure 5.7 Load-displacement relationships (Case 2)

Moreover, the result for shear resistance mechanisms are shown in **Figure 5.8**. It was worthy note that the degradation of shear strength with increased pre-crack width was mainly attributed to the degradation of arch action, while the beam actions, truss actions and concrete contributions were not obviously affected by section pre-crack.

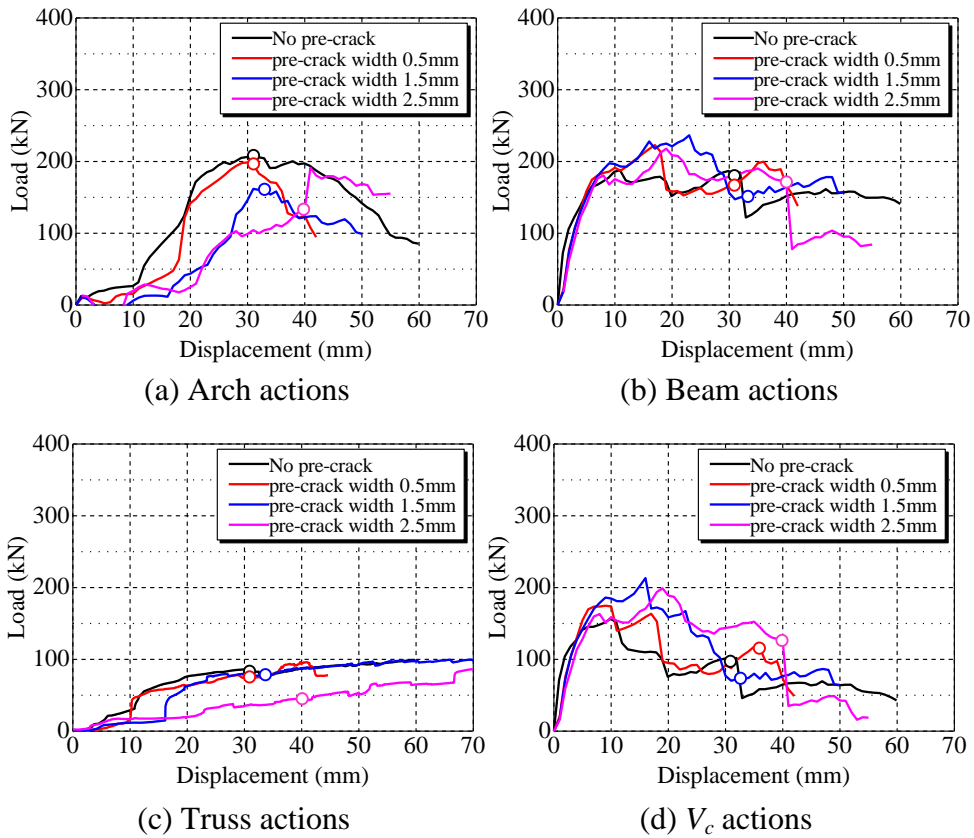


Figure 5. 8 Result of shear resistance mechanisms (Case 2)

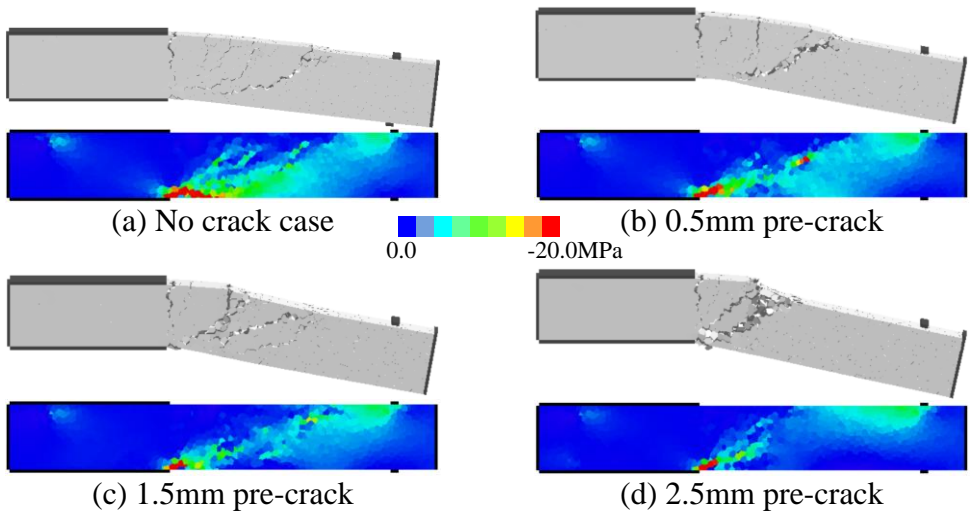


Figure 5. 9 Deformations and axial compressive stress distributions (Case 2)

The degradation of arch action due to section pre-crack also could be understood by the comparisons of deformations and axial compressive stress states as shown in **Figure 5.9**. For the deformation behaviors, the critical shear cracks of the pre-cracked columns, which crossed initial pre-cracks, developed more severely than that of the no pre-crack case. And the fan-shaped stresses along the critical shear cracks of the pre-cracked columns were evidently lower than that of the non-pre-cracked case, and the wider pre-crack led to the severer stress loss, which signified that the formation of section pre-crack $1.0d$ away from the footing-column intersection caused the degradation of arch action.

5.3.3 Section pre-crack $2.0d$ far away from footing-column intersection (Case 3)

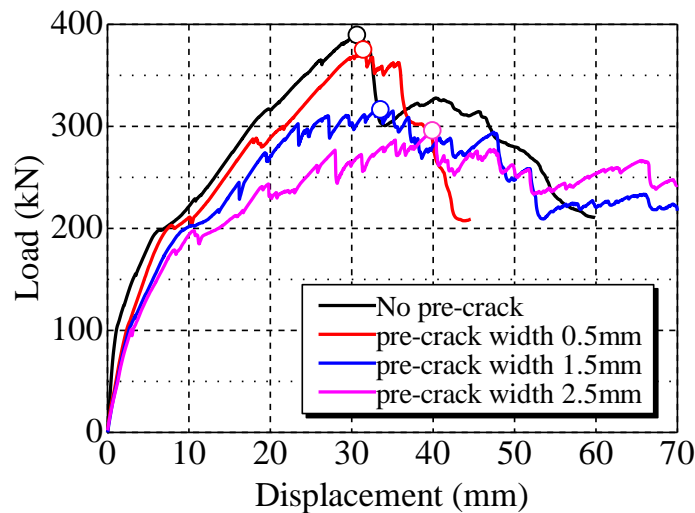


Figure 5. 10 Load-displacement relationships (Case 3)

With respect to the results for the section pre-crack $2.0d$ far away from the footing-column intersection, the load-displacement relationships for evaluation of shear strengths are shown in **Figure 5.10**. Very similar to the effect of section pre-crack on shear strength shown in **Figure 5.7**, the shear strength was significantly decreased with the increased pre-crack width as well. In particular, in the case of the pre-crack width exceeding 0.5 mm, the decreasing rate suddenly became high, and the shear strength of the 2.5 mm pre-cracked column was decreased to 64% of the non-pre-cracked one. Thus, it was learned

that both the section pre-cracks $1.0d$ and $2.0d$ far away from the footing-column intersection would cause obvious degradation of shear strength.

Additionally, the decoupling shear resistance mechanisms are illustrated in **Figure 5.11**. It was clarified that the arch action was reduced with the increase of pre-crack width, and this resulted in the degradation of shear strength shown in **Figure 5.10**, while the beam actions, truss actions and concrete contributions were not greatly affected by the section pre-cracks.

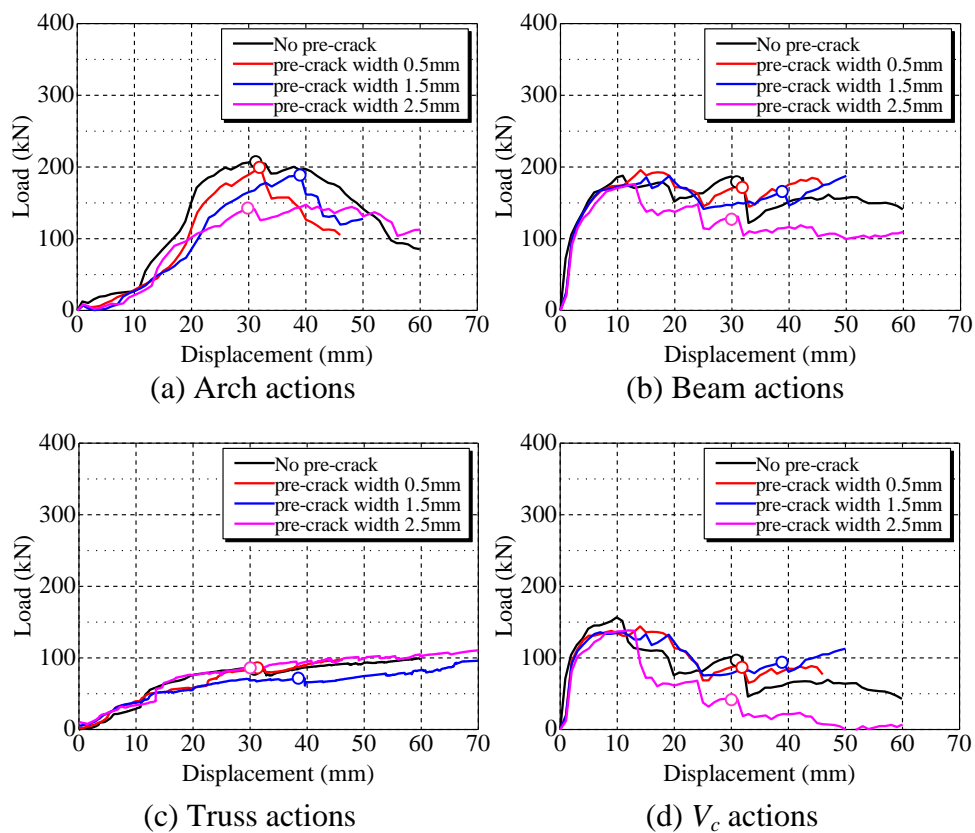


Figure 5. 11 Result of shear resistance mechanisms (Case 3)

The deformations and axial compressive stress states of the four cases at maximum load points are shown in **Figure 5.12**. It could be apparently observed that the critical shear cracks of the pre-cracked columns crossed the initial section pre-cracks and presented severer damage. The fan-shaped axial stresses along the critical shear cracks of

the pre-cracked columns became lower than that of the non-pre-cracked case. The wider the pre-crack was, the severer the stress loss became.

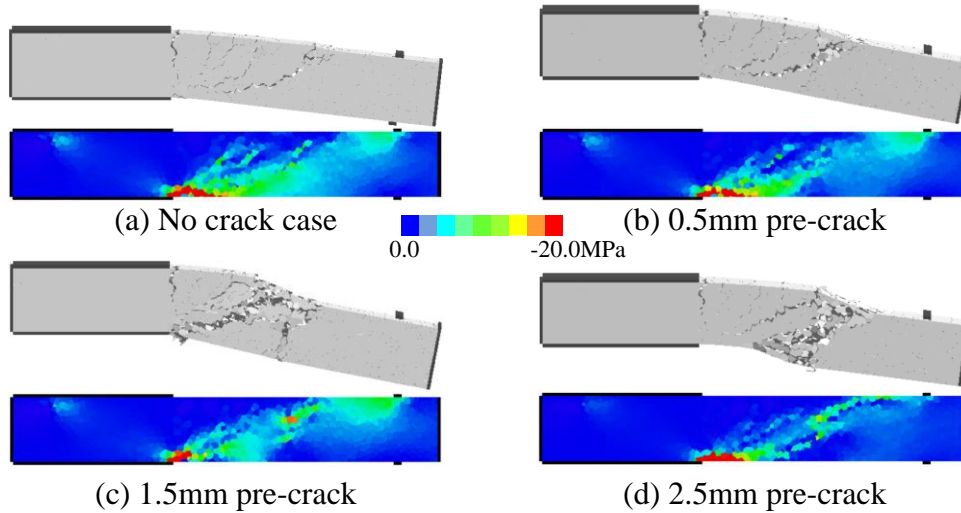


Figure 5. 12 Deformations and axial stress distributions (Case 3)

5.4 Summary and conclusions

In this chapter, in order to confirm the mechanical reason of typical arch action degradation of RC member subjected to cyclic loading, the author numerically investigated the effect of the section pre-crack, which usually form due to cyclic loading, on the degradations of shear strength and arch action. As a consequence, it was clarified that the formation of section pre-cracks located at the position $1.0d$ or $2.0d$ (d : effective depth of column) far away from the footing-column intersection was a primary factor for the degradation of arch action, while the section pre-crack located at the footing-column intersection had very minor effect on the shear strength.

6. Experimental Investigation of Effect of Section Pre-crack on Shear Strength and Mechanism of Shear Strength Degradation due to Section Pre-crack

6.1 Introduction

The first degradation of arch action has been pointed out to be the main reason of shear strength degradation and shear failure after yielding under cyclic loading (refer to chapters 3 and 4). In chapter 5, it is numerically clarified that the formation of section crack, which ordinarily forms at the plastic hinge of RC member under cyclic loading, can significantly reduce arch action. The effect of section crack, however, has not been experimentally verified.

As introduced in chapter 1.2.4, to date, only a few researches studied the effect of section crack on shear. Pimanmas and Maekawa (2001a) for first time experimentally penetrated multiple section pre-cracks in RC beams (the shear span to depth ratio is 2.4) designed in shear by 4-point reversed flexural loading; thereafter, they found that the section pre-cracks enhanced the shear strength compared with the non-cracked beam by 3-point loading, because the pre-cracks obstructed the continuous propagation of diagonal shear cracks, which was further demonstrated by their finite element analyses (Pimanmas

and Maekawa 2001b, 2001c). The section pre-cracks by 4-point reversed loading dispersedly located at the entire shear span, and the crack widths varied in a large range from 0.02 to 5.0 mm and could not be accurately controlled. Quite differently, however, the section cracks due to cyclic loading generally initiate and propagate only at the zone where high moment affects, and usually present a similar width at a certain loading stage. Thus, it is desirable to develop an experimental method to introduce a section pre-crack located at high bending zone of shear span and investigate its damage to shear performance.

In this study, firstly an experimental approach was attempted to introduce section pre-cracks at the high bending zone of RC beams designed for shear. In detail, one non-cracked RC beam for behavioral comparison and two beams with 0.5 and 1.0 mm-wide section pre-crack, respectively, were 3-point loaded, and the effect of pre-crack on shear strength was clarified. Secondly, a numerical approach by employing 3-D RBSM was put forward to simulate the different shear behaviors of the test beams with and without section pre-cracks. Finally, the shear resistances by numerical analysis of the three beams were decoupled into the contributions of beam action and arch action by utilizing the local stress result with an intention to understand the mechanism of shear strength degradation due to section pre-crack.

6.2 Experimental setup

6.2.1 Design of specimens

One non-cracked RC short beam (No. A) and two beams with a single section pre-crack 0.5 and 1.0 mm in width, respectively (No. B and No. C), were tested. The three beams in same dimension were designed failing by shear. As shown in **Table 6.1** and **Figure 6.1**, the beams are 1,600 mm long and have a cross section of 300 mm×150 mm. The shear span to effective depth ratio is 2.36 so that the beams ordinarily suffer shear

compression failure. Two tension reinforcing bars of type D29 were arranged with a concrete cover thickness of 45 mm, i.e., the tension reinforcement ratio is 3.36%, and the elastic modulus and the yield strength of them are 182 GPa and 358 MPa, respectively. In order to facilitate the observation of shear behavior, the stirrups of type D6 were arranged in one side (the left span in **Figure 6.1**) to fail the beams in the other span, where the shear behavior was focused on and video recorded. By standard cylinder compression test, it was known that the concrete compressive strength of No. A, C and No. B are 34.1 MPa and 29.2 MPa, respectively.

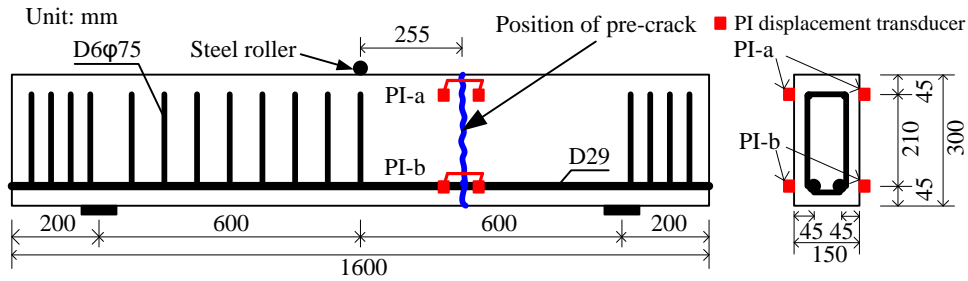


Figure 6. 1 Details of RC beams

Table 6. 1 Material property of RC beams

Beam No.	a/d	Tension reabr (D29)			Compressive strength of concrete f_c (MPa)	Width of pre-crack w (mm)	Designed shear cracking load V_{con} (kN)	Designed shear strength V_u (kN)
		ρ_t (%)	f_y (MPa)	E_s (GPa)				
A					34.1	0.0	141	211
B	2.35	3.36	358	182	29.2	0.5	134	190
C					34.1	1.0	141	211

According to the studies by Niwa et al. (1983 and 1986), the shear cracking load V_{con} and the shear strength under shear compression failure V_u for the three beams were predicted (see **Table 6.1**) by the previous Equation 3.3 and Equation 6.1, without considering the effect of pre-crack. And the current JSCE standard specification (2012) are on the basis of these equations:

$$V_u = \frac{0.24 f_c'^{2/3} (1 + \sqrt{100 \rho_t}) (1 + 3.33 r/d)}{1 + (a/d)^2} b_w d \quad 6.1$$

where, f_c' is the concrete compressive strength; b_w is the width of beam; a is the length of shear span; d is the effective depth of beam; ρ_t is the tension reinforcement ratio; r is the width of loading plate along beam axis.

Herein, as an improving factor for shear strength, the width of loading plate r is as small as 20 mm, because the shear load was applied through a steel roller in our experiment (see **Figure 6.1**).

6.2.2 Approach for introducing section pre-crack

In beams No. B and C, a 0.5 mm and 1.0 mm wide single pre-crack was introduced, respectively, in the target section which was the effective depth (255 mm) far away from the loading point, since it was considered that the section crack due to cyclic loading ordinarily forms nearby this position where relatively high bending moment affects.

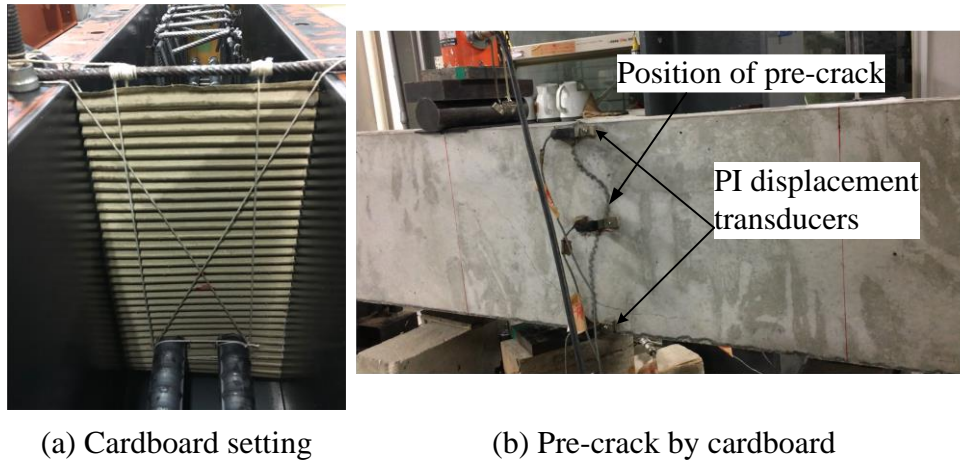


Figure 6. 2 Details of RC beams

In order to introduce section pre-crack with a desirable width, the soft corrugated cardboards, i.e., the inlayers of common carton box, were set at the target section inside the steel framework before concrete casting (see **Figure 6.2a**), considering that the corrugated shape of the cardboard can generate interlocking effect in crack interface. The desirable pre-crack widths were achieved by superimposing cardboard (0.25 mm-wide

for one piece), two pieces for 0.5 mm and four pieces for 1.0 mm. Moreover, the cotton thread was utilized to fix the cardboard in framework, to prevent the movement of cardboard caused by concrete flow during casting and vibrating as far as possible. The image of introduced pre-crack in beam No. C is illustrated in **Figure 6.2b**.

In the process of shear loading, not only the shear load and the vertical displacements at loading and support points were measured but also the opening and closure behaviors of section pre-crack were recorded by PI-shape displacement transducers, which were set along the pre-crack on compression (PI-a) and tension (PI-b) sides, respectively (see **Figure 6.1** and **Figure 6.2b**).

6.3 Experimental result

6.3.1 Load-displacement relationship and failure mode

The load-displacement relationships by experiment are displayed by solid curves in **Figure 6.3**. In addition, the shear cracking loads V_{cr} and the shear strengths V_{ur} are listed in **Table 6.2**. Overall, it was notable that the initial stiffness of pre-cracked beams significantly decreased compared with the non-cracked one, attributed to the closure behavior of pre-crack. And the decreasing rate was higher in the wider pre-cracked beam (No. C). In terms of shear cracking load, the non-cracked beam (A3 in **Figure 6.3**, 136 kN) was slightly lower than the previous prediction (141 kN for No. A in **Table 6.1**). In contrast, the shear load in pre-cracked beam No. B nearly was in same grade (B4 in **Figure 6.3**, 142 kN) and that in pre-cracked beam No. C was slightly lower (C4 in **Figure 6.3**, 108 kN), which implied that the section pre-cracks had minor effect on load for critical shear cracking. With regard to the shear strength result, the non-cracked beam No. A presented a higher grade (A5 in **Figure 6.3**, 234 kN) than the prediction (211 kN for No. A in **Table 1**) as previously explained, and it was worthy note that the strengths of pre-cracked beams obviously declined compared with that of the non-cracked one, 38%

decrease for beam No. B (144 kN) and 41% decrease for beam No. C (139 kN). Therefore, it became clear that the pre-cracks in the section which was effective depth far away from loading point can significantly reduce the shear strength of short beam, which presented a same effect of the section pre-crack on shear strength of RC column obtained in chapter 5. This result was incompatible to the conclusions in the study by Pimanmas and Maekawa (2001a) where the multiple section pre-cracks enhanced the shear strength of RC short beams.

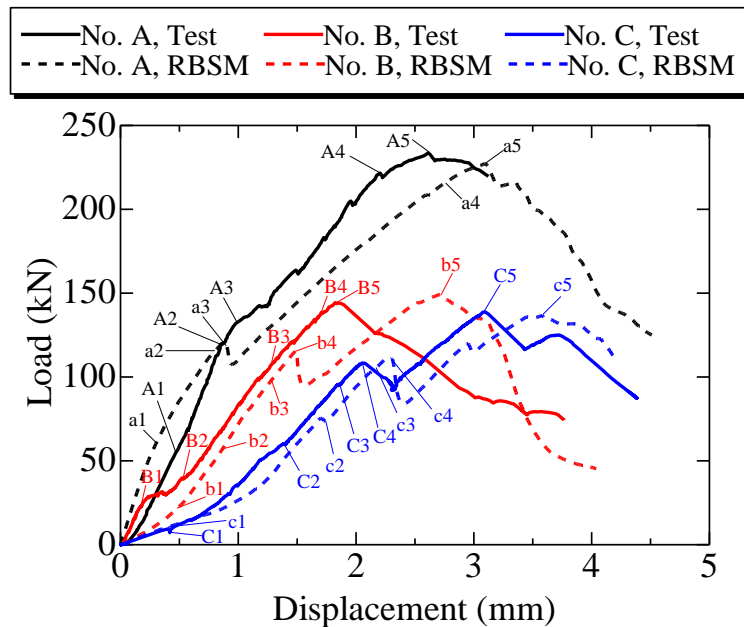


Figure 6. 3 Load-displacement relationships

Table 6. 2 Result of shear load

Beam No.	Width of pre-crack w (mm)	Tested shear cracking load V_{cr} (kN)	Numerical shear cracking load V'_{cr} (kN)	Tested shear strength V_{ur} (kN)	Numerical shear strength V'_{ur} (kN)
A	0.0	136	121	234	227
B	0.5	142	116	144	149
C	1.0	108	111	139	137

Figure 6.4 compares the test result in this study and the result by Pimanmas et al. (2001), where the horizontal axis standards for average section crack width in shear span and the vertical axis standards for ratio of shear strength by loading test to the shear

strength calculated based on Equation 6.1. Consequently, it was understood that, for Pimanmas's result, the shear strength of reference beam without section crack presented an obvious lower grade than the calculation by Equation 6.1 while the shear strengths of the section cracked beams showed similar grade to the calculation, which means that the section cracks increased the loading carrying capacity because of the excessively low grade of the reference beam. On the contrary, the shear strength of our reference beam presented a similar grade to that of the calculation, and the decrease of shear strength due to section crack was very evident.

The failure modes of the three beams are illustrated in **Figure 6.5**. It was observed that at ultimate stage the shear compression failure occurred nearby the loading plate together with a severe spalling of concrete cover in the three beams. However, as the deformation characteristics of pre-cracked beams No. B and C, a second diagonal crack above the critical one and a horizontal crack along tension reinforcing bars were noted (see **Figure 6.5b-c**). The process of crack propagation will be more detailed discussed in the following chapter 6.4.3.2 to explain the effect of pre-crack on shear behaviors.

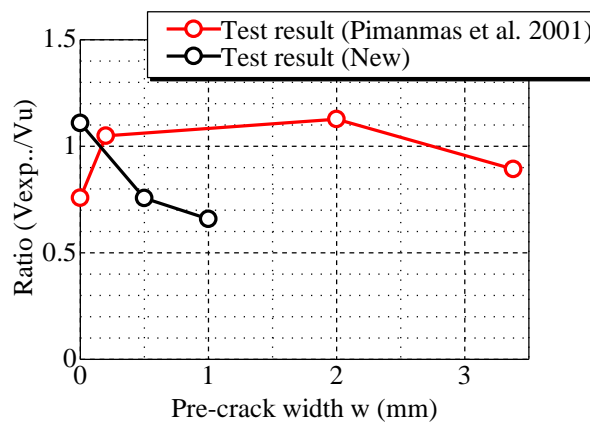
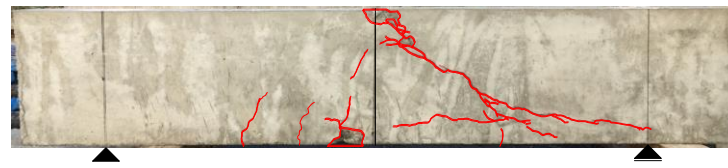
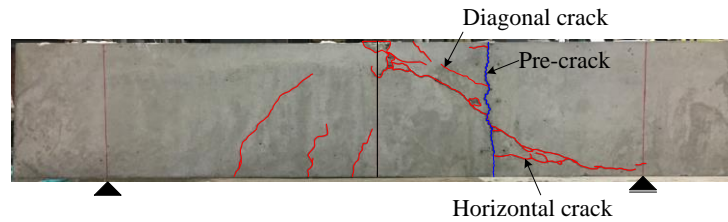


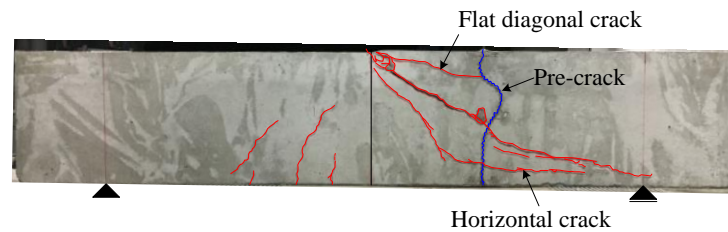
Figure 6. 4 Comparison of test result with the result by Pimanmas et al. (2001)



(a) Beam No. A



(b) Beam No. B



(c) Beam No. C

Figure 6. 5 Crack patterns after shear failure

6.3.2 Opening and closure behaviors of section pre-crack

The opening and closure behaviors of the pre-cracks recorded by PI-shape displacement transducers (measurement points are shown in **Figure 6.1**) are displayed in **Figure 6.6** by solid curves, combined with the load-displacement relationships. Herein, the average measurement by PI-a or PI-b on front and back surfaces are presented and the negative width in diagram standards for a closure procedure.

Figure 6.6a shows the result of beam No. B. In terms of closure behavior by PI-a at compression side, it was understood that the pre-crack closed at a constant speed since the start of loading until the point D1 and thereafter the closure speed began gradually decrease. The closure width at point D1, which was 0.41 mm, was identified as the approximate width of pre-crack and it was close to our target, i.e, 0.5 mm. Afterward the

pre-crack completely ceased to close at point D2 when the closure width approached 0.5 mm, and simultaneously the formation of critical shear crack was confirmed. After point D2, shear behavior governed the structural performance until ultimate stage. In terms of opening behavior by PI-b at tension side, it was seen that the pre-crack opened at a constant speed until the failure point where the maximum opening width was relatively small (i.e., 0.19 mm), and afterward an obvious decrease of opening width was noted resulted from the dramatic development of shear deformation.

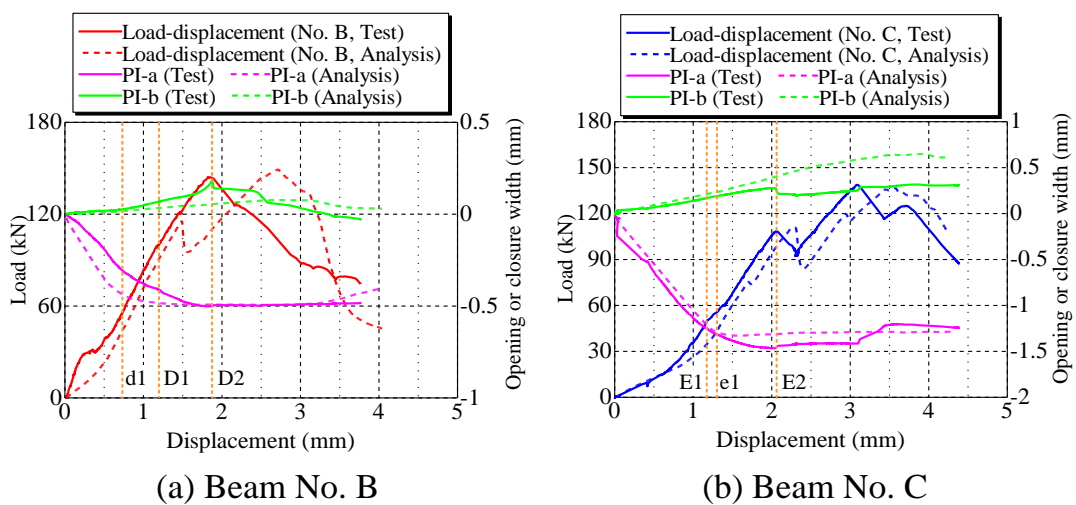


Figure 6.6 Behavior of section pre-crack

The behavior of pre-crack of beam No. C is shown in **Figure 6.6b**. Similar to the result of beam No. B, at compression side, the pre-crack first closed at a constant speed and after point E1 the closing speed gradually decreased until the occurrence of critical shear crack (point E2). By the closing width at point E1, the pre-crack width was identified as 1.22 mm. At tension side, the pre-crack opened at a constant speed until the occurrence of critical shear crack at point E2, and afterward ceased to open since shear behavior became dominant.

Based on the above opening and closure behaviors of pre-crack, it was proved that the experimental method for introducing pre-crack was practical and effective. In particular,

the target pre-crack width could be approximately achieved, which means that a parametric investigation of the effect of pre-crack on shear performance, concerning different pre-crack widths and positions in RC member, becomes available.

6.4 Numerical analysis for test beams

6.4.1 Analytical model

In chapter 6.3, by experiment, it was lessoned that the section pre-cracks with a width around 0.5 and 1.0 mm can significantly reduce the shear strength of a RC beam. But it was desirable to understand the mechanical role of pre-crack in shear performance, i.e. mechanism of shear strength degradation due to section pre-crack. Therefore, a numerical analysis employing 3-D RBSM was performed to simulate the shear behaviors of test beams. The RBSM models of test beams with average element size of 15 mm are shown in **Figure 6.7**, and the same material properties of concrete and reinforcing bar listed in **Table 6.1** were utilized. The parameters and constitutive models applied in 3-D RBSM have been discussed in previous chapter 2.

6.4.2 Procedure for introducing section pre-crack

For pre-cracked beam, before loading analysis, section pre-crack was introduced by the way applying loading on link elements for longitudinal reinforcing bar, which was a similar approach to that employed in chapter 5 for introduction of section pre-crack (see **Figure 6.7**).

In the procedure of pre-crack introduction by 3-D RBSM, as first step, four link elements in longitudinal reinforcing bars located at the same section that 150 mm far away from loading point were fixed, and meanwhile another four link elements located at the same section 350 mm far away from loading point were horizontally tensioned by displacement control (see step 1 in **Figure 6.7**). Consequently, due to high deformability

of reinforcing bars, a pre-crack would be generated approximately in the middle plane (250 mm far away from loading point) between the previous two sections where the link elements located at, that is, a pre-crack at the same position as that of the test beams was introduced (see step 2 in **Figure 6.6**). With regard to the width of pre-crack, it was determined by the displacement control of the tensioned link elements.

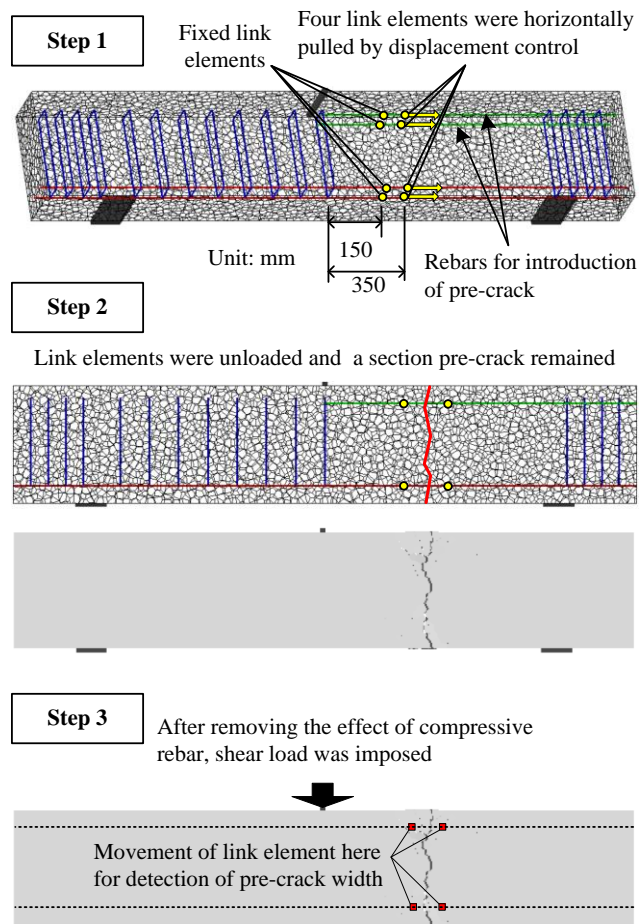


Figure 6. 7 Analytical model and procedure for introduction of section pre-crack

Then in second step, once a pre-crack with desirable width was achieved, the previously tensioned and fixed link elements were to be unloaded and became completely free in movement. The pre-crack, however, would remain there due to the residual deformation of longitudinal reinforcing bars (see step 2 in **Figure 6.7**).

By above two steps, a desirable pre-crack with a width of 0.5 or 1.0 mm could be

introduced. And after that, in third step, shear load analysis would be performed by displacement control to investigate shear behavior and strength. Before shear loading, the effect of compression reinforcing bars, which were for introducing pre-crack, were removed, because we did not arrange compressive reinforcing bars in actual experiment. Moreover, the investigation of opening and closure behaviors of pre-cracks in numerical analysis was also taken into account, which were surveyed by the relative horizontal displacements of link elements nearby the section pre-cracks at compression and tension sides (see step 3 in **Figure 6.7**).

6.4.3 Analytical result

6.4.3.1 Load-displacement relationship and behavior of section pre-crack

In this subsection, the result of numerical analysis is discussed by comparing with the previous experimental result.

The global load-displacement relationships by numerical analysis are plotted in previous **Figure 6.3** by dotted lines and the analytical shear cracking loads and shear strengths are listed in previous **Table 6.2**. It was evident that the numerical result overall captured the global behaviors of the three beams including the reduction of initial stiffness in pre-cracked beams. Furthermore, similar to the experimental result, the shear cracking loads were not remarkably affected by pre-cracks (see a3, b4, c4 in **Figure 6.3** and **Table 6.2**), nevertheless the shear strengths were considerably reduced in pre-cracked beams (see a5, b5, c5 in **Figure 6.3** and **Table 6.2**).

The opening and closure behaviors of the pre-crack in beam No. B obtained from the relative displacements of link elements are displayed in previous **Figure 6.6a** by dotted lines. Similar to the experimental result, at compression side, the pre-crack closed at a constant speed from the start of loading until the point d1 when the closure width was 0.40 mm, and this was regarded as the approximate width of pre-crack created by numerical analysis which was close to the experimental result, i.e., 0.41 mm. Then after

the point d1, the closure speed was mildly decreased to nearly zero when a critical shear crack formed. With regard to the opening behavior, at tension side, the pre-crack steadily opened in the same way as the experimental result until the failure stage, but the opening speed was relatively lower.

The opening and closure behaviors of the pre-crack in beam No. C by numerical analysis are presented in previous **Figure 6.6b**. Referring to the change point e1 of closure speed, the approximate width of pre-crack was found to be 1.24 mm, which was close the experimental result, i.e., 1.22 mm. Moreover, it was seen that at compression side the pre-crack steadily opened at a higher speed than the experimental one until the failure point.

Based on the above comparison of results by experiment and numerical analysis, it was proved that 3-D RBSM can simulate the global shear behavior of test beams with a high accuracy. Meanwhile, the good agreement of experimental and numerical analysis in turn is a good evidence of the effectiveness of the experimental method for introducing a section pre-crack and the fact of shear strength reduction due to section pre-crack.

6.4.3.2 Crack propagation

On purpose to understand the effect of section pre-crack on shear behavior, the crack propagations of the three beams based on results by experiment and numerical analysis are focused on in this section.

Figure 6.8-6.10 display the crack patterns at representative critical stages observed in experiment and numerical analysis for the three test beams, and the critical stages are marked in **Figure 6.3**. In the result of numerical analysis, the scale of crack width varies from 0.01 to 0.5 mm while the deformation is magnified by 15 times.

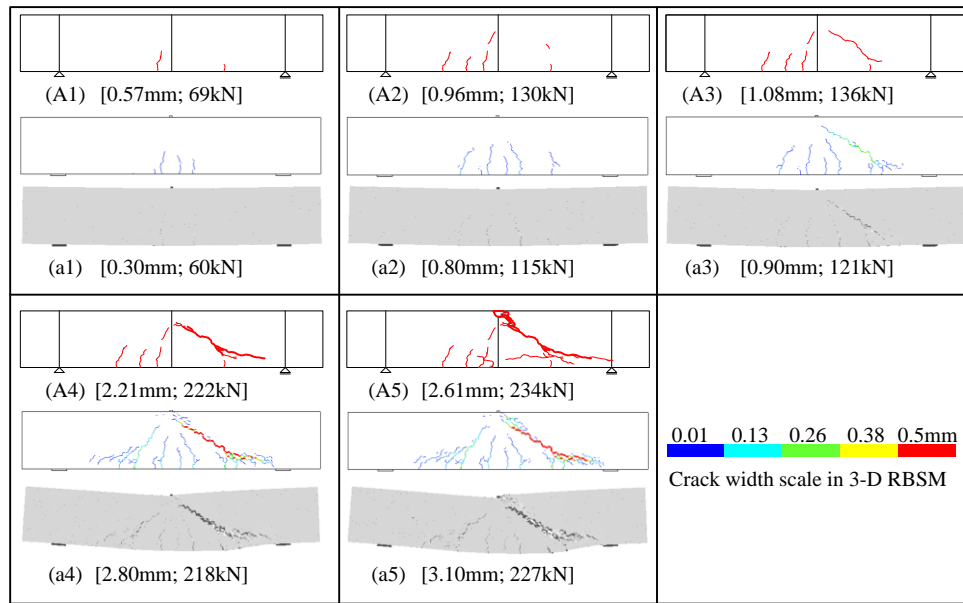


Figure 6. 8 Crack propagation of beam No. A

As the experimental result of the non-cracked beam No. A (see **Figure 6.8**), it was observed that visible flexural cracks first initiated from the bottom surface under the loading point (A1), when the load was increased to 69 kN. Subsequently, the preceding flexural cracks propagated upward to the loading point and simultaneously new flexural cracks initiated in the shear spans, when the load was increased to 130 kN (A2). Afterward, a critical shear crack appeared for first time as a result of the propagation of the preceding flexural crack in shear span when the load reached 136 kN (A3), and then shear behavior dramatically developed, that is, the critical shear crack propagated rapidly to the loading point and the support point with an increase of crack width (A4). Ultimately, as mentioned in chapter 6.3, the critical shear crack further developed and resulted in the compression failure of concrete nearby loading point, when the load reached peak, i.e. 234 kN (A5).

On the other hand, in numerical analysis, the similar behaviors such as flexural cracking (a1-a2) and critical shear cracking (a3-a4) were confirmed at the corresponding load stages. Moreover, the failure mode, i.e. compression failure due to shear at loading point, also was well simulated (a5).

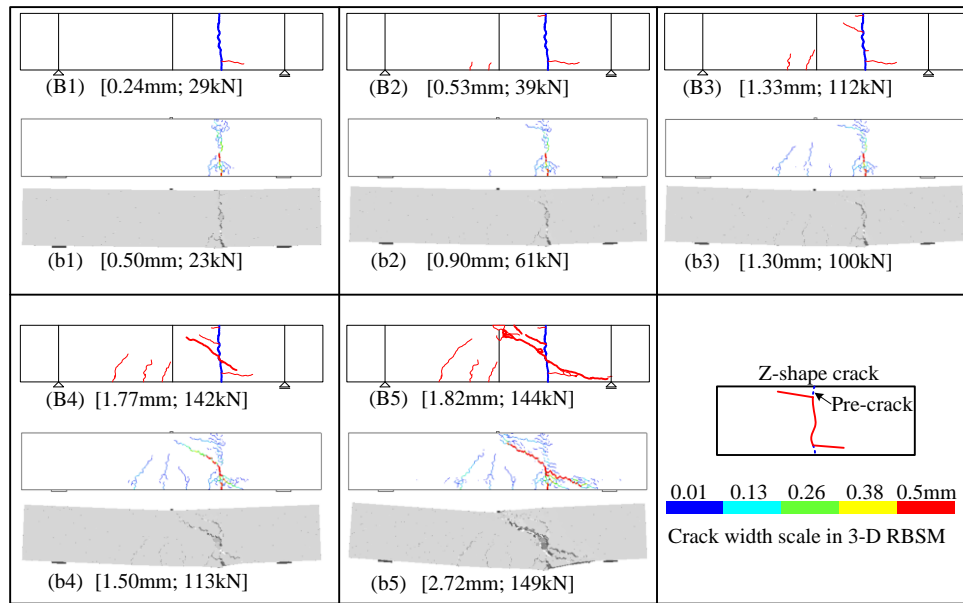


Figure 6.9 Crack propagation of beam No. B

In terms of the result for pre-cracked beam No. B (see **Figure 6.9**), in the experiment, a minor horizontal crack first initiated from the section of pre-crack and propagated toward the support point along the tension reinforcing bars (B1), instead of the first formation of flexural cracks that was observed in the non-cracked beam No. A (see A1 in **Figure 6.8**). Thereafter, two flexural cracks initiated from the bottom surface under the loading plate when the load was increased to 39 kN (B2). After that, a flat diagonal crack at compression side originated from the section of pre-crack. Herein, it was worth noting that the combination of the flat diagonal crack, the previous horizontal crack along tension reinforcing bars and the vertical pre-crack formed a Z-shape crack (see image of Z-shape crack in **Figure 6.9**) which was identified as a unique deformation caused by section crack (Pimanmas and Maekawa 2001a). Finally, the critical shear crack rapidly extended and crossed the section pre-crack when the load was increased to 142 kN (B4), leading to the compression failure of concrete near loading plate (B5).

With respect to the result by numerical analysis, the first occurrence of Z-shape crack was successfully achieved (b1-b4), i.e. a flat diagonal crack at compression side (b2) and

a horizontal crack along tension reinforcing bars (b4) were observed. Nearly at the same time of the formation of horizontal crack, the critical shear crack was generated across the section of pre-crack (b4) and ultimately led to the compression failure of concrete near loading plate (b5).

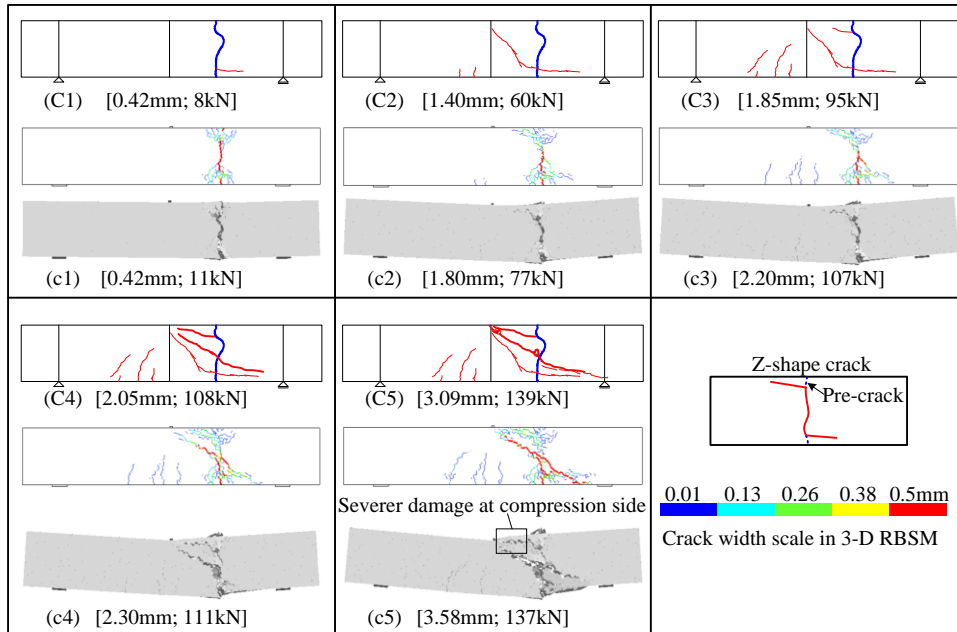


Figure 6. 10 Crack propagation of beam No. C

Because of the high similarity of the crack propagation between beam No. B and No. C, the crack behavior of pre-cracked beam No. C will be briefly described in **Figure 6.10**. In the experiment, with the increase of load, besides flexural cracks, a horizontal crack along tension reinforcing bars (C1) and a flat diagonal crack from pre-crack at compression side (C3) first initiated and formed a Z-shape crack (C3). Subsequently, a critical shear crack across the pre-crack was generated (C4) and dramatically developed, triggering a compression failure of concrete near loading point (C5).

A similar crack behavior to that in the experiment has been confirmed in the result by numerical analysis, i.e. an obvious initiation of Z-shape crack was first captured (c2-c3) and thereafter a critical shear crack began govern the deformation behavior (c4);

ultimately, a compression failure of concrete near loading plate occurred.

By contrasting the results between non-cracked and pre-cracked beams, it became clear that although the section pre-crack caused typical behavior of Z-shape crack, the critical shear cracks in pre-cracked beams could form by nearly same inclination as that in non-cracked beam. These observations were opposite to the shear-effect of multiple pre-cracks uniformly distributed in shear span reported by Pimanmas and Maekawa (2001a), where the continuous development of critical shear crack was obstructed by section pre-cracks. In addition, it was also notable that the deformation of concrete near loading point at failure stage became much severer in the pre-cracked beams (see a5 in **Figure 6.8** and c5 in **Figure 6.10**).

6.5 Mechanism of shear strength degradation caused by section pre-crack

In this section, the hysteresis of shear load by numerical analysis shown in **Figure 6.3** were decomposed into the contributions of shear resistance mechanisms, i.e. beam action and arch action, with an intention to verify the conclusion obtained in chapter 5 that section pre-crack is the basic reason for degradation of arch action. Moreover, the primary role of section pre-crack in stress transmission in concrete was explained.

6.5.1 Decoupling result of shear resistance mechanism

The decoupling approach with the use of the local stress output from 3-D RBSM analysis has been detailed introduced in chapter 2 and practically applied in the studies of chapters 3-5. By the same way, the hysteresis of shear loads shown in **Figure 6.3** were decomposed into various shear resistance mechanisms. It should be noted that the elementary unit dx along beam for calculation of shear resistance mechanism was determined to be 100 mm.

Consequently, the average beam action and arch action, at each deformation, of all units dx located in target shear span were computed for the three beams, and the results are displayed in **Figure 6.11a-c**, combined with the analytical load-displacement relationships that discussed in **Figure 6.3**.

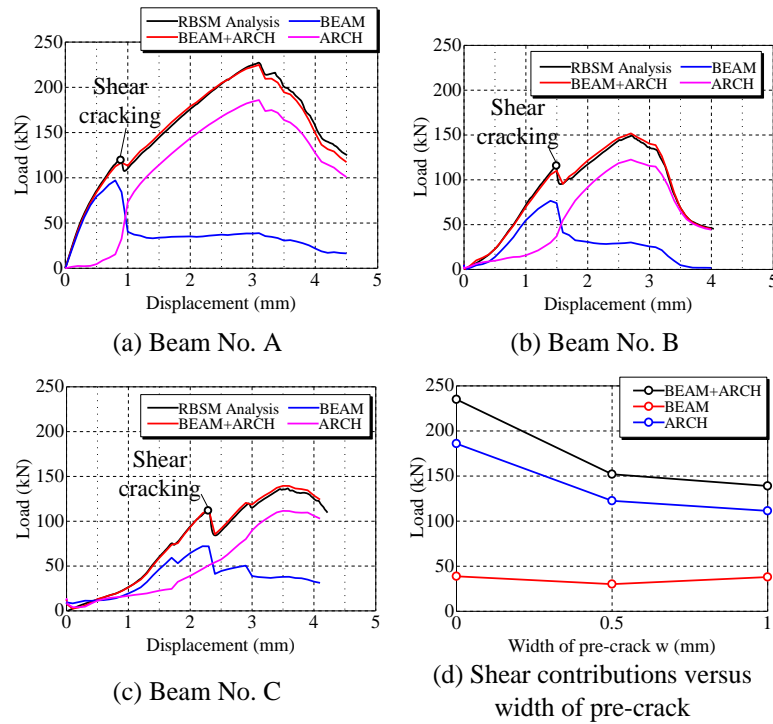


Figure 6. 11 Decoupling of shear resistance into average beam action and arch action

It was apparent that the combination effects of beam action and arch action were perfectly in agreement with the hysteresis of shear load by 3-D RBSM for the three beams, that is, the decomposition method was applicable and effective. For non-cracked beam No. A (see **Figure 6.11a**), it was seen that the beam action first provided shear resistance since the start of loading, nevertheless the arch action was nearly not generated. A rapid shift in resistant effect of beam action and arch action, later on, was noted at the initiation of shear crack, that is, the beam action declined steeply to around 40 kN while the arch action rose sharply and became dominant to the development of shear resistance. It should

be kept in mind that the arch action developed much more than the maximum effect of beam and governed the shear strength while the beam action decreased to a low grade after shear cracking.

For the pre-cracked beams (see **Figure 6.11b-c**), similar developments of beam action and arch action to those of the non-cracked one, particularly the shift in the role of beam action and arch action, were confirmed. For understanding the primary role of arch action, the beam actions and arch actions corresponding to shear strengths were picked out and compared in **Figure 6.11d**. It was concluded that the arch actions governed the shear strengths for the three beams, and the significant degradation of shear strength due to pre-crack was attributed to the decrease of arch action while the beam actions of the three beams were in similar grade.

6.5.2 Primary role of section pre-crack in degradation of shear resistance mechanism

Moreover, the specific resistance components in arch actions were investigated. The components for maximum arch actions by concrete compression related effect (short for compression effect, item $C_c \cdot dj_{Cc}/dx$ in Equation 2.4) and concrete tension related effect (short for tension effect, item $T_c \cdot dj_{Tc}/dx$ in Equation 2.4) are illustrated in **Figure 6.12** in the form of distribution along beam axis that obtained in each elementary unit dx . Herein, the lower limit and upper limit of the horizontal coordination in **Figure 6.12-6.14** represent the location of loading point and support point, respectively. As a consequence, it was seen that, overall, the arch action was nearly completely provided by the compression effect, whereas the tension effect was minor and could be neglected. For the compression effect of non-cracked beam (**Figure 6.12a**), it was noted that the arch action was in a relatively high grade nearby loading plate and was gradually decreased toward the support point. In contrast to that of the non-cracked beam, the compression effect in pre-cracked beam was overall in a lower grade, particularly in the zone between loading point and section of pre-crack, directly leading to the degradation of average arch action.

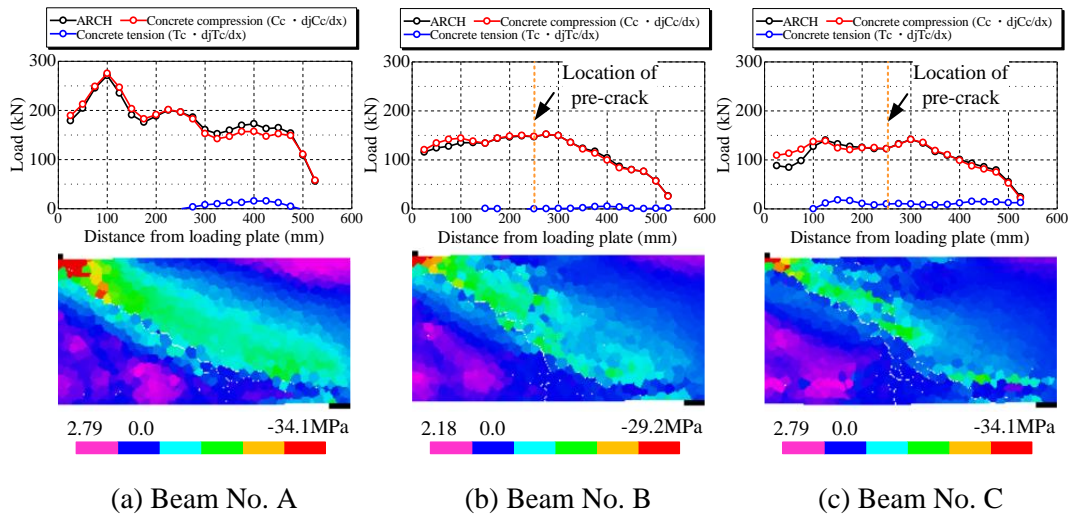


Figure 6.12 Longitudinal distributions of decoupling arch action and axial stress states in central cross section at maximum load

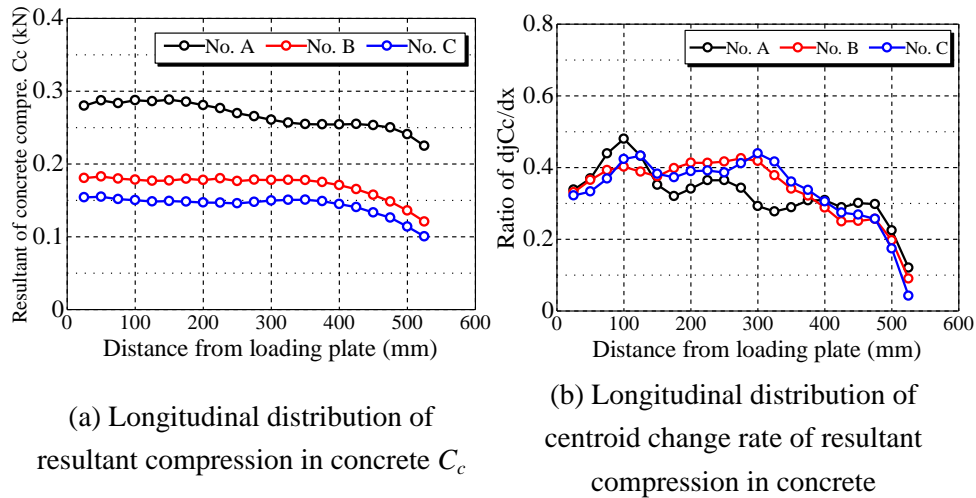


Figure 6.13 Result of the factors for calculation of arch action

For a deeper interpretation of the reason for degradation of compression effect, the relevant factors for calculation of compression effect, i.e. the resultant compression C_c in concrete and the change rate of its centroid along longitudinal direction (dj_{Cc}/dx) would be discussed in **Figure 6.13**, respectively. With respect to resultant compression (C_c) (see **Figure 6.13a**), it was observed that its distribution considerably declined in pre-cracked

beams, and the wider the pre-crack was the higher the decline rate became. The different grade of resultant compression (C_c) can be intuitively understood by the different axial stress states in target shear span shown in **Figure 6.12** (hereby the lower and upper limits in stress legends stand for the tensile and compressive strengths of concrete), that is, the area of high compression zone nearby loading plate at compression side of the cracked beams were evidently smaller and the range of inclined arch-shape stress flow were obviously narrower compared with those of the non-cracked beam.

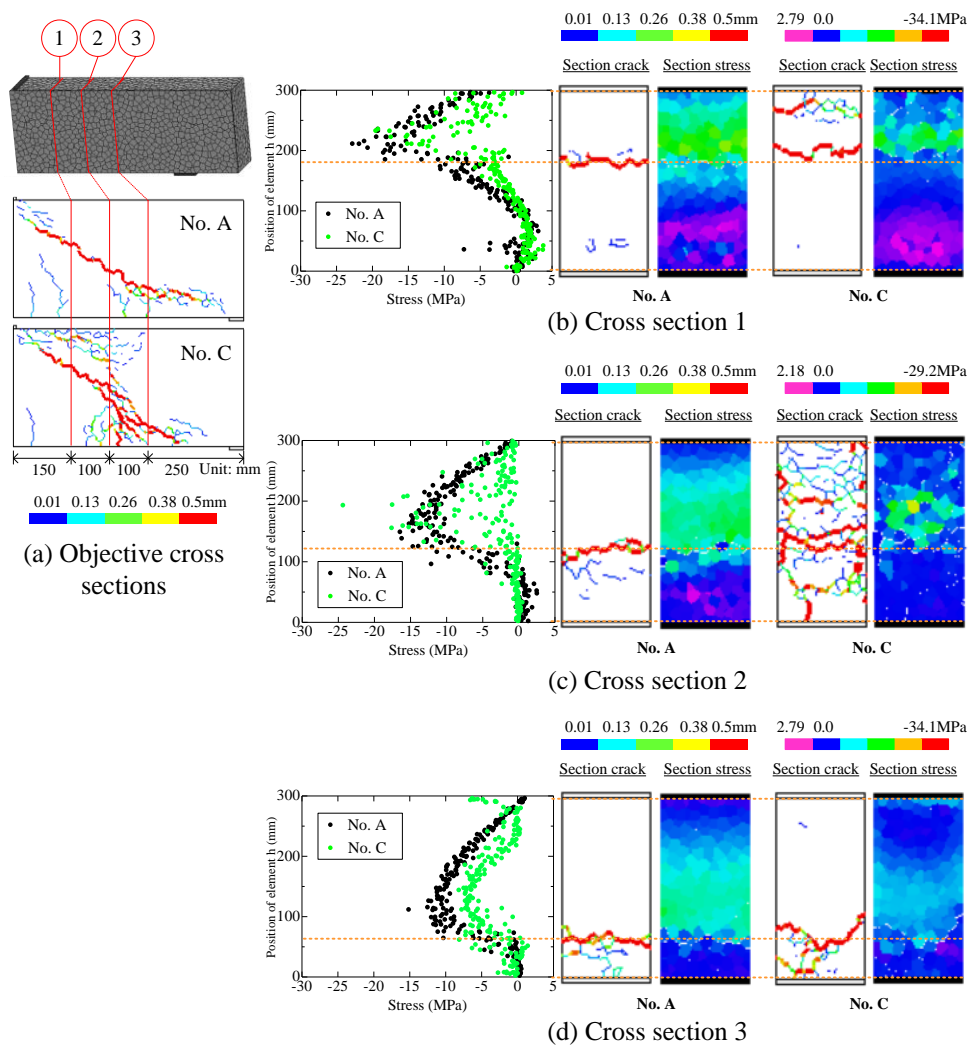


Figure 6. 14 Comparison of axial compressive stress states in cross section of concrete between beam No. A and C

On the other side, because of the similar orientation of critical shear crack in the three beams, a roughly same shape of distribution of centroid change rate was confirmed, namely, the centroid change rates of the three beams were in close grade in the entire span and were gradually decreased from loading point to support (see **Figure 6.13b**). Thus, it became clear and should be emphasized that the overall decrease of resultant compression (C_c) was dominant to the degradation of arch action in pre-cracked beam.

The primary role of section pre-crack is more detailed explained in **Figure 6.14**, where the different axial stress states between non-cracked beam No. A and pre-cracked beam No. C in three critical sections are compared. The locations of the cross sections 1-3 are shown in **Figure 6.14a** combined with the crack patterns at maximum loads. In **Figure 6.14b-c** for contrast of results between beam No. A and No. C in cross sections 1-3, the diagrams on left side illustrate the axial stress intensities in cross section obtained from concrete elements while the graphs in middle and right side display the corresponding crack patterns and axial stress contours for beam No. A and No. C.

As a result, for cross section 1, it was seen that the compressive stress in beam No. C was overall in a lower grade than the non-cracked beam one (see diagram in **Figure 6.14b**). Moreover, compared with those in beam No. A, it was observed that an extra crack (i.e., Z-shape crack mentioned in previous discussion) formed above the critical shear crack in the pre-cracked beam No. C (see crack patterns of **Figure 6.14b**), and the extra crack was likely to lead to the dramatic reduction of stress at its location (see stress contour in No. C of **Figure 6.14b**). For cross section 2 where the pre-crack was generated, the reduction of stress in pre-cracked beam No. C became more significant, namely, the majority of stresses nearly declined close to zero (see diagram in **Figure 6.14c**), which was attributed to the much severer crack damage, i.e. larger number of cracks (see crack patterns in **Figure 6.14c**). This was further confirmed by the remarkable loss of stress in the crack zone (see stress contour in No. C of **Figure 6.14c**). Therefore, it was concluded that the section pre-crack in this study played a primary role in inducing extra crack

behaviors and obstructing the transfer of axial compressive stress in concrete, leading to the overall decline of resultant compression in concrete C_c and the degradation of arch action discussed in previous content. With respect to the result for cross section 3, an entire reduction of stress, by a relatively low percentage compared with that for cross section 2, in pre-cracked beam No. C was seen (see diagram in **Figure 6.14d**). Different from the mechanism in cross sections 2, however, the reduction of stress in cross section 3 was likely to be a subsequent process caused by the obstruction of stress transfer in cross section 2, because a similar crack pattern was clarified in the two beams.

6.6 Summary and conclusions

On purpose to investigate the effect of section pre-crack on shear behavior of RC member, an experimental method by utilizing cardboard for introducing pre-crack with desirable width at target position into RC beam was attempted, and its effectiveness and applicability were confirmed by the measurement of opening and closure behaviors of the pre-cracks in the RC beams under shear loading.

Shear loading was applied on a non-cracked beam and two beams with a single 0.5 mm and 1.0 mm section pre-crack, respectively, and it was found that the section pre-cracks can lead to a significant degradation of shear strength compared with that of the non-cracked beam.

By employing 3-D RBSM, the shear behaviors including load-displacement relationship, crack propagation and pre-crack opening/closure of the test beams were simulated. Particularly, the unique deformation behavior of Z-shape cracking in pre-cracked beams was well reproduced. The numerical result also supported the finding of the shear strength degradation due to section pre-crack that has been mentioned in previous chapter 5.

On the basis of the local stress states obtained from 3-D RBSM, the developments of

shear resistances for the three beams were decomposed into the contributions provided by beam action and arch action. And it was lessoned that the shear strengths of the three beams were governed by the contributions of arch action, and the degradation of the shear strengths in pre-cracked beams was attributed to the reduction of maximum arch action.

Moreover, the arch actions for shear strengths were decomposed into the resistant components of compression effect ($C_c \cdot djC_c/dx$) and tension effect ($T_c \cdot djT_c/dx$). As a result, the arch actions were found mainly being provided by the compression effect ($C_c \cdot djC_c/dx$), and the reductions of maximum arch action in pre-cracked beams were caused by the overall reduction of resultant compression (C_c).

In addition, the comparison of axial compressive stresses in critical cross sections between non-cracked and pre-cracked beams was carried out, and it was concluded that the section pre-crack played a primary role in inducing extra crack behaviors such Z-shape crack and obstructing the transfer of compressive stress in axial direction after shear cracking, which was the essential reason why the resultant compression in concrete (C_c) and arch action degraded.

7. Effect of Rebar Cutoff on Shear Resistance Mechanisms

7.1 Introduction

The cutoff in longitudinal reinforcement (short for rebar cutoff) is ordinarily designed in many RC bridge piers and walls. As one frequent-occurring earthquake damage, however, the shear failure has been often reported occurring at the point of rebar cutoff. A lot of researches have studied the effect of rebar cutoff on shear strength and proposed some empirical equations to assess shear strength at rebar cutoff zone based on a large amount of loading experiments (Ferguson et al. 1959, Baron 1966, Kao et al. 1975, Ozaka et al. 1986 and 1987). Moreover, the seismic evaluation methods to determine whether shear failure would occur at point of rebar cutoff or at footing-column joint of RC bridge piers, under seismic load, were established (Kawashima et al. 1995, Kosa et al. 2008). In recent years, various numerical methods for simulating shear performance of RC structures with rebar cutoff (Sakai et al. 2009, Sasaki et al. 2010), and the seismic retrofit method for point of rebar cutoff (Zhang et al. 2012) have become hot topics.

In this chapter, aiming to understand the effect of rebar cutoff on shear resistance mechanisms, the author simulated the different shear performances between the RC beams with and without rebar cutoff by 3-D RBSM, and clarified the effect of rebar cutoff on shear resistance mechanisms: beam action and arch action.

7.2 Objective experiment

Ozaka et al. (1986) carried out a large number of 3-point loading tests for RC beams to investigate the effect of rebar cutoff on the shear failure mode and the shear strength, by changing the certain variables such as tension reinforcement ratio, shear span to effective depth ratio, shear reinforcement ratio and position of rebar cutoff point.

Based on the test result, four failure types for RC beams were concluded by Ozaka et al. (1986) based on the different shear performances (see **Figure 7.1**). For the failure type I, the shear resistance drops soon after the diagonal shear cracking at rebar cutoff point (Y1) and the RC beam presents a very brittle shear failure (U1). Both the long bars and cutoff bars are not yielded. For the failure type IIa, the long bars at rebar cutoff point are first yielded (Y2), and thereafter the shear failure occurs at rebar cutoff point (U2a). For the failure type IIb, the tension rebars nearby the loading point are first yielded (Y3), and later on, the shear failure occurs at rebar cutoff point (U2b). The tension rebars at rebar cutoff point are not yielded in the whole loading process. For the failure type III, the tension rebars nearby the loading point are yielded (Y3), and then the beam fails attributed to the compression failure of concrete (U3). This failure type shows a good deformability.

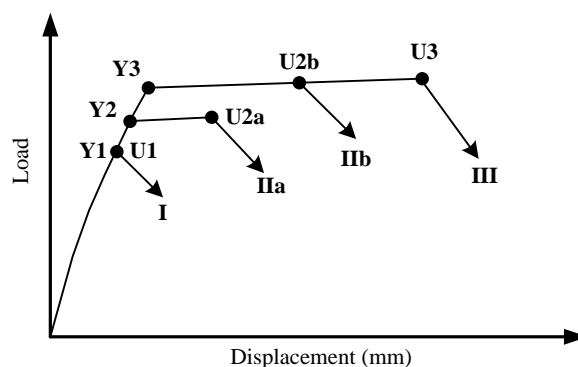


Figure 7. 1 Classification of failure types

Among the experimental beams, the author selected three beams, damaged by three different failure types, and conducted numerical analyses by 3-D RBSM. The beams M1,

M7 and M8, the numbers of which were remained same as the original research, suffered from shear failure type IIa, I and III, respectively. The details of the objective RC beams are listed in **Table 7.1** and the design drawings are shown in **Figure 7.2** (only the target shear spans, for shear failure, are drawn). The beams have a cross section 400 mm×500 mm and the shear span length a is 1400 mm, i.e. the shear span to effective depth ratio is 3.5. Six tension rebars (D19, yield strength $f_{y1}=402$ MPa) and four compression rebars (D6, yield strength $f_{y2}=392$ MPa) were arranged. Three tension rebars were cutoff for the beam M7 and the beam M8. The cutoff length L_{cut} , distance from the support point to the cutoff point, is 465 mm, i.e. L_{cut}/a is 0.33. In addition, the rebar cutoff zone of the beam M8 was shear reinforced by stirrups (D6, yield strength $f_{yw}=392$ MPa), i.e. the shear reinforcement ratio is 0.151%. The concrete strengths are listed in **Table 7.1** as well.

The effect of rebar cutoff on shear performance can be known by comparing the results between the beam M1 and the beam M7, and the enhancement effect of stirrups to rebar cutoff zone can be comprehended by comparing the results between the beam M7 and the beam M8.

Table 7. 1 Details of objective RC beams

Case No.	Shear span to effective depth ratio	Shear span length	Position of cutoff point		Tension reinforcement ratio	Shear reinforcement ratio	Concrete	
			L_{cut} (mm)	L_{cut}/a			Compressive strength	Tensile strength
	a/d	a (mm)	L_{cut} (mm)	L_{cut}/a	ρ_t (%)	ρ_w (%)	f_c' (MPa)	f_t' (MPa)
M1			-	-			26.3	2.43
M7	3.5	1400	465	0.33	0.83		26.7	2.72
M8						0.151	23.4	2.81

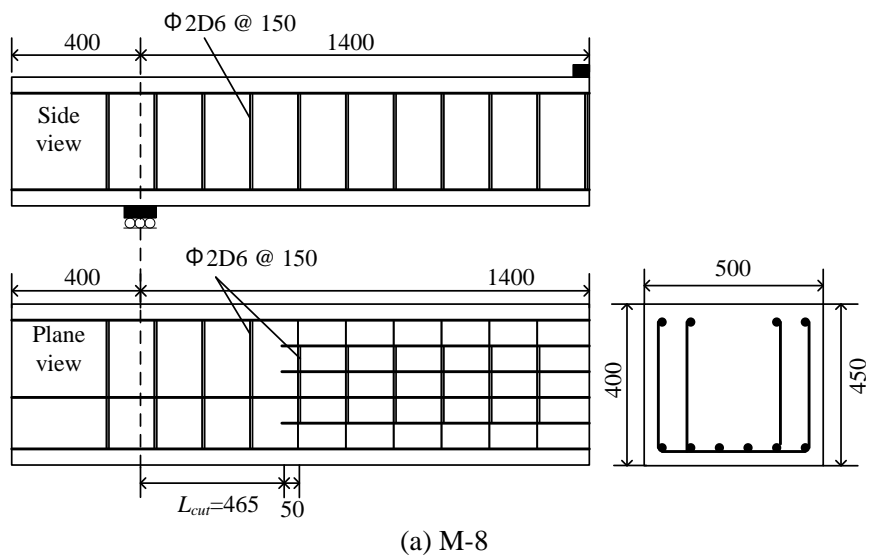
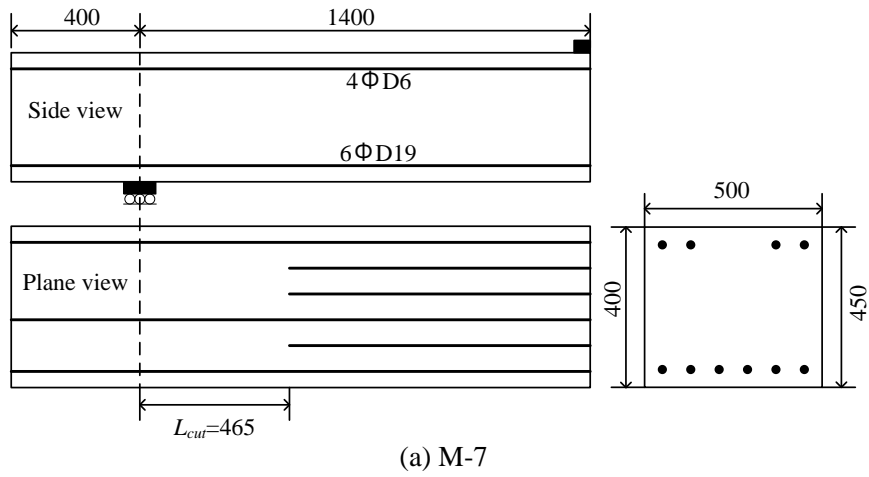
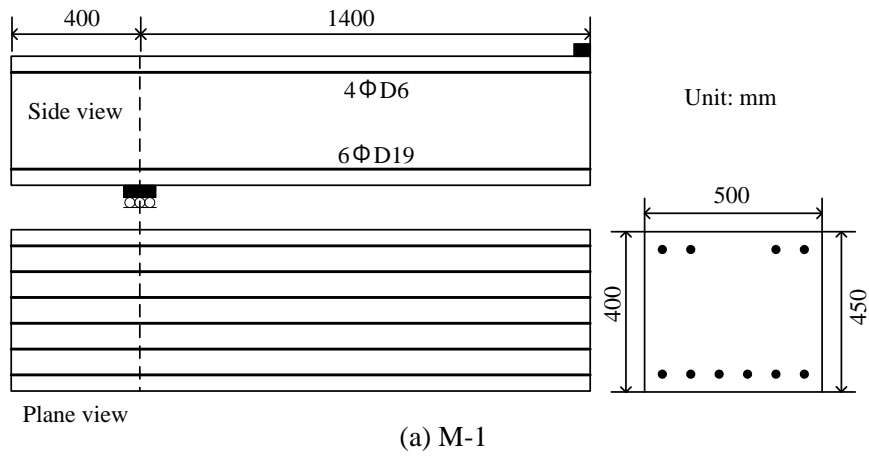


Figure 7. 2 Drawing of RC beams

7.3 Analytical model

According to the dimensions of RC beams and the material properties introduced in chapter 7.2, the numerical models were built (see **Figure 7.3**) with the concrete being created by 3-D RBSM and the rebars being modeled by beam element. When modeling concrete, on the purpose of reducing the calculation consumption, the 30 mm element in average was arranged for shear span at right side (see **Figure 7.3a**), while the target shear span for shear failure was modeled by the 15 mm element in average, suggested by Yamamoto et al. (2008). The rebar cutoff zones in the beam M7 and the beam M8 are shown in **Figure 7.3c-d**, and the stirrups were modeled in target shear span for the beam M8. By the way, large amounts of stirrups were set in the right shear span to restrict the shear failures occurring in the target shear spans (see **Figure 7.3b-d**). The loading plates and the support plates, 50 mm wide, were modeled by the rigid prisms, and the vertical load was imposed by displacement control.

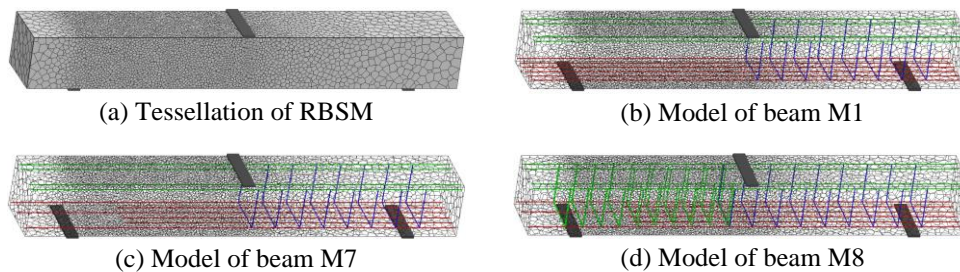


Figure 7. 3 Analytical models

7.4 Analytical result

The analytical load-displacement relationships are shown in **Figure 7.4**, together with the test result for the beam M7 and the beam M8 by dash curves (the load-displacement relationship for the beam M1 is not available in the original literature). Additionally, the deformations and crack patterns at failure points by analyses and the critical shear cracks from the test are given in **Figure 7.5** (the critical shear crack for the beam M8 is not

available in the original literature). For the beam M1 without rebar cutoff, the shear cracking load was found as 347 kN, at the point a, which was slightly greater than the test result, 314 kN; later on, the beam was yielded, at the point b, when the load was increased to 386 kN; ultimately, the shear failure after yielding occurred, at the point c, when the load was 396 kN (395 kN for test). Thus, it was confirmed that the analysis well reproduced the behavior of the failure type IIb for beam M1. The deformation (magnified by eight times) and the crack damage by analysis, at the failure point c, are shown in **Figure 7.5a**, combined with the critical shear crack observed in test, and the criterion for the analytical crack was determined by the damage condition of normal spring between two concrete particles. As a result, the position and the orientation of critical shear crack in test was well reproduced.

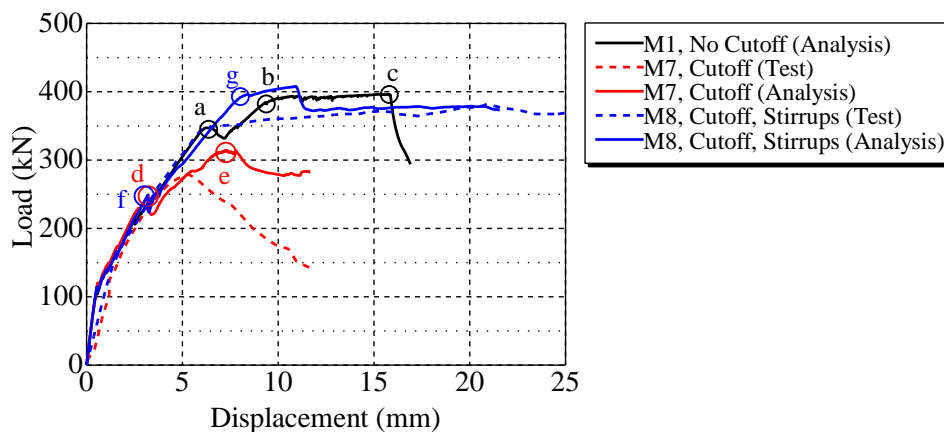


Figure 7. 4 Load-displacement relationships

For the beam M7 with rebar cutoff, the shear cracking load by analysis was identified as 248 kN, at the point d, which was slightly lower than the test result, 272 kN. And it was seen that the diagonal shear crack formed at the rebar cutoff point and then rapidly propagated to loading point and support point (see **Figure 7.5b**). After that, the shear failure occurred, at the point e, when the load was increased to 314 kN (290 kN for the test). Thereby, the analytical result did not fail immediately after diagonal shear cracking,

which slightly differed from the test result, the failure of which was more brittle, type I. Actually, the shear behavior and the deformability by analysis was between the failure type I and IIa, and the analysis roughly reproduced the effect of rebar cutoff. Obviously, the rebar cutoff contributed to the shear failure at the rebar cutoff point, and reduced the shear strength compared with that of the beam M1.

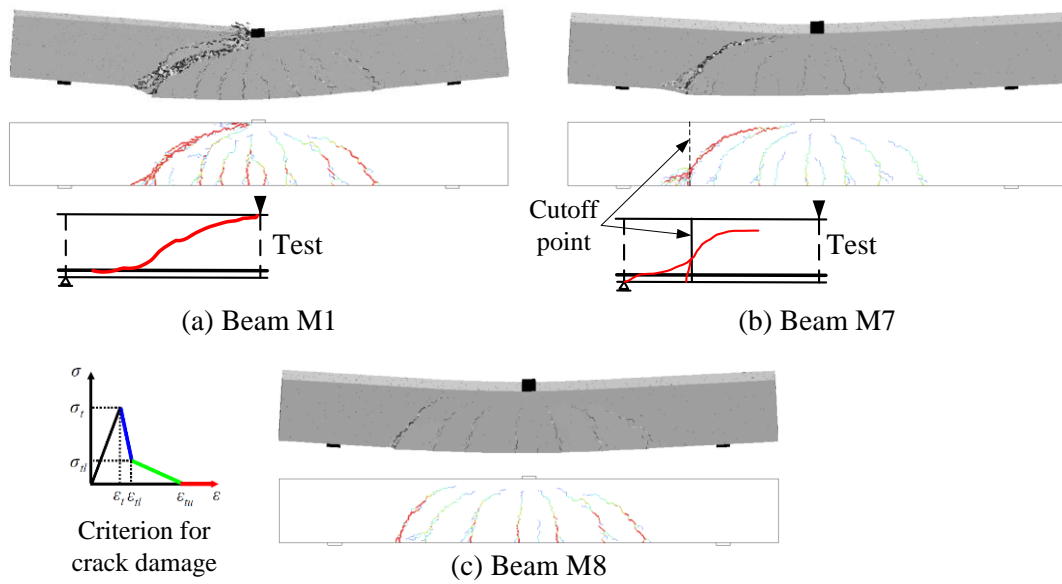


Figure 7. 5 Deformations and crack patterns

Regarding to the beam M8 with rebar cutoff enhanced by stirrups, the similar shear cracking load, 249 kN, at the point f, to that of the beam M7 was obtained. Then, the beam was yielded at the point g (394 kN), which was slightly later than the test result. It was evident that arrangement of stirrups greatly reduced the shear deformation, compared with the beam M7 (see **Figure 7.5c**) and the beam M8 displayed better deformability. Finally, the beam M8 failed due to the flexural compression failure, instead of the shear failures found for the beam M1 and the beam M7, which was a same failure type as the test result, type III.

In summary, based on the above analytical result, it was confirmed that 3-D RBSM can roughly capture the different shear performances among the three beams, particularly the

effect of rebar cutoff.

7.5 Effect of rebar cutoff on shear resistance mechanisms

As the most important part, aiming to clarify the effect of rebar cutoff on the shear resistance mechanism, the author decoupled the analytical load-displacement hysteresis for the beam M1 and the beam M7 shown in **Figure 7.4** into the capacity curves for beam action and arch action, and investigated the primary role of rebar cutoff in the shear performance. Although it has been reported that if the anchorage length of cutoff rebar is sufficient, the rebar cutoff would not obviously reduce the shear performance of RC beam (Ozaka et al. 1986), the target of this chapter was to clarify the reason of degradation of shear strength caused by rebar cutoff and the RC beam with sufficient anchorage length of cutoff rebar was not set as the research object in this chapter.

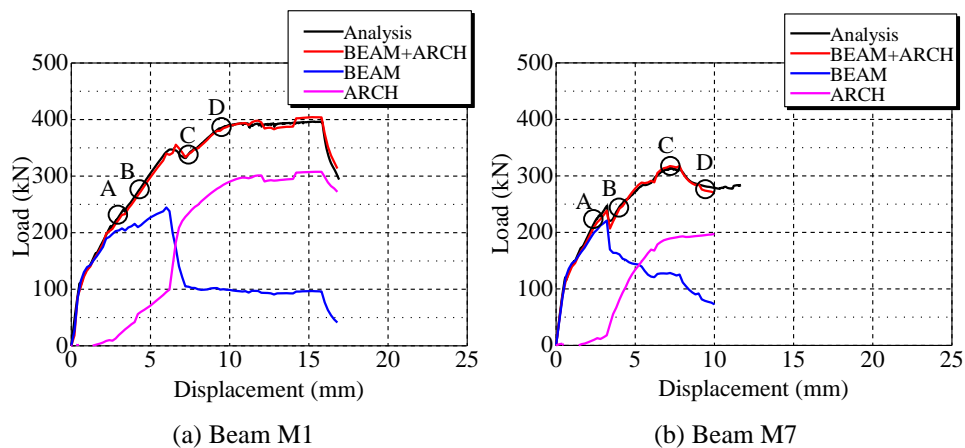


Figure 7. 6 Decoupling beam action and arch action

Herein, the elementary unit dx along beam axis in the target shear span for integration of shear resistance mechanism was determined as 100 mm. The decoupling results of beam action and arch action are shown in **Figure 7.6**, combined with the analytical load-displacement relationships. The good agreement between the combined effect of shear

resistance mechanisms and the analytical result was confirmed. For the two beams, the beam actions initially provided the majority of shear resistance before the diagonal shear cracking. Later on, the beam actions sharply dropped when the diagonal cracks were generated. The maximum beam actions were in close grade between the two beams, i.e. 245 kN for M1 and 221 kN for M7. After the diagonal shear cracking, the arch actions started to take effect. The arch action for beam M1 was consecutively increased until the yielding (point D) and thereafter was kept stable. Ultimately, the sudden decline of arch action caused shear failure. The arch action for beam M7 was consecutively increased until the beam about to fail (point C) and thereafter was kept a constant. The maximum grade of it, however, was much lower than the former one for beam M1, which was the reason of its lower shear strength. The consecutive drop of beam action, other than the drop of arch action, was found leading to the ultimate shear failure for the beam M7.

Therefore, it was concluded that the significant different developments of arch action between the two beams was the fundamental reason for their different shear strengths. And in order to clarify this difference, the critical factors on beam action and arch action were analyzed for the four loading stages, the point A-D in **Figure 7.6** (The points A-D in **Figure 7.6a** and **Figure 7.6b** correspond to the same displacements).

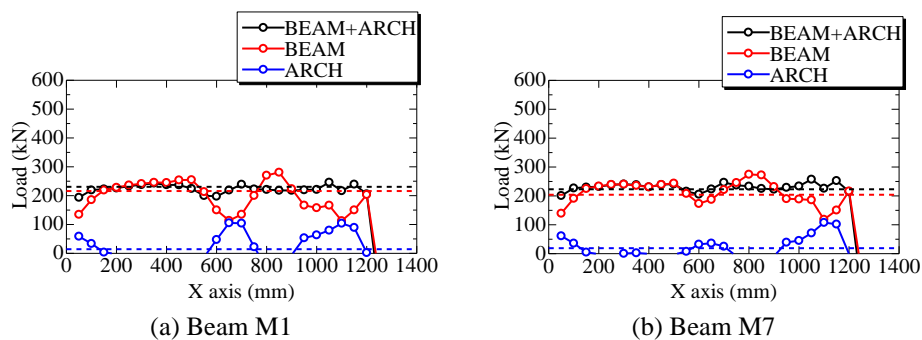


Figure 7. 7 Beam actions and arch actions at stage A

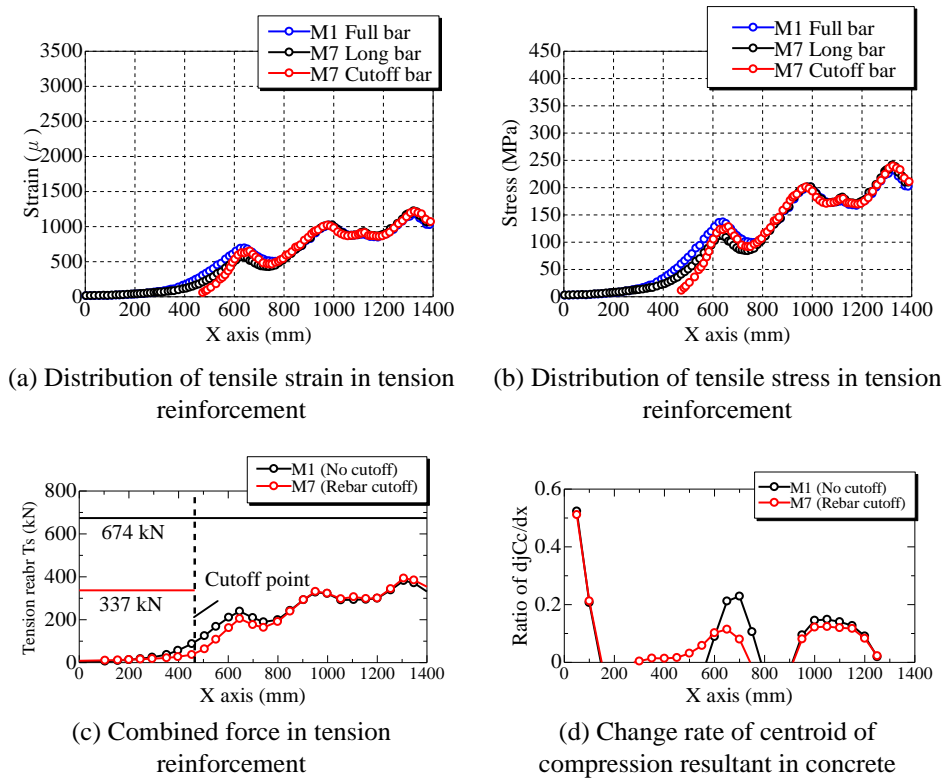


Figure 7. 8 Result of local force for the two beams at stage A

Figure 7.7 shows the result for beam action and arch action in each elementary unit dx along beam axis for the two beams at stage A, before diagonal shear cracking. The dash lines in diagrams standard for the mean value of each action, and the lateral coordinates 0 and 1400 represent for the support point and the loading point. As seen, the beam action provided the great majority of shear resistance at stage A, as mentioned before. **Figure 7.8a** shows the tensile strain distributions in tension rebars along beam axis, and the result for the beam M7 was classified by cutoff bar and long bar. Similarly, **Figure 7.8b** shows the tensile stress distributions. The strain and stress presented similar distributions with a similar slope from loading point to support point. Thereby, the combined tensile forces by all tension reinforcement also presented similar distributions, and this similar and evident slope (dT_s/dx) resulted in the similar grade of beam actions for the two beams (see **Figure 7.8c** where the straight lines are for reference of combined tensile force when all

tension reinforcement are yielded). **Figure 7.8d** shows the change rate of centroid of compression resultant in concrete (dj_{Cc}/dx) for each elementary unit dx along beam axis. The change rate of centroid was very minor because no diagonal crack formed, which explained the minor grade of arch action.

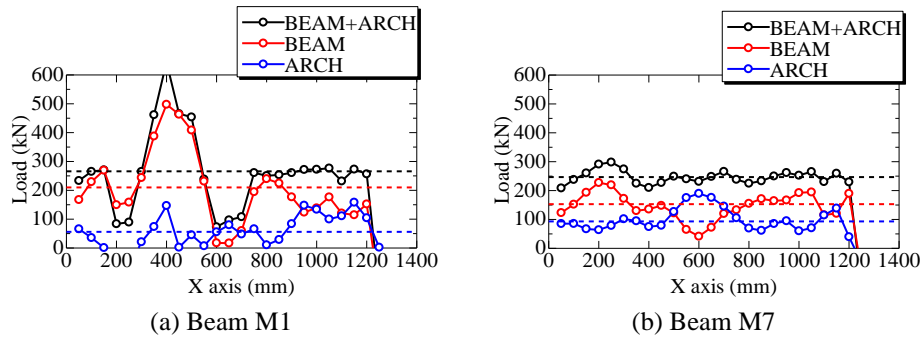


Figure 7.9 Beam actions and arch actions at stage B

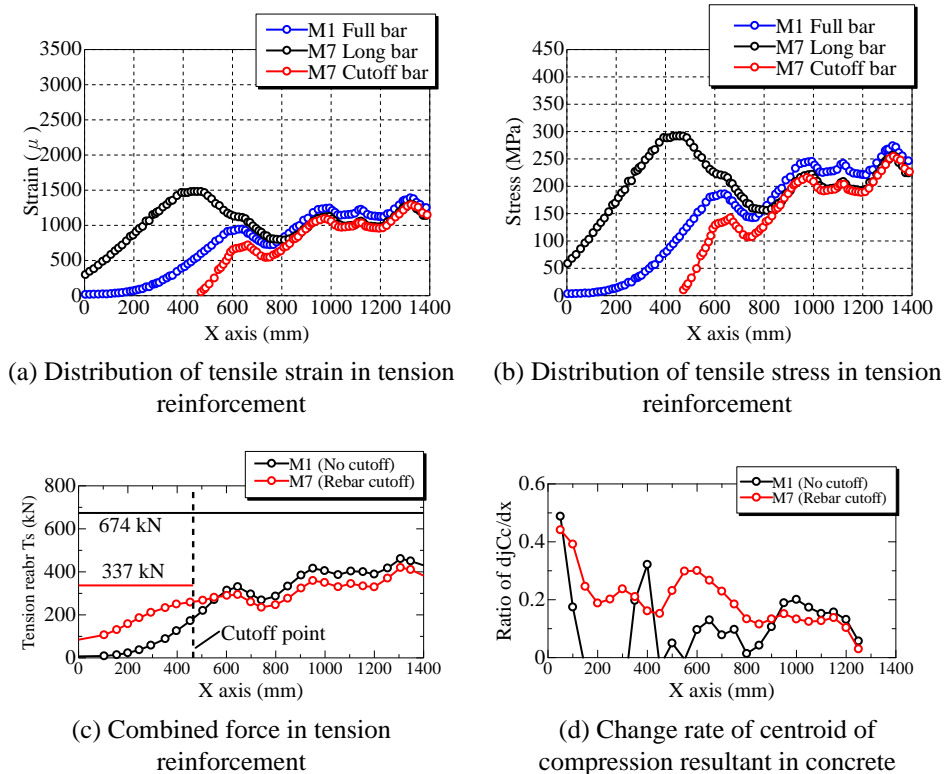


Figure 7.10 Result of local force for the two beams at stage B

Then, the similar result at stage B-D will be discussed. The stage B is a typical point after diagonal cracking for the beam M7. For the beam M1, the beam action kept rising while the arch action was still very minor, because the diagonal crack did not form (see **Figure 7.9a**). For the beam M7, however, the beam action was decreased compared with that at stage A, while the arch action had started to rise at a relatively high rate, so that the combined effect of the two actions was slightly increased (see **Figure 7.9b**).

Because of the diagonal shear cracking for the beam M7, the general rising of tensile strain in long bars at rebar cutoff point was seen (see **Figure 7.10a**), whereas the tensile strain in cutoff bars remained same as that at stage A, due to the bond damage between rebar and concrete at the rebar cutoff point. The similar distributions of tensile stresses are observed in **Figure 7.10b**. This rising of tensile stress in long bars for the beam M7 contributed to the general rising of combined tensile force at rebar cutoff zone more than that of the beam M1 (see **Figure 7.10c**); in turn, the slope of combined tensile force (dT_s/dx) became lower than that at stage A, so that the beam action was overall decreased (Compressive forces by compression reinforcements were extremely minor and were omitted). On the contrary, the change rate of centroid (dj_{CC}/dx) overall was increased, which contributed to the rising of arch action (see **Figure 7.10d**).

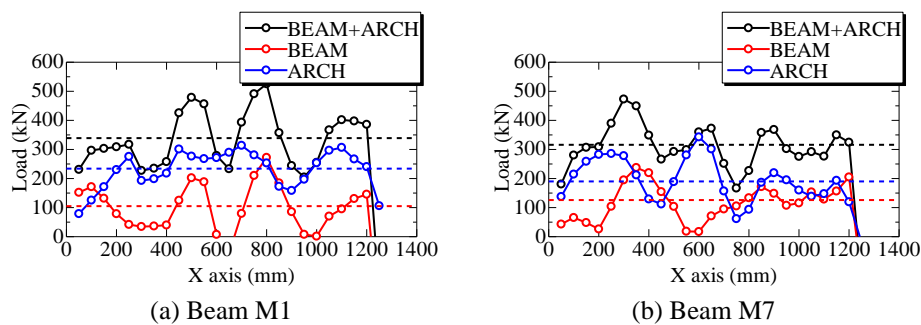


Figure 7. 11 Beam actions and arch actions at stage C

The stage C is the failure point for the beam M7. The result at stage C is discussed as follows. No big difference was found between the beam actions and the arch actions

between the two beams (see **Figure 7.11**). For the beam M1, the arch action was increased a lot while the beam action was dramatically decreased, compared with those at stage B, because of the diagonal shear cracking not long before (see **Figure 7.11a**). For the beam M7, the beam action was kept decreasing and the arch action approached to the maximum grade (see **Figure 7.11b**).

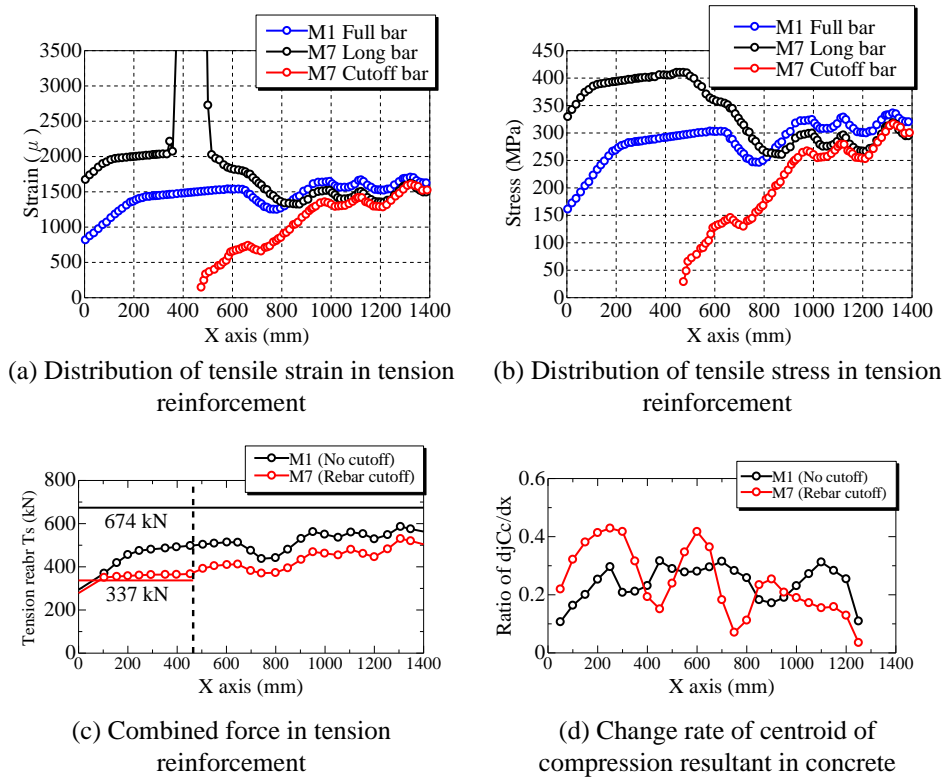


Figure 7. 12 Result of local force for the two beams at stage C

The tensile strain of the beam M1, in general, was significantly increased, particularly nearby the support point (see **Figure 7.12a**). For the beam M7, the tensile strain of long bars overall greatly rose and had been yielded at the rebar cutoff zone (yielding strain: 2020μ , according to the original literature), while that of cutoff bars was slightly increased nearby loading point at a low rate. The similar distributions of tensile stresses are shown in **Figure 7.12b**, and the upper limit of tensile stress (around 400 MPa) was confirmed

for the long bars at rebar cutoff zone. The drop of beam actions for the beam M1 as well as the beam M7 could be understood from the lower slopes of combined tensile force (dT_s/dx) at rebar cutoff zone (see **Figure 7.12c**), compared with those at stage A. Because of the similar mean levels of the compression resultant (C_c) (nearly same as tensile force in tension reinforcement T_s) and the change rates of centroid (dj_{C_c}/dx), the arch actions of the two beams presented close grades (see **Figure 7.12c-d**). Also, because of the similar mean levels of the slope of combined tensile forces (dT_s/dx), the beam actions of the two beams displayed similar grades.

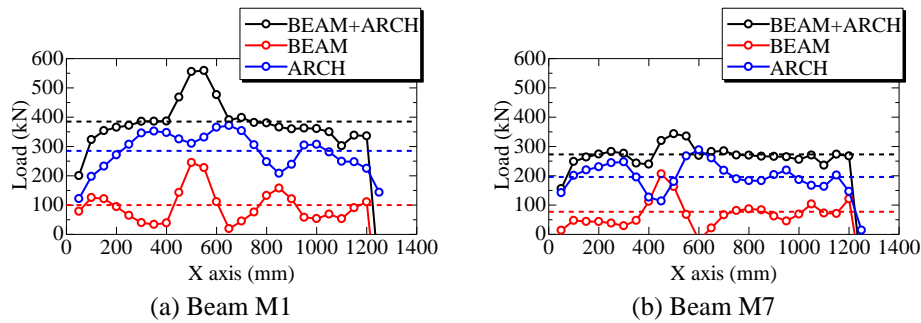


Figure 7. 13 Beam actions and arch actions at stage D

Moreover, it was concluded and should be emphasized that the drop of beam action for the beam M7 after the diagonal shear cracking, which resulted in the ultimate shear failure, was caused by the rising of tensile strain in tension reinforcement at rebar cutoff zone, which reduced the slope of combined tensile force (dT_s/dx).

The stage D is the yielding point for the beam M1. And the shear components at stage D is explained as follows (see **Figure 7.13**). The arch action for the beam M1, in general, was further increased, whereas no promotion of it could be seen for the beam M7, compared with the previous stages. Meanwhile, the beam actions for the two beams continued decreasing and presented low grades.

The tensile strain of the beam M1 was further increased and had been yielded in the entire shear span (see **Figure 7.14a**). For the beam M7, only the tensile strain of long bars

greatly rose at the rebar cutoff zone because of great shear cracking there, while that of cutoff bars was not sensitive to the greater loading. The similar distributions of tensile stresses are shown in **Figure 7.14b**, and it was seen that the tensile stress of the beam M1 also approached to the upper limit while the tensile stresses for the beam M7 nearly remained unchanged compared with that at stage C. As shown in **Figure 7.14c**, the combined tensile force greatly rose for the beam M1; in the meantime, it was remained unchanged for the beam M7, since it was dominated by the upper limit (337 kN) at the rebar cutoff zone. This evident difference explained the big gap between the grades of arch actions between the two beams, because the other factor (dj_{Cc}/dx) presented similar levels (see **Figure 7.14d**).

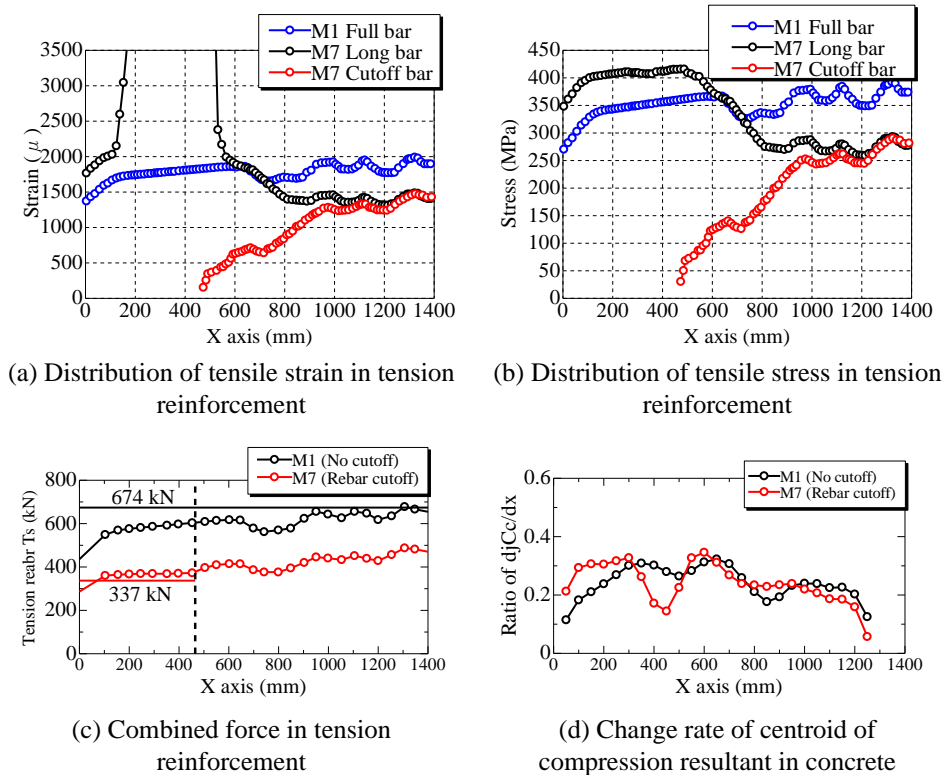


Figure 7. 14 Result of local force for the two beams at stage D

Thus, it was learned that the great difference of arch actions between the two beams was originated from the different load carrying capacities of tension reinforcement, that

is, the upper limit of the combined tensile force in tension reinforcement of the beam M7 was significantly reduced because of the rebar cutoff.

7.6 Summary and conclusions

In this chapter, the different shear performances including shear strength between the RC beams with and without rebar cutoff in longitudinal reinforcement were simulated by 3-D RBSM, and the effect of rebar cutoff on shear resistance mechanisms was further investigated. The following conclusions are included.

Firstly, it was confirmed that 3-D RBSM was able to reproduce the distinct shear performances between the two beams, i.e. the shear failure after yielding, defined as failure type IIb for the beam M1 and the relatively brittle shear failure at rebar cutoff point for the beam M7, defined as failure type I.

Secondly, it was clarified that the drop of beam action for the beam M7 after the diagonal shear cracking, which resulted in the ultimate shear failure, was caused by the rising of tensile strain in tension reinforcement at rebar cutoff zone, which reduced the slope of combined tensile force (dT_s/dx); the great difference of arch actions between the two beams was originated from the different load carrying capacities of tension reinforcement, that is, the upper limit of the combined tensile force in tension reinforcement of the beam M7 was significantly reduced because of the rebar cutoff.

8. Summary and Conclusions

8.1 Conclusions

In this study, the author, employing 3-D RBSM as a main tool, simulated shear behaviors of a number of RC members, i.e. the RC column for bridge pier (chapters 3, 4 and 5), the RC beam with section pre-crack (chapter 6) and the RC beam with rebar cutoff (chapter 7), under different loading conditions. And the theory of shear resistance mechanisms was combined with 3-D RBSM, that is, it was succeeded in decoupling the development of shear resistance into beam action, arch action, truss action and concrete contribution, by using the local stress output from 3-D RBSM. By this way, the author investigated three significant issues in shear for RC members, i.e. the mechanism of shear failure after yielding due to cyclic loading, the effect of section crack on shear resistance mechanism and the essential mechanism of shear strength reduction due to rebar cutoff. The conclusions derived from this study are included as follows.

1. As a general summary, the effectiveness and applicability of 3-D RBSM for simulating structural behaviors of RC members with different main variables and under different loading conditions was proved by the comparison of analytical result and experimental result in this study.
2. Chapter 3 studied the mechanism of shear failure after yielding, i.e. mechanisms of shear strength degradation, for a RC column subjected to cyclic loading, which

is explained as that the initial shear strength was first decreased to a grade close to the shear demand corresponding to flexural strength because of the progressive degradation of arch action, while the original capacity of beam action was well maintained; then after the high percentage loss of arch action, the beam action began decrease induced by the degradation of concrete contribution; finally the shear strength became lower than the shear demand corresponding to flexural strength and shear failure occurred. On the contrary, the arch action, under one-side repeated loading, presented very limited degradation with the increase of displacement ductility.

3. In chapter 4, a parametric study for the effects of structural variables, i.e. shear reinforcement ratio, shear span to effective depth ratio, tension reinforcement ratio and axial compression load, on the mechanism of shear failure after yielding for RC columns was performed. As a consequence, the reliability of the failure mechanism included in chapter 3 was demonstrated, that is, the progressive degradation of arch action with increased displacement ductility was the essential reason for the degradation of shear strength, regardless of the varying structural factors. As effect of variables on failure mechanism, it was learned that more arrangement of shear reinforcement could effectively delay the start ductility point for dramatic degradation of arch action and shear strength; smaller shear span to effective depth ratio could dramatically advance the start ductility point for dramatic degradation of arch action and shear strength; more arrangement of tension reinforcement could similarly advance the start ductility point for dramatic degradation of arch action and shear strength; higher axial compression load effect could advance the start ductility point for dramatic degradation of arch action and shear strength as well.
4. In chapter 5, in order to clarify the critical factor for the degradation of arch action due to cyclic loading, section pre-crack was numerically introduced into RC

columns and its effect on shear strength and arch action was numerically investigated. As a result, it was apparent that the formation of section cracks located at the position $1.0d$ or $2.0d$ (d : effective depth of RC column) far away from footing-column intersection could dramatically cause degradation of arch action, whereas the section crack located at footing-column intersection did not affect shear strength.

5. In chapter 6, the section pre-cracks, $1.0d$ (d : effective depth of RC beam) far away from loading point, were introduced into RC beams and their effect on shear performance was studied by 3-point loading experiment and numerical analysis. Consequently, it was clarified that section crack could greatly reduce shear strength of RC beam, which was found being caused by the degradation of arch action. Moreover, as the reason of arch action degradation, the section pre-cracks was discovered playing a primary role in obstructing the transfer of axial compressive stress in concrete along beam axis.
6. Chapter 7 shows the result of monotonic loading analyses for two RC beams with same structural details except for one with cutoff point in longitudinal rebar, where the degradation of shear performance such as shear strength and deformability caused by rebar cutoff point was confirmed. Moreover, it was clarified that the shear strength degradation caused by rebar cutoff point was attributed to the degradation of arch action, and the degradation of the capacity of arch action was originated from the lower load capacity sustained by tension rebar, i.e. the load capacity maintained by tension rebar when they were yielded, because of the reducing of number of tension rebar at rebar cutoff zone.

8.2 Recommendations for future study

This study has clarified the mechanism of shear failure after yielding of RC member

subjected to cyclic loading that degradation of arch action with increased displacement ductility governs shear strength degradation and is probably attributed to the formation of section cracking behavior. The effective measurement for inhibition of arch action degradation and development of section crack, however, has not been put forward. Based on the achievement from chapter 5, i.e. section crack nearby footing-column intersection nearly has no damage to arch action and shear strength, a practical method that limiting section crack only forms at footing-column intersection by arranging a bit more tension reinforcement in plastic hinge zone (range from $1.0d$ to $2.0d$ far away from footing-column intersection) is considered. But this method needs experiment to verify.

Furthermore, an approach to introducing section pre-crack into RC beam has been proposed in chapter 6 and the section pre-crack was found playing a primary role in resulting in severer internal crack damage reducing transfer of compressive stress. And it will be more acceptable if those extra section cracks can be directly observed in experiment. Thus, it is suggested that same loading test for RC beam with section pre-crack should be conducted with an intention to observe the internal crack damage caused by section pre-crack by cutting cross section of specimen.

At last, in this study, the effect of rebar cutoff on shear resistance mechanism of RC beam under monotonic loading has been explained. However, it is widely known that RC member with rebar cutoff sometimes fails by shear at rebar cutoff point. For example, some cyclic loading tests for bridge piers with rebar cutoff showed that the shear failure occurred at cutoff point because of the insufficient anchorage length of cutoff rebar (Kawashima et al. 1995). Thus, it is necessary to simulate the shear failure at rebar cutoff point of the RC member with rebar cutoff under cyclic loading, and investigate the shear failure mechanism based on the analysis of the degradation progresses of beam action and arch action.

References

- Applied Technology Council (1983). Seismic Retrofitting Guidelines for Highway Bridges. ATC 6-2, Redwood City, CA, ATC.
- Ang, B. G., Priestley, M. J. N. and Paulay, T., (1989): “Seismic Shear Strength of Circular Reinforced Concrete Columns.” *ACI Struct. J.*, 86(1): 45-59.
- Bolander, JE. and Hong, GS., (2002). “Rigid-Body-Spring Networks Modeling of Prestressed Concrete Members.” *ACI Struct. J.*, 99(5): 595-604.
- Building code requirements for structural concrete and commentary, (2015). ACI 318M-14, *American Concrete Institute (ACI)*, Farmington Hills.
- Baron, M.J. (1966): “Shear Strength of Reinforced Concrete Beams at Points of Bar Cutoff.” *ACI Journal*, 63(6): 127-134
- Choi, K. K. and Park, H. G. (2010). “Evaluation of inelastic deformation capacity of beams subjected to cyclic loading.” *ACI Structural Journal*, 107(5): 507.
- Comite Euro-Fédération Internationale du Béton, (1990). CEB-FIB Model Code 1990 First Draft, *CEB*, Paris.
- Comite Euro-Fédération Internationale du Béton, (2010). CEB-FIB Model Code 2010, Vol.2, Final Draft, *CEB*, Lausanne Switzerland.
- Collins, M. P. and Kuchma, D. (1999). “How safe are our large, lightly reinforced

- concrete beams, slabs, and footings?." *Structural Journal*, 96(4): 482-490.
- CEB model code for seismic design of concrete structures, (1985). No. 165.
- Design for Earthquake Resistant Reinforced Concrete Buildings Based on Ultimate Strength Concept. (1988). *Structural Committee, Architectural Institute of Japan (AIJ)*.
- Eurocode 2: Design of Concrete Structures: Part 1-1: General Rules and Rules for Buildings, (2004). *British Standards Institution*.
- Fu, L., Nakamura, H., Yamamoto, Y. and Miura, T., (2016a). "Numerical investigation of effect of through crack on shear strength degradation of RC column." *Proceedings of the Japan Concrete Institute*, 36: 865-870.
- Fu L., Nakamura H., Furuhashi H., Yamamoto Y. and Miura T. (2016b). "Mechanism of Shear Strength Degradation of RC Column Subjected to Cyclic Loading." *Structural Concrete: the Journal of the fib*, Wiley Online Library, 18: 177-188.
- Ferguson, P. M. and Mat-Loob, F. N., (1959). "Effect of Bar Cutoff on Bond and Shear Strength of Reinforced Concrete Beams." *ACI Journal*, 56(7): 5-24.
- Gedik, Y. H., Nakamura, H., Yamamoto, Y., Kunieda, M. and Furuya, N., (2011). "Analysis of Compression Failure of Concrete by Three Dimensional Rigid Body Spring Model." *Cement & Concrete Composites*, 33:978–991.
- Ichinose, T., Ogishi, S., Yabunouchi, T., Aoyama, H. and Watanabe. F. (1988). "Shear Design of Reinforced Concrete Beam and Column Members-Truss Action and Arch Action." *AIJ Tokai Chapter Architectural Research Meeting*, Architectural Institute of Japan, 37-140. (in Japanese)
- Iwamoto, T., Nakamura, H., Fu, L., Yamamoto, Y. and Miura, T., (2017). "An

- investigation on shear resistant mechanism of RC beam based on beam action and arch action.” *Journal of JSCE*, 73(1): 70-81. (in Japanese)
- Ishibashi, T., Nakayama, Y. and Tsuyoshi, T., (2001). “Failure Mode of Reinforced Concrete Column without Hoop Reinforcement.” *Journal of JSCE*, 676: 13–18. (in Japanese)
- Kinugasa, H. and Nomura, S. (1994). “Failure Mechanism under Reversed Cyclic Loading after Flexural Yielding.” *Concrete Research and Technology*, 5(2): 21-32. (in Japanese)
- Kim, W. and Jeong, J. (2011). “Decoupling of arch action in shear-critical reinforced concrete beams.” *ACI Structural Journal*, 108(4): 395.
- Kani, G. N. J. (1964). “The riddle of shear failure and its solution.” *ACI, In Journal Proceedings*, 61(4): 441-468.
- Kani, G. N. J. (1966). “Basic facts concerning shear failure.” *ACI, In Journal Proceedings*, 63(6): 675-692.
- Kao, A. M. and Untrauer, R. E., (1975). “Shear Strength of Reinforced Concrete Beams with Bars Terminated in Tension Zones.” *ACI Journal*, 72(12): 720-722.
- Kawashima, K., Hoshikuma, J. I. and Unjoh, S., (1995). “A Seismic Evaluation Method for Reinforced Concrete Bridge Piers with Inadequate Anchoring Length at Termination of Main Reinforcements.” *Journal of JSCE*, 525: 83-95.
- Kawashima, K. and Koyama, K., (1988). “Effect of Number of Loading Cycles on Dynamic Characteristics of Reinforced Concrete Bridge Pier Columns.” *Structural Engineering/Earthquake Engineering*, Proceedings of JSCE No.392, 5(1): 183-191.

- Kosa, K., Tsuyoshi, T., Kato, K. and Hamamoto, T., (2008). "A Study on Damage Mechanism of a PC Girder Bridge Damaged at the Cut-off Point." *Journal of Structural Engineering. A*, 54: 343-352. (in Japanese)
- Mattock, A. H. (1969). "Diagonal tension cracking in concrete beams with axial forces." *Journal of the Structural Division*, 95(9): 1887-1900.
- Mizuno, E., Suzuki, M. and Kameda, Y., (2010). "An Experimental Study on Deformational Behavior of RC Columns under Cyclic Loading." *Science and Technology Research*, 22: 65-72.
- Mishima, T., Hara, N. and Maekawa, K. (1992). "The Analytical Approach to the Effect of Cyclic Loading on The Reduced Shear Stiffness of RC Crack Planes." *Journal of JSCE*, 1992(442): 191-200.
- Nakamura, H., Niwa, J. and Tanabe, T. A. (1992). "An analytical evaluation of the ductility of reinforced concrete members." *Journal of JSCE*, 1992(442): 127-135.
- Niwa, J., Yamada, K., Yokozawa, K. and Okamura, H., (1986). "Revaluation of the Equation for Shear Strength of Reinforced Concrete Beams without Shear reinforcement." *Journal of JSCE*, 372: 167-176. (in Japanese)
- Niwa, J., (1983). "Shear Strength Formula for Deep Beams Based on FEM Analysis." *Proceedings of JCI 2nd Colloquium on Shear Analysis of RC Structures*. Oct., 25-26. (in Japanese)
- Okamura, H. and Higai, T. (1980). "Proposed design equation for shear strength of reinforced concrete beams without shear reinforcement." *In Proceedings of the Japan Society of Civil Engineers*, Japan Society of Civil Engineers, 300: 131-141.
- Ohe, R. and Yoshikawa, H., (2002). "Study on Shear Strength Degradation of Single

- Reinforced Concrete Columns under Repeated Large Deformation.” *Journal of JSCE*, 711: 59–71. (in Japanese)
- Ohta, M. (1979). “An Experimental Study on the Behavior of Reinforced Concrete Bridge Piers under Cyclic Loadings” *Journal of JSCE*, 292: 65 – 74. (in Japanese)
- Ozaka, Yoshio, Suzuki, M., Terasawa, M. and Kobayashi, S., (1986). “Effect of Bar Cutoff on Shear Strength of Reinforced Concrete Beams.” *Journal of JSCE*, 366: 133-142.
- Ozaka, Y., Suzuki, M., Miyamoto, M. and Kobayashi, S., (1987). “Evaluation of Shear Strength for Reinforced Concrete Beams with Bars Terminated in Tension Zones and Its Application to Design.” *Journal of JSCE*, 378: 89-96.
- Papadakis, G. (1996). “Shear failure of reinforced concrete beams without stirrups.” *PhD diss.*, Department of Civil Engineering, Aristotle University of Thessaloniki, Thessaloniki, Greece (in Greek).
- Park, R. and Paulay, T., (1975). Reinforced concrete structures. *John Wiley & Sons*.
- Priestley, M. N., Verma, R. and Xiao, Y. (1994a). “Seismic shear strength of reinforced concrete columns.” *ASCE Journal of structural engineering*, 120(8): 2310-2329.
- Priestley, M. N., Seible, F., Xiao, Y. and Verma, R. (1994b). “Steel Jacket Retrofitting of Reinforced Concrete Bridge Columns for Enhanced Shear Strength-Part 1: Theoretical Considerations and Test Design.” *ACI Structural Journal*, 91(4): 394-405.
- Priestley, M. N., Seible, F. and Xiao, Y. (1994c). “Steel Jacket Retrofitting of Reinforced Concrete Bridge Columns for Enhanced Shear Strength--Part 2: Test Results and Comparison with Theory.” *ACI Structural Journal*, 91(5): 537-551.

- Park, R., (1982). "Ductility of Square-Confined Concrete Columns." *ASCE ST4*, 108(4): 929-950.
- Panagiotakos, B., T. and Fardis, N., M., (2001). "Deformations of Reinforced Concrete Members at Yielding and Ultimate." *ACI Struct. J.*, 98(2): 135-148.
- Priestley, M. J. N., (1981). "Ductility of Spirally-Confined Concrete Columns." *ASCE ST1*, 107(1): 181-202.
- Priestley, M. J. N., Seible, F. and Carvi, G. M., (1996). "Seismic Design of Retrofit of Bridges." *A Wiley-Interscience Publication*.
- Pimanmas, A. and Maekawa, K., (2001a). "Influence of Pre-crack on RC Behavior in Shear." *Journal of JSCE*, 669: 277-291.
- Schlaich, J., Schäfer, K. and Jennewein, M. (1987). "Toward a consistent design of structural concrete." *PCI journal*, 32(3): 74-150.
- Suga, M., Nakamura, H., Higai, T. and Saito, S., (2001). "Effect of Bond Properties on the Mechanical Behavior of RC Beam." *Proceedings of Japan Concrete Institute*, 23(3): 295-300. (in Japanese)
- Standard Specifications for Concrete-Design, (2012). *Japan Society of Engineers (JSCE)*.
- Saatcioglu, M., (1991). "Deform Ability of Reinforced Concrete Columns." *ACI Struct. J.*, 127: 421-452.
- Seismic retrofitting guidelines for highway bridges, (1983). *Applied Technology Council (ACT6-2)*, Redwood City, Calif..
- Sakai, J. and Unjoh, S., (2009). "Dynamic Response Analyses Using Fiber Element for Shake Table Test of Full-Scale Reinforced Concrete Bridge Column that Failed in Shear at Cut-Off Point of Longitudinal Reinforcement." *Journal of JSCE. A1*, 65: 406-

416.

Sasaki, T., Kurita, H., Kawashima, K., Ukon, H. and Kajiwara, K., (2010). “Effect of Loading Protocols on the Failure Modes of RC Bridge Columns with Termination of Main Reinforcements at Two Heights.” *Journal of JSCE. A*, 66(1): 37-55.

Watanabe, H. and Kawano, H. (1999). “Study on the Mechanism of Shear Strength Decay of RC Members Under Load Reversals.” *Journal of JSCE*, 1999(613): 85-102.

Wong, Y. L., Paulay, T. and Priestley, M. J. N., (1993). “Response of Circular Reinforced Concrete Columns to Multi-directional Seismic Attack.” *ACI Struct. J.*, 90(2): 45-59.

Yamamoto, T., Iishibashi, T., Otsubo, M. and Kobayashi, S. (1984). “Experimental Studies on Seismic Resistance of A Pier with Reinforcement Terminated in A Tension Zone.” *Journal of JSCE*, 348: 61-70. (in Japanese)

Yamamoto, Y., Nakamura, H., Kuroda, I. and Furuya, N., (2008). “Analysis of Compression Failure of Concrete by Three Dimensional Rigid Body Spring Model.” *Journal of JSCE*, 64: 612–630. (in Japanese)

Yamamoto, Y., Nakamura, H., Kuroda, I. and Furuya, Nobuaki., (2014). “Crack Propagation Analysis of Reinforced Concrete Wall under Cyclic Loading Using RBSM.” *European Journal of Environmental and Civil Engineering*, 18(7-8): 780-792.

Zhang, G., Hoshikuma, J. and Sakai, J., (2012). “Experimental Study on Seismic Retrofit of RC Bridge Pier with Cut-off Section of Reinforcement for Upgrading Flexural Strength and Ductility.” *Journal of Structural Engineering. A*, 58: 343-352.